

~~CONFIDENTIAL~~

13846

12

C72 72556

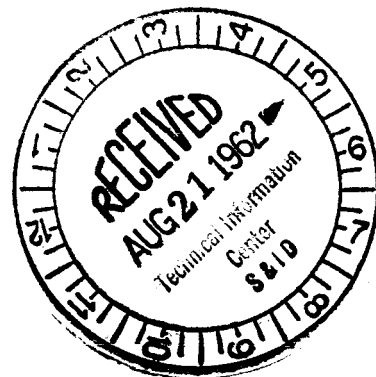
REFERENCE NO. 64 322

COPIES

APOLLO

BELLCOMM, INC.
1100 17th ST., N.W.
WASHINGTON 6, D. C.
(UNCLASSIFIED TITLE)

APOLLO HEAT SHIELD
PHASE I
MONTHLY PROGRESS REPORT



Prepared by

RESEARCH AND ADVANCED DEVELOPMENT DIVISION
AVCO CORPORATION
Wilmington, Massachusetts

RAD-SR-62-165
Letter Contract M2H43X-406012
Avco Report Series 201

THIS REPORT WAS PREPARED IN ACCORDANCE WITH NAA/S&ID LETTER CONTRACT M2H43X-406012. IT IS SUBMITTED IN PARTIAL FULFILLMENT OF THE CONTRACT AND IN ACCORDANCE WITH NAA/S&ID PROCUREMENT SPECIFICATION MC304-0001 AND SIN62-420 (PARAGRAPH 4.0.)

(NASA-CR-127994) APOLLO HEAT SHIELD, PHASE
1 Monthly Progress Report (Avco Corp.,
Wilmington, Mass.) 150 p

N79-76593

10 August 1962

Unclass
00/34 11693

Prepared for

NORTH AMERICAN AVIATION, INC.
SPACE AND INFORMATION SYSTEMS DIVISION
Downey, California

DOWNGRADED AT 3 YEAR INTERVALS
DECLASSIFIED AFTER 12 YEARS

~~CONFIDENTIAL~~

CLASSIFICATION CHANGE

TO UNCLASSIFIED

By authority of [signature]
Changed by [signature]
Classified Document Master Control Station, NASA
Scientific and Technical Information Facility

Date 12/3/82

Goal Information Facility

RAD-SR-62-165

(5)

AVCO

~~CONFIDENTIAL~~

C 7 2 7 2 5 5 6
(UNCLASSIFIED TITLE)

APOLLO HEAT SHIELD
PHASE I
MONTHLY PROGRESS REPORT


Prepared by
RESEARCH AND ADVANCED DEVELOPMENT DIVISION
AVCO CORPORATION
Wilmington, Massachusetts

RAD-SR-62-165
Letter Contract M2H43X-406012
Avco Report Series 201

THIS REPORT WAS PREPARED IN ACCORDANCE WITH NAA/S&ID
LETTER CONTRACT M2H43X-406012. IT IS SUBMITTED IN
PARTIAL FULFILLMENT OF THE CONTRACT AND IN ACCORD-
ANCE WITH NAA/S&ID PROCUREMENT SPECIFICATION MC304-
0001 AND SID62-420 (PARAGRAPH 4.0.)

10 August 1962

APPROVED


E. Offenhartz
Project Manager
Apollo R&D


C. F. Berninger
Project Director
Apollo Project Office

Prepared for
NORTH AMERICAN AVIATION, INC.
SPACE AND INFORMATION SYSTEMS DIVISION
Downey, California

~~CONFIDENTIAL~~

~~CONFIDENTIAL~~

(NOT USED)

-ii-

~~CONFIDENTIAL~~

CONTENTS

I.	Current Status	1
A.	Design	1
B.	Materials Development and Evaluation	12
C.	Reliability and Quality Assurance	22
D.	Manufacturing	23
E.	Administration and Documentation	24
II.	Problems and Actions	26
A.	Design	26
B.	Materials Development and Evaluation	28
C.	Reliability and Quality Assurance	29
D.	Manufacturing	30
E.	Administration and Documentation	30
III.	Forecasts	31
A.	Design	31
B.	Materials Development and Evaluation	32
C.	Reliability and Quality Assurance	34
D.	Manufacturing	35
E.	Administration and Documentation	36
IV.	Analysis	37
A.	Design	37
B.	Materials Development and Evaluation	96

~~CONFIDENTIAL~~

(NOT USED)

-iv-

~~CONFIDENTIAL~~

ILLUSTRATIONS

Figure 1	Avcoat X5026 -- Rate of Reaction versus Temperature for Different Heating Rates	16
2	Comparison of Longitudinal Convective Heat Transfer Distribution	38
3	Radiative Heat Transfer, Trajectory 1, Point 1	41
4	Radiative Heat Transfer, Trajectory 1, Point 2	42
5	Radiative Heat Transfer, Trajectory 1, Point 3	43
6	Radiative Heat Transfer, Trajectory 1, Point 4	44
7	Radiative Heat Transfer, Trajectory 1, Point 5	45
8	Heat-Transfer Rate Measurements	46
9	Heat-Transfer Rate Measurements -- High-Stagnation Enthalpy ($\rho_1 = 0.025$ cm, $\alpha = 33^\circ$)	47
10	Heat-Transfer Rate Measurements -- High-Stagnation Enthalpy ($\rho_1 = 0.005$ cm, $\alpha = 33^\circ$)	47
11	Apollo Trajectory 1, NAA Heating, Predicted Local Weight Loss of Avcoat X5026, Charring Analysis	49
12	Time-Temperature Histories for Apollo Command Module with C-5 Nominal Ascent Trajectory and Abort Heating	51
13	Isochronal Temperature Gradients for Apollo Command Module with C-5 Nominal Ascent Trajectory and Abort Heating	52
14	Additional Heating and Cooling Capability of the Internal Air Conditioning System	53
15	Heat Shield Insulation Weight (w_{INS}) versus $\sqrt{\frac{\rho k}{C_P}}$	54
16	Blunt Face -- Typical Weight Penalty Associated with Safety Factor on Structure Temperature	56
17	Temperature Histories for Several Exposed Fastener Materials at a Depth Equal to That of the First Face Sheet of the Honeycomb -- Stations 16 - 19	57

ILLUSTRATIONS (Cont'd)

Figure 18	Temperature Histories for Several Exposed Fastener Materials at a Depth Equal to That of the First Face Sheet of the Honeycomb - Stations 12 - 15, Trajectory 1	58
19	Temperature Histories for Several Exposed Fastener Materials at a Depth Equal to That of the First Face Sheet of the Honeycomb - Stations 12 - 15, Trajectory 4	59
20	Temperature at First Interface versus Depth from Surface ..	60
21	Temperature at First Interface versus Thickness of Embedded Fastener, Trajectory 1	61
22	Energy - Wave No. $\times 10^{-4}$ versus Internuclear Separation - Å	62
23	Wave Function - Vibrational Quantum State, $V' = 10$, $B^2\pi$ State of NO (No. 1)	63
24	Wave Function - Vibrational Quantum State, $V' = 10$, $B^2\pi$ State of NO (No. 2)	64
25	Potential Functions of NO	66
26	Potential Functions of N_2	67
27	Potential Functions of O_2	68
28	Geometry	70
29	Required Bond Allowable Tensile Stress versus Bond Elastic Modulus	76
30	Tangential Deflection versus Distance from Apex - Case 1.4	77
31	Tangential Deflection versus Distance from Apex - Case 1.0	78
32	Radial Deflection versus Distance from Apex - Case 1.4 ...	79
33	Radial Deflection versus Distance from Apex - Case 1.0 ...	80
34	Radial Deflection versus Distance from Apex - Case 1.1 ...	81

ILLUSTRATIONS (Cont'd)

Figure	35	Radial Deflection versus Distance from Apex — Case 1.2 ...	82
	36	Radial Deflection versus Distance from Apex — Case 1.3 ...	83
	37	Toroidal Shells of Varying Stiffness	84
	38	Meridional Stresses in Outer Skin versus Distance from Apex — Case 1.4	85
	39	Meridional Stresses in Outer Skin versus Distance from Apex — Case 1.3	86
	40	Meridional Stresses in Outer Skin versus Distance from Apex — Case 1.2	87
	41	Meridional Stresses in Outer Skin versus Distance from Apex — Case 1.1	88
	42	Meridional Stresses in Outer Skin versus Distance from Apex — Case 1.0	89
	43	Avcoat X5026 Thermal Gradients — Run 2947	90
	44	Turbulent Tube Specimen of Avcoat X5026	92
	45	Turbulent Tube Specimen of Avcoat X5019	93
	46	Avcoat X5026 Thermal Gradients — Run 2953	94
	47	Avcoat X5026 Thermal Gradients — Run 2963	95
	48	Moisture Absorption versus Time	100
	49	Ultimate Tensile Strength, Modulus of Elasticity, and Total Strain to Failure versus Temperature	101
	50	Overall View of Tested OVERS Samples A-1 and A-3	104
	51	Photomicrograph of Half Section of Sample A-1 (left) and Sample A-3 (right)	105
	52	Overall View of OVERS Tested Samples A-2 and A-4 (Similar composition to X5026-22, but less dense)	106

ILLUSTRATIONS (Cont'd)

Figure 53	Photomicrograph of Half Section of X5026-22B Test Samples A-2 (left) and A-4 (right)	107
54	Overall View of OVERS Test Samples A-2 and A-5 Material (Similar to X5026-22 Except Phenolic Micro-balloons Omitted from Formulation)	108
55	Photomicrograph of Half Section of Test Samples A-2 (left) and A-5 (right)	109
56	Overall View of OVERS Tested Samples A-3 (X5026-22B, S.G. = 0.73), PL-2 (X5026-22), and DB3 (X5026, S.G. = 0.487)	110
57	Photomicrographs of Half Section of Tested Samples A-3 (a), PL-2 (b), and DB3 (c)	111
58	Overall View of OVERS Tested Samples II A5-2A, H45-2A, and II A4-5A	112
59	Photomicrograph of Half Section of Tested Samples II A5-2A (a), H45-2A (b), and II A4-5A (c)	113
60	Overall View of OVERS Tested Samples II A4-2A, II A5-5A, and H45-5A	114
61	Photomicrograph of Half Section of Tested Samples II A4-2A (a), II A5-5A (b), and H45-5A (c)	115
62	Overall View of OVERS Tested Samples 3, 4, and 5B (H46)	116
63	Photomicrograph of Half Section of Tested Samples 3 (a), 4 (b), and 5B (c)	117
64	Overall View of Instrumented OVERS Test Samples [(2) X5026-29, left; (2) X5026-22, center; (2) X5026-23, right]	118
65	Photomicrographs of Tested Samples X5026-29, Low Heat Flux (left) and High Heat Flux (right)	119
66	Photomicrographs of Tested Samples X5026-22, Low Heat Flux (left) and High Heat Flux (right)	120

ILLUSTRATIONS (Concl'd)

Figure 67	Photomicrographs of Tested Sample X5026-23, Low Heat Flux (left) and High Heat Flux (right)	121
68	Slope of Temperature Histories of Sample 21, Plate 16, Avcoat X5026-22 during Heating Period	124
69	Slope of Temperature Histories of Sample 21, Plate 52, Avcoat X5026-23 during Heating Period	125
70	Temperature Distribution History of Sample 21, Plate 16, Avcoat X5026-22 during Heating Period	126
71	Temperature Distribution History of Sample 21, Plate 52, Avcoat X5026-23 during Heating Period	127
72	Effect of an Error in Driving Temperature on Computed Emissivity Error at 50 Seconds, Case 4	130
73	Predicted Penetration into Avcoat X5026	132
74	Temperature Distribution in Back-up Plate	134
75	Spectral Emittance of Avcoat X5026-29 after Exposure to Low-Enthalpy Arc (Measurements at 26 °C)	135
76	Spectral Emittance of Avcoat X5026-29 after Exposure to High-Enthalpy Arc (Measurements at 26 °C)	136

TABLES

Table I	Status of Structural Development Tests	4
II	Excerpt from Matrix of Franck-Condon Factors: NO-Bands ..	73
III	Different Methods Used to Compute the Equilibrium Radiative Heat Transfer	73
IV	Effect of Diluent on High-Viscosity Resins	97
V	Tensile Strength of Modified DC-731 as a Function of Borax Concentration and Cure Temperature	98
VI	Tensile Strength (Single Lap Shear) of DC-601 Bonded to Primed PH 15-7 Mo Stainless Steel	98
VII	Analysis of Microballoons	99
VIII	OVERS Arc Test Data on Instrumented Test Samples	123
IX	Effective Thermal Diffusivities Calculated Using Program 1077 for Sample 21, Plate 16, Avcoat X5026-22	128
X	Effective Thermal Diffusivities Calculated Using Program for Sample 21, Plate 52, Avcoat X5026-23	128

~~CONFIDENTIAL~~

I. CURRENT STATUS

Avco's program accomplishments during the period 9 through 31 July 1962 continue to reflect increased technical activities and include the work statement and documentation negotiations during the last part of the month.

A. DESIGN

1. Heat Transfer

Information has been made available by NAA on the abort trajectory. A report has been completed giving a summary of the techniques used in the analysis of the heating on the Apollo command module.

Comparisons have been made between the revised NAA theoretical (received July 1962) and Avco theoretical and experimental cold-wall convective heating rates.

An exploratory study of the necessity and/or feasibility of using the non-similar solutions of the laminary boundary layer equations for the determination of the spherical face convective heating has been initiated.

A study has been initiated to develop a more refined theoretical method of predicting the stagnation-point heating rates on nonaxisymmetric bodies.

Comparisons between the NAA radiative heating calculations (received July 1962) and the Avco radiative heating calculations have been made for trajectory 1.

The study of multicomponent species injection is continuing. A simplified technique has been completely formulated and examined to determine its applicability. The species properties are still being studied and appropriate molecular models selected.

Convective heat transfer tests conducted in the 1.5- and 6.5-inch diameter shock tubes have been completed. The heat-transfer rate distribution about the basic configuration at 33 degrees angle of attack at an enthalpy level of $H/RT_0 = 72$ has been obtained and check runs along the blunt body have been completed for enthalpy levels between $H/RT_0 = 240$ and 510.

At the enthalpy level of $H/RT_0 = 72$ the previous data along the lee side of the cone (obtained with string-supported models) have been checked by tests using wire-supported models.

~~CONFIDENTIAL~~

~~CONFIDENTIAL~~

Models for the radiative heat-transfer tests are due to arrive from the vendor at the end of August.

The initial models for the shape-parameter study have arrived from the vendor and are being instrumented.

2. Thermodynamic Analysis

Based on the analysis of Avcoat X5026 as a charring ablator, predictions have been obtained for the total local mass loss over most of the re-entry vehicle for trajectory 1. The results, presented as a function of the rear face design temperature, are based upon the property estimates previously reported.

A thermal analysis for combined ascent and abort heating was initiated to determine the thermal adequacy of the design thicknesses on the Apollo command module forecone. The NAA S&ID "patched" trajectory, Saturn C-5 nominal boost followed by trajectory 5, was considered. Resulting structure temperatures are far below the re-entry design limit.

An estimate of the total heat load on the environmental control system was made assuming various values for the composite insulation capacity (or thermal resistance) of the heat-shield-substructure-insulation composite.

Preliminary estimates of the weight penalties associated with various methods of applying factors of safety is continuing. The two methods of applying safety factors under direct consideration are: a) a safety factor applied to structure temperature, and b) a safety factor applied to material properties. The results of these studies are very critical in arriving at a satisfactory factor of safety.

New heat-shield thicknesses based on revised properties of Avcoat X5026 have been determined. A thermal analysis of selected stations on the command module for the entire boost through re-entry sequence (no space flight) has been completed.

The feasibility of umbilicals and shear ties in the blunt face was investigated and recommendations for further analytical and experimental study were made. Various mechanical fasteners are being studied for their thermodynamic behavior throughout all phases of the Apollo trajectory.

Emphasis was placed upon obtaining solutions to the Schrödinger equation for the various vibrational levels in the $X^1 \Sigma_g^+$, $A^3 \Sigma_u^+$ and $B^3 \frac{1}{11g}$ electronic

~~CONFIDENTIAL~~

~~CONFIDENTIAL~~

states of the N_2 molecule together with the overlap integrals and Franck-Condon factors associated with the permissible transitions between vibrational levels in the different electronic states. In addition, the writing of a digital program for evaluating the spectral distribution of the total equilibrium radiant heat input at the various vehicle stations was commenced.

The potential energy function of the $X^2\Sigma_g^+$ electronic state of N_2^+ was constructed in the same manner as the potential functions previously reported for other molecules of importance to the radiant heating problem.

A digital computer program for calculating the equilibrium radiant heat transfer at the stagnation point of the vehicle was completed. This program represents a refinement of the plane-slab methods currently in use in that it accounts for self-absorption and curved-shock geometry. This program is strictly applicable only in regions in which the temperature and density of the flow field are uniform. The output gives the total radiant input to a perfectly black wall. No information on the spectral distribution of the heating is given. It is proposed to utilize this program for calculation of the total radiant heating at the stagnation point pending completion of the more sophisticated program for calculating spectral heating caused by a nonuniform flow field.

The study of stresses around cutouts is being continued so that information on stress concentrations around cutouts may be obtained. Present effort consists of the determination of the effect of edge reinforcement in addition to the stress distribution in a plate with multiple cutouts.

The shallow spherical-shell section of the blunt end has been investigated for all symmetrical pressure-loading conditions. These were preliminary and did not include any cutouts in the structure.

Current methods of bond-stress concentration analysis were deemed inadequate and a more rigorous approach is being attempted.

A bond stress parametric study (based on current methods) to define cold-soak requirements has been completed.

A study of ablator-panel buckling and gap requirements has been started.

Free ablator-panel deflection and resulting fastener load histories versus time are in progress for a selected distribution of stations throughout the command module. These histories are being completed for ascent, cold, and re-entry trajectory environments using ablator materials Avcoat X5026-22 and X5019.

Stress histories for the bonded ablator to substructure shell have been run for ascent and trajectory 1, with both Avcoat X5026 and X5019 ablators.

~~CONFIDENTIAL~~

~~CONFIDENTIAL~~

The problem of determining thermal stresses and displacements in a three-layer visco-elastic body was attempted. It was felt that further consideration of this problem at this time was not feasible because of the mathematical difficulties involved.

Investigation and correlation were made of parts of information received from NAA S&ID concerning abort and tumbling abort. Only one time definition of abort was received. This definition directs the use of trajectory 5 in the ascent C-5 booster curves of procurement specification MC-364-001.

Three tubes of Avcoat X5026-22 and two tubes of Avcoat X5019 were tested in the 10-megawatt arc facility. Data are being reduced.

The status of testing is shown in Table I.

Detail drawings of fasteners were received and fabrication started. The status of the test program is shown in the accompanying table.

TABLE I

STATUS OF STRUCTURAL DEVELOPMENT TESTS

Cold Soak Beam and Panel Tests (G301-101-3100) (Refer to list of notes for explanations)		
Test Objective	Specimen Number*	Status
Gross effects	I-1	Tested 6/23/62; Epoxylite failed
	I-2	Tested 6/15/62; Epon 931 failed
	I-3	Tested 6/28/62; DC-731, no failure
	I-4	Tested 6/30/62; EccoSil 4712, no failure
	I-5	HT-424 failure during cure

~~CONFIDENTIAL~~

~~CONFIDENTIAL~~

TABLE I (Cont'd)

Cold Soak Beam and Panel Tests (G301-101-3100) (Refer to list of notes for explanations)		
Test Objective	Specimen Number*	Status
Gross effects	I-6	Tested 7/13/62; SC-71 failed
	I-7	Tested 7/18/62; EccoSil 4640, no failure
	I-8	Tested 7/25/62; DC-601 failed at 45°
	I-9-14	Note 7
	I-15-28	Note 8
	II-(Table II)* 1, 3, 5, 9, 11, 13	Specimen being prepared; notes 1, 2, and 3
	II-(Table II)* 2, 4, 6, 8, 10, 12, 14	Notes 1, 2, 3, and 8
	V-1, 2, 3, 4	Note 9
Substantiate analysis	III-1, 3	Tested 7/26/62; fasteners in X5026 at 260°F showed no crazing or notch effects
	III-2, 4	Specimens 1 and 3 being prepared; note 8
	IV 1, 3, 5	Notes 1, 2, and 3
Substantiate strength	IV 2, 4, 6	Notes 1, 2, 3 and 8
	Composite	Three tests to be planned after 9/9
	Lapped	Three tests to be planned after 9/9

~~CONFIDENTIAL~~

~~CONFIDENTIAL~~

TABLE I (Cont'd)

Composite Beam and Panel Heat and Load Tests (G301-101-2100) (Refer to list of notes for explanations)			
Test Objective	Specimen Number*	Test Condition	Status
Gross effects	I-1	Hot soak	Canceled due to cold failure
	I-2	Hot soak	Canceled due to cold failure
	I-3	Hot soak	0.20 psi shear failure at 600°F
	I-4	Hot soak	Specimen ready for test on 7/23/62
	I-5	Hot soak	Canceled due to cold failure
	I-6	Hot soak	Canceled due to cold failure
	I-7	Hot soak	Tested 7/26/62; failure due to poor surface preparation; will be re-run.
	I-8	Hot soak	Canceled due to cold failure
	I-9-14	Hot soak	Note 7
	I-15-28	Hot soak	Note 8
	I-1-28	Transient heat	Notes 4 and 6
	II-(Table II)* 1, 3, 5, 9, 11, 13	Transient heat	Specimens being prepared; notes 4 and 6
	II-(Table II)* 2, 4, 6, 8, 10, 12, 14	Transient heat	Notes 4, 6 and 8

~~CONFIDENTIAL~~

~~CONFIDENTIAL~~

TABLE I (Cont'd)

Composite Beam and Panel Heat and Load Tests (G301-101-2100) (Refer to list of notes for explanations)			
Test Objective	Specimen Number*	Test Condition	Status
Gross effects	V-5, 6	Hot soak	Note 9
Substantiate analysis	III-5, 6, 8	Hot soak	Specimens being prepared
	III-7, 9	Hot soak	Note 8
	IV-1, 3, 5	Hot soak	Specimens to be prepared 8/20/62; notes 1, 2 and 6
	IV-1, 3, 5	Transient heat	Specimens to be prepared 8/20/62; notes 1, 2, 4, 5 and 6
Substantiate strength	Composite	Hot soak	Three tests to be planned after 9/9
	Lapped	Hot soak	Three tests to be planned after 9/9
Fastener Tests (G301-101-2200) (Refer to list of notes for explanations)			
Test Objective	Specimen Number*	Test Condition	Status
Evaluate strength	II (Table I)* 1	Cold soak	Avcoat X5026 (unbonded and attached by two fixed fasteners) failed in tension
	II (Table I)* 2-10	Cold soak	Note 10
	II (Table I)* 2-10	Hot soak	Note 10
Substantiate strength	Tensile	Hot and cold	A series of 200 tests will be planned after 9/9
	Shear	Hot and cold	A series of 200 tests will be planned after 9/9

~~CONFIDENTIAL~~

~~CONFIDENTIAL~~

TABLE I (Cont'd)

Turbulent Tube Tests

(G301-101-1600)

Test Objective	Specimen No.	Status
Evaluate E and α at high temperatures for preliminary design purposes	1 (Avcoat X5026)	Tested 7/9/62; data being reduced
	2 (Avcoat X5026)	Tested 7/10/62; data being reduced
	3 (Avcoat X5026)	Tested 7/11/62; data being reduced
	4 (Avcoat X5019)	Tested 7/10/62; data unacceptable
	5 (Avcoat X5019)	Tested 7/12/62; data unacceptable
	6 (Avcoat X5019)	Test suspended until difficulties in instrumentation are corrected
Evaluate E and α at high temperatures for final design purposes	1 (Final Material)	To be tested after selection of final material
	2 (Final Material)	To be tested after selection of final material
	3 (Final Material)	To be tested after selection of final material

Acoustic, Vibration, and Shock Tests

(G301-101-5100)

(Refer to TR S220-T-0 for detailed test plan)

Test Objective	Specimen No.	Status
Acoustic Tests	1	Test facility being selected
	2	Test plan being written using reference design concept
Vibration and Shock	3-resonance survey	Support test fixture being constructed
	4-resonance survey	Substructure test completed 6/28/62; specimen being bonded
	5-sinusoidal vibration	Specimen ready; shakers not available
	6-sinusoidal vibration	Material not available until 8/1

~~CONFIDENTIAL~~

~~CONFIDENTIAL~~

TABLE I (Concl'd)

Test Objective	Specimen No.	Status
Vibration and Shock	7-shock	Test plan being written using reference design concept
	8-shock	Test plan being written using reference design concept
	9-shock	Test plan being written using reference design concept
	10-vibration and temperature	Waiting for reply from NAA S&ID defining environment.

*Specimens are numbered in Avco RAD Apollo Structural Development Test Programs, TR-S220-T-21 (10 July 1962)

LIST OF NOTES TO TABLE I

- Note 1: Specimens cannot be prepared because of lack of facility item 9, schedule III (a-1). Thermocouples cannot be installed.
- Note 2: Test data cannot be recorded efficiently because of lack of facility item 25, schedule III (c). Present system causes extreme delay in data reduction and recording.
- Note 3: Test temperatures cannot be controlled accurately causing difficulty in maintaining cooling rate caused by lack of facility item 26, schedule III (c).
- Note 4: Quartz lamp heating cannot be applied to the test specimens because of lack of approval of special test equipment — quartz lamp furnaces.
- Note 5: Combined heating and loading tests cannot be run until test fixture is approved under special test equipment.
- Note 6: Deflections cannot be measured because of lack of displacement transducer fixture which is awaiting approval as special test equipment.
- Note 7:** Adhesive material not received at Avco RAD.

~~CONFIDENTIAL~~

~~CONFIDENTIAL~~

- Note 8: Ablator material Avcoat X5019 not available for preparation of specimens.
- Note 9: Epoxy adhesive not yet selected by Materials Group for evaluation.
- Note 10: Fastener material not available at Avco RAD; material is on order. Fasteners will be fabricated upon receipt of material.

The application of Avcoat X5026-22 to a 12 by 18-inch substructure panel (to be used for vibration tests) has been completed and the ablative material was ground to a 1-inch thickness, including the bond. The bonding material has been radiographically and ultrasonically checked and a uniform adherence exists between the Avcoat material and the substructure panel. There are four areas (each 1/4-inch long) in the overlapping joint between the two Avcoat tiles where there is not any bonding material.

Aluminum and steel brackets are being machined to mount the 18 by 36-inch substructure on its vibration fixture. Holes have been drilled in this panel to bring it in conformance with the design on drawing SK-8660.*

Delivery of the magnesium vibration fixture has been delayed to 31 July because of the vendor's low estimate of the machining time required.

A detailed test plan for the acoustic environment tests is being written.

Modes of ablator failure were defined and transmitted to J. M. Kerr at NAA S&ID.

a. Heat-Shield Fairing Studies and Weights

Thickness values were computed for use in determining the mass-loss and cg location for eight time points during re-entry. Fairing layouts are in process. As soon as they are completed, weight calculation will be made.

b. Aft Compartment

In response to SEM No. 003 (item 4), drawings LA-4192 and LA-4193 were prepared and completed showing Avco's proposed revisions to S&ID design for the tension tie and umbilical receptacle located through the aft-compartment heat shield.

A layout study is in process to determine a new tile arrangement based on the tension tie and umbilical receptacle located through the aft compartment. Later information received from NAA on 30 July concerning additional details will be incorporated into the layout.

*Drawings will be presented separately from this report.

~~CONFIDENTIAL~~

~~CONFIDENTIAL~~

Detail tile arrangement analysis was made using two different methods. Drawing LA-4175 shows a bonded tile arrangement using lapped edges and mechanical fasteners as backup.

c. Crew Compartment

Layout studies were made of different tile arrangements and the optimum arrangement, using the existing cutout information, resulted in that shown on Drawing LA-4195.

The layout study on the roll rocket apertures at 135 and 225 is still in process. An interference was encountered between the rocket engine nozzle and a structural frame. To continue the study, the frame was relocated approximately three degrees.

d. Forward Compartment

A layout study (LA-4196) was completed showing an optimum tile arrangement based on existing cutout information.

A detail layout study is in process for the pitch rocket apertures at 180 degrees.

e. Fasteners

The following detail drawings were completed:

LA-4188 "B" Details — Fixed and Loose Fasteners
LA-4191 "A" Detail — Plastic Screw-Floating Insert
LA-4194 Detail — Access Door Attachment

Mechanical samples are being fabricated to the above drawings for experimental evaluation.

Studies of other fasteners are continuing in order to establish a simple, but optimum, configuration.

During this reporting period, the following items have been accomplished:

- a. The Project Procedure for Apollo has been released for integration into the RAD Drafting Practice Manual.
- b. R & Q submitted a manuscript for RAD-E700001, Series 401, Environmental Design and Test Criteria Specification for Apollo. This manuscript was circulated to various cognizant activities where it is now being reviewed.

~~CONFIDENTIAL~~

~~CONFIDENTIAL~~

B. MATERIALS DEVELOPMENT AND EVALUATION

1. Materials Development

Laboratory production of the reference Avcoat 5026-22 continued at the rate of approximately 45 panels for the 3-week period. The density range was 0.86 to 0.96 gm/cc.

The investigation of replacing phenolic microballoons with glass or silica microballoons is continuing. Panel densities are appreciably higher, especially with the glass microballoons.

Replacing the phenolic microballoons in the X5026-22 formulation with porous carbon gave excessively high densities — 1.37 gm/cc.

Fiberglass honeycomb has been received and work is now in progress making panels with microballoon-filled systems.

A possible source of hollow-glass fibers has been found. Pittsburg Plate Glass has such fibers in the developmental stage. Contact has been made with their laboratories, but final arrangements for purchase of a suitable quantity has yet to be made. Hollow fibers should give lower density and conductivity.

Vacuum drying of phenolic microballoons is continuing. Also, the specially packaged phenolic microballoons from Union Carbide have been received. In spite of these steps taken to reduce volatiles, moisture can be picked up during processing (humidity control in the processing area may be necessary).

A number of dry-blended formulations were made up and molded using glass microballoons, silica microballoons, and chopped fibers.

Samples of moldings made with a pregelled dry blend and with a nongelled dry blend were extracted with acetone and submitted for infrared examination to determine if any unreacted anhydride is present. A visual examination showed more material extracted from the nongelled system.

Viscosity and gel time vs temperature data were obtained for more flexible resin formulations for use in modified Avcoat X5019. Room temperature viscosities were taken of three highly viscous resins diluted with various amounts of a low-viscosity, flexible epoxy resin.

Eccosil SC-71, an RTV silicone rubber, was used to bond tiles of X5026-22 to 15-7 stainless-steel honeycomb panels (4 by 12-inch). Two specimens were made, one failed at room temperature, because of shrinkage of the adhesive on cure; the other failed between room temperature and -260°F. Preliminary analysis of strain gage data did not reveal the failure temperature.

~~CONFIDENTIAL~~

~~CONFIDENTIAL~~

SC-71 contains some solvent or thinner which escapes during cure, resulting in shrinkage. From this standpoint, SC-71 appears unsuitable.

Eccosil 4640, an RTV silicone rubber containing silica microballoons (Eccospheres) was used to bond tiles of X5026-22 to 15-7 stainless-steel honeycomb panels. Both specimens were taken to -260°F in 2 hours, held for 2 hours, and allowed to return to room temperature overnight. Strain gage data and visual inspection revealed no sign of failure. These panels will be tested at 600°F glue-line temperature with an applied shear load of 10 pounds per tile.

Dow Corning 601, an RTV silicone rubber, was used to bond two instrumented tiles of X5026-22 material to PH 15-7 Mo stainless-steel panels, 0.040 inch thick. These specimens will be tested under environmental conditions of RT to -260°F and RT to 600°F . Preliminary test results already obtained on DC 601 adhesive used to bond these adherents has indicated that the specimens should pass this evaluation.

Test specimens bonded with DC 731, a single-component RTV silicone adhesive, have withstood exposure to glue-line temperatures of up to 600°F for 10 minutes under shear stress of 10 pounds per tile. Similar test specimens, bonded with Eccosil 4712, an epoxy-silicone mixture, have withstood an exposure to glue-time temperature of 600°F for 1 hour under shear stress of 10 pounds per tile.

a. Ballistics Impact Test Specimens

Tiles of heat-shield material, X5026-22, were bonded to aluminum sheet stock, 2024 T3, and to aircraft steel, type 4130. DC 601 adhesive was used. Early indications are that the test panels have withstood exposure to -100°F . Impact test results have shown less damage to the tile than panels bonded with Epoxylite 5403. Further testing, at liquid nitrogen temperature, is planned.

Tiles of X5019 heat-shield material were bonded to aluminum with Eccosil 4640 foam silicone RTV rubber for similar impact tests.

b. Modification of DC 731 RTV Silicone

This material, which depends on atmospheric moisture to cure, has been cured by adding small amounts of polyhydrates such as borax ($\text{Na}_2\text{B}_2\text{O}_7 \cdot 10 \text{H}_2\text{O}$) and raising the glue-line temperature to release the needed water. In an effort to assess the effect of borax on the strength of the adhesive bond, a series of butt-tensile specimens were made with X5026-22 and 15-7 stainless steel. Test results indicate that not only does the available moisture in the borax cure the 731 RTV, but that some improvement in room temperature strength is realized. Since one of the main drawbacks in using DC 731 adhesive is the fact that it will not cure in thick and large sections because of a lack of exposure to atmospheric moisture, this experimental program will be continued.

~~CONFIDENTIAL~~

Four additional stainless-steel honeycomb panels were received from NAA. Two of these will be covered with Avcoat X-5026-22 and the remaining two will be covered with Avcoat X5019. Half of these panels are for structural tests and half are for dynamic test.

Two panels received previously are in the process of being tiled with Avcoat X5026-22. Eight chromel-alumel thermocouples were installed on the honeycomb structure. In addition, five cromel-alumel thermocouples were installed at various depths in a 0.750-inch diameter plug of X5026; the plug was bonded into the X5026 panel with Shell Epon No. 931. The Thermocouples were located at the following depths in the heat shield material:

- No. 1 — 0.060 inch
- No. 2 — 0.125 inch
- No. 3 — 0.250 inch
- No. 4 — 0.500 inch
- No. 5 — 0.625 inch

This panel is to be shipped 31 July 1962. A dynamic panel is now ready for covering and will be shipped 4 August 1962. A silicone adhesive, Eccosil 4640, was used to bond the tiles to the honeycomb on these two panels.

To evaluate the stability of the ablative heat-shield material in vacuum, the following consecutive tests were run on a specimen of X5026. The initial pressure was approximately 10^{-6} mm Hg in each test, but increased as heat was applied to the specimen.

Starting Pressure (mm Hg)	Pressure at Temperature (mm Hg)	Temperature (°F)	Time (hrs)	Weight Loss (g/cm ² of surface)
1. 1×10^{-6}	1×10^{-5}	350	3	0.00236
2. 1×10^{-5}	3×10^{-3}	350	3	0.00045
3. 1×10^{-6}	6×10^{-5}	250	3	0.00023

These results indicate a high initial weight loss that decreased in succeeding runs at the same and lower temperatures.

The program of evaluating the stability of candidate materials for the exterior surface of the vehicle is progressing on schedule. Preliminary screening tests are being performed to reduce the number of required final

~~CONFIDENTIAL~~

environmental tests. The gasification of the ablative heat shield in vacuum, or under ascent heating, may cause blistering or peeling of an exterior coating. This possibility is being investigated.

Several lap shear panels were pumiced, electrocleaned, and electroetched in an attempt to obtain preferential pitting. Current, voltage, and time were controlled in order to produce pitting. This work was performed to see if a flask-type pit could be etched in the structure material and if possible, whether it would act as an added mechanical bond for the heat-shield material.

Lap shear panels were heat treated and the surfaces prepared for adhesive bonding of the heat-shield material. All material used in the above tests was 15-7 Mo stainless steel.

Development of analytical methods for trace amounts of elements in the refractory X5026 formulations continues to present many problems.

The Parr bomb method appears to liberate effectively the organically bound chlorine in X5026-29. The resulting solution, however, contains such a large amount of sodium nitrate that analysis for the trace amount of chloride ion becomes difficult. A potentiometric titration of the chloride with silver nitrate gave a very distorted curve. A polarographic determination of the chloride will be tried next.

A standard Kjeldahl determination for the small amount of nitrogen in X5026-22 did not prove sensitive enough. A spectrographic procedure for the determination of trace amounts of nitrogen in X5026 formulations is being investigated.

Additional continuously weighed and torsion-effusion decomposition runs have been completed. Torsion-effusion experiments have been run at various heating rates and on precharred samples. Figure 1 shows the effect of increasing the rate of temperature rise of the furnace on the rate of production of volatiles in the X5026 degradation.

c. Nondestructive Testing

Radiographic testing of approximately 50 X5026 tiles was performed during this reporting period. About 70 percent of these were different process variations of the X5026-22 formulation. Overall quality is about the same as that previously reported. Although stainless-steel equipment is now being used for mixing, metallic inclusions continue to be present in concentrations varying from light to heavy. Corings have been taken for chemical and metallographic examination. When the nature of these inclusions has been identified, studies will be undertaken to determine their source and methods for their elimination. Fiber

~~CONFIDENTIAL~~

CONFIDENTIAL

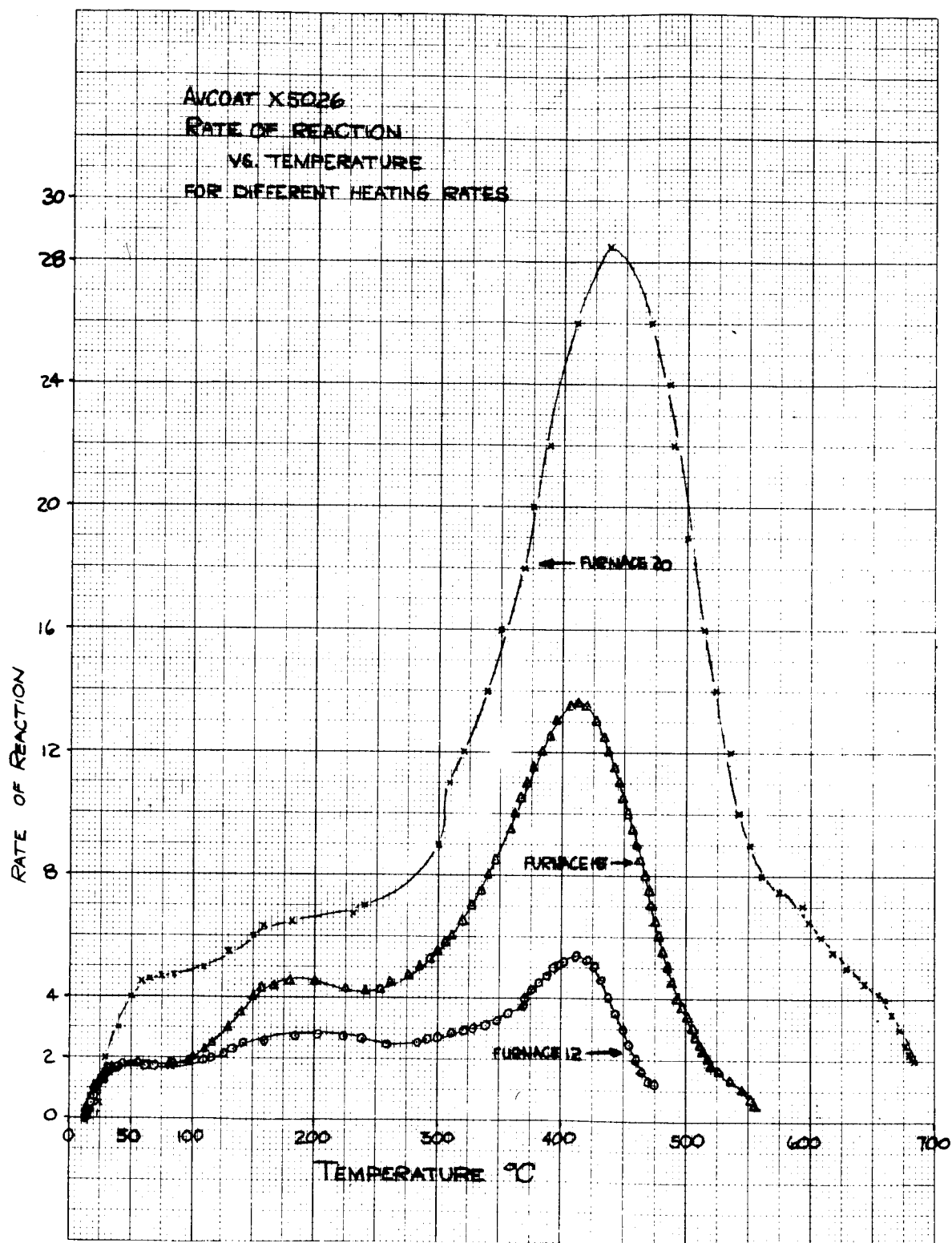


Figure 1 AVCOAT X5026 - RATE OF REACTION VERSUS TEMPERATURE
FOR DIFFERENT HEATING RATES

CONFIDENTIAL

~~CONFIDENTIAL~~

clumping appears to be present in about the same amounts as previously found. The incidence of the microballoon segregation, however, has decreased significantly.

Ultrasonic examination of 45 X5026 tiles was performed during the reporting period. These tiles were from six formulations, chiefly X5026-22. Gross laminar defects, such as those seen in some X5026-22 tiles, were not detected in tiles of other formulations. This may be a statistical phenomenon or may be associated with the elimination of phenolic microballoons. Flaws seen in other formulations by this technique do not cause total loss of back reflection and therefore are tentatively identified as localized areas of nonuniformity. Cores have been submitted for metallographic examination to identify these areas.

Ultrasonic velocity and attenuation studies are continuing. Correlations with density have been held up because of apparent variations through the plate thickness. Cores are now being sectioned into thin wafers for further study.

d. Physical Testing

Engineering curves of tensile properties of X5026-22 have been completed. This study was performed only to delineate curve shapes and has no statistical significance. A single plate of average density, uniform, and free of gross flaws was fabricated into standard 5-inch long tensile specimens. Three tests were performed at each of the temperatures: -100°, 0°, 78°, 150°, 250°, 350° and 600°F. Values obtained at the three previously tested temperatures of -100°, 78° and 350°F agreed sufficiently well with available data to indicate that the panel tested was representative.

A study of the effect of interconnected porosity on moisture expansion of X5026-22 has been performed.

Adhesive bond and mechanical fastener samples are undergoing test.

e. Metallography

Studies during this period have included OVERS test samples, quartz lamp test panels, and NDT flaw and inclusion identifications. Examinations of specimens subjected to heating tests continue to indicate that low heat-flux conditions are critical for the X5026 materials. Such conditions result, in general, in frangible chars with cracking both parallel and perpendicular to the surface. In some instances, cracks in the undergraded material below the char also occur.

~~CONFIDENTIAL~~

~~CONFIDENTIAL~~

f. Chemistry

Bulk density measurements were made on thermal conductivity arc, tensile thermal expansion,* heat capacity, and chemistry specimens taken from X5026-22B, Plate 141, X5026-22, Plate 113 and 141, and X5026-22 made with dried microballoons - a total of 50 samples. In addition, the bulk density, percent porosity, and percent resin of 180 samples of various formulations of X5026 mentioned in the last report were completed.

Volatiles, sinkers, and density measurements were made on five lots of phenolic microballoons (one lot vacuum dried), urea microballoons, and eccospheres.

Vacuum encapsulations were measured for density and percent inorganic content.

Infrared spectra have been obtained on a sample of unfilled X5026-22 and benzene and acetone extracts of X5026-22 in an effort to pin down the cause of cracking.

An ultraviolet absorption spectrum of the vacuum distillate from phenolic microballoons indicated free aromatic material.

A new procedure for the analysis of anhydride and free acids has been completed and written. A method for the analysis of hydrolyzable and free acetic acid is under investigation.

New methods for more rapid analyses of carbon-hydrogen and nitrogen are under investigation in the laboratory.

g. Liaison

Coordination of a program for raw material vender qualifications has been initiated. Materials Department liaison personnel will link together the functions of Plastics, Chemical Analysis, Quality Control, and Purchasing in this effort, and will prepare technical inputs to raw-material specifications.

2. Materials Evaluation

Several new groups of Avcoat X5026 material that have been tested in the Model 500 arc have been analyzed and compared. The silhouette ablation films have been read for a total of seven groups of specimens, but have

*Also percent resin and dry weight.

~~CONFIDENTIAL~~

~~CONFIDENTIAL~~

not been incorporated in the results reported, since the change in the heats of ablation is small. The best estimate of the transpiration factor is also given for each material.

The calibration of the recording pyrometer is presently being completed.

Screening tests were continued in the OVERS arc facility. Samples tested (18) had either formulations similar to X5026 (with variations similar to those reported in the previous progress report) or were based on porous silica substructures with and without various impregnants. Samples of X5026-22 having specific gravity variations of 0.9 to 0.49 showed the sample of lowest density to be almost void of cracks in the char layer but to ablate more readily than the more dense X5026 material. Tests were performed on porous silica materials, with and without impregnants. The samples of this class of materials had high thermal diffusivities based on char depth (except the specimen with no impregnant, which had no char). Surface ablation was negligible for these materials. In addition to the above screening tests, data were reduced for six instrumented X5026 samples (which were reported previously).

The slopes of the temperature histories of plate 16, sample 21, and plate 52, sample 21 have been calculated. The slopes give strong indications of chemical reactions between 800 to 1200°F. Using program 1077 effective thermal diffusivities, α -values were obtained for the same specimens. Most of the α -values were of the same magnitude as previously reported for specimens S and T of Avcoat X5026-22.

The checkout of program 1105, which is used for the calculating thermal conductivity k and specific heat C_p from transient temperature measurements, was continued and additional options have now been checked. As discussed in the previous progress report, the separate determination of thermal conductivity and specific heat requires knowledge of the heat flux somewhere in the body in addition to several internal temperature histories. The correlation between k and C_p is being investigated for the several methods of introducing heat flux information.

A program was begun to study the effect on emissivity (calculated from program 958) of variations from the exact value of specific heat and conductivity. A series of calculations are being made to determine the emissivity from program 958 for several values of C_p and k differing from the exact value by as much as 25 percent. Because of recent difficulties with program 958, these calculations have not been completed.

Temperature data from three tests on the OVERS arc have been made available. Internal temperatures were measured during a period in which the specimen was cooling by radiation. Because of the difficulty with program 958, only one set of results has been completed. Calculated surface

~~CONFIDENTIAL~~

~~CONFIDENTIAL~~

temperatures agree well with the brightness temperatures measured with the optical pyrometer. Agreement was within 3 percent during the period of maximum surface temperature. Difficulties with the measurements of total radiation make it impossible to evaluate the accuracy of the computed surface heat flux. Values of emissivity computed from the data, being greater than unity, are obviously wrong.

An attempt was begun to reduce the oscillations in computed values of emissivity induced by errors in the temperature which drives program 958. The procedure employed was to smooth values of heat flux and surface temperature by fitting a parabola through five successive points. As the apparent period of the oscillations was greater than five time steps, the reduction in the amplitude of the oscillation was small.

During this period primary emphasis was devoted to thermal property measurements of Avcoat X5026, calibration of the degradation apparatus discussed in the last report, and the measurement of degradation of Avcoat X5026.

The reliability of the Apollo vehicle against the meteorite threat has been evaluated for 1- and 14-day missions, assuming the heat-shield material to be Avcoat X5026 and that the particle-penetration energy relationship follows the trends shown for a target impacted at room temperature. The results show that the Apollo capsule having a minimum heat-shield thickness of 0.200 inch will provide the necessary reliability (0.997 for mission success) for a 1-day mission. The calculated reliability for a 14-day mission was 0.973, which is below minimum value.

Most of the planned impact tests of Avcoat X5026 at room temperature have been completed and results indicate that the penetration into Avcoat X5026 is somewhat greater than predicted, which implies that the reliability calculation is at best an optimistic estimation of the system reliability.

Several test firings of glass spheres (mass = 0.1 gram) into targets which were cooled to -100° and -260°F have been completed. Preliminary data indicate that there is some reduction in penetration occurring at -100°F . The target behaved well at these conditions, with little spall and no visible fracture occurring, and the bond (DC 601 RTV silicone rubber) held up well. At -260°F , the target debonded before the test and the target fractured near the edge. Impacts were nevertheless made into these targets and resulting penetration does not differ very much from the room-temperature results.

During the current period the total spectral reflectance of six samples which had been tested for ablation properties was measured. On the assumption that $(1-n)$ can be used for determination of the emittance, the emittance of these various samples has been determined for the purpose of providing the ϵ_{λ} and eventual correction of surface brightness temperature to true temperature during arc tests.

~~CONFIDENTIAL~~

~~CONFIDENTIAL~~

Some caution must be used in applying these results to analytical work since the transmittance has not been measured on these samples. Plans to evaluate the spectral transmittance have been formulated and test specimens are being processed.

The data reduction program (RAD 1275), anticipated in our last report, has not been completed because of unanticipated delays and time consumed in data reduction automation.

Although new apparatus has been designed (to produce radiative fluxes), the final construction and installation of the apparatus has been held up pending approval of special test equipment. Initial efforts to produce a radiative heat-flux source (using surplus carbon arc motion projector lamps) were unsuccessful because of an unreliable long-time (5 minutes) operation. These lamps produced an incident radiative flux of 50 Btu/ft²-sec for short times. Longer operating times caused misalignment of lenses and excessive heating of the projector causing a rapid falloff in the radiative flux to a sample. The schedule originally presented called for four tests of formulation X5026 up to 1 August 1962. Approval of the STE will result in a new test schedule.

Five preliminary tests have been run in simulated trajectory environments. This simulated trajectory consists of an initial convective heat pulse of approximately 350 Btu/ft²-sec at an enthalpy of 19,000 Btu/lb for 2 minutes. The sample is removed and the arc is then adjusted (approximately 2 to 4 minutes) to give a lower heat flux and enthalpy of 40 Btu/ft²-sec and 8000 Btu/lb respectively. The sample is then put back into the jet and tested for approximately 10 minutes. All of the samples tested in this environment have been uninstrumented. Only X5026 formulation-type materials have been investigated. The purpose of these tests was to study the char characteristics which in all cases had horizontal cracks. Future studies will use instrumented samples in order that data be made available for the analytical models. In addition preliminary experiments are being performed to determine if gas enthalpies of 25,000 Btu/lb can be achieved, and if a complete programmed trajectory environment is possible. The application of these preliminary tests to the OVERS depends on the approval of STE.

Pipe test apparatus for the OVERS is currently being fabricated (including calorimeters). It is anticipated that high enthalpies, 3000 to 15,000 Btu/lb, low heat fluxes, less than 30 Btu/ft²-sec, and running times of 10 to 20 minutes can be achieved in the OVERS facility. A laminar-pipe test section for the 10-megawatt arc will be constructed and installed for other low shear pipe tests upon approval of STE.

~~CONFIDENTIAL~~

C. RELIABILITY AND QUALITY ASSURANCE

1. Reliability

The study of nondestructive test techniques under development by NDT specialists was continued. Applicability to reliability evaluation appears promising to date. The Design Review Group is most interested in determining the following probable discrepancies within each heat-shield panel: internal flaws, voids, density variations, moisture content, surface cracks, tensile strength, modulus of elasticity, reparation, specific heat variations, and bond quality.

Work is progressing on the development of a math model to demonstrate the reliability of the Apollo heat shield. The reliability of the heat shield is defined as the probability that the back-face temperature will be less than 600°F. The approach being taken is to express the back-face temperature as a function of those design parameters and environmental conditions that affect this temperature. These functional relationships are being investigated with a view to using them in reliability math models.

An additional technique is being developed in this area. It utilizes a sequential randomized block design, coupled with factorial experiments. It is believed that this will lead to the maximum utilization of test data, consistent with the limitations of environmental test equipment and measuring techniques. The general approach being considered is to subject specimens of heat-shield material to environmental treatments, either singly or in combinations, and to record the back-face temperature. The temperature measurement is to be performed either during or after the environments (preferably during). The data are then analyzed utilizing the analyses of variance techniques.

2. Tasks in Process

- a. IBM 1620 computer programming is continuing in the development of a series of programs to perform regression and correlation analyses. The programs are tailored to analyze materials and physical property data relating to reliability prediction and demonstration.
- b. A complete review of the reliability program and demonstration plans is continuing to determine appropriate data collection, failure-recurrence control, and analysis techniques and methods needed to implement reliability plans and programs.
- c. A definitive investigation of nondestructive radiation measurement versus specific gravity property relationship of various experimental materials is continuing.

~~CONFIDENTIAL~~

d. In association with an experimental testing procedure developed, an investigation of a statistical analytical procedure is in process for the purpose of deriving simultaneous estimates, at defined confidence levels, of specific heat and thermal conductivity properties of Apollo ablative materials.

2. Quality Assurance

Letters outlining quality-assurance requirements have been sent to proposed vendors by Purchasing. Quality Control will begin vendor surveillance as answers are received. Coordination with Quality, Material Engineering, and Purchasing is being maintained.

All honeycomb panels furnished by NAA S&ID and Avco Nashville have been tested as required to the latest quality-assurance technical releases on radiography.

An investigation to determine possible automated ultrasonic inspection techniques for the purpose of cutting costs and manpower has been initiated. From discussions held, practicability and techniques are encouraging, and a report is forthcoming.

D. MANUFACTURING

1. Master Facility Tools

Tool designs of the master facility tools for the forward, crew, and aft compartments have been released to tool manufacturing per schedule.

2. Pilot Ablative Panel-Molding Dies

The following tool designs have been completed and released to tool manufacturing.

- a. 18 by 24-inch flat molding die
- b. 24 by 30-inch flat molding die
- c. Representative molding die in the toroidal area
- d. Representative molding die of a semi-conical configuration.

Tool designs for further pilot ablative panel molding dies are progressing per schedule.

~~CONFIDENTIAL~~

~~CONFIDENTIAL~~

3. Other Tool Designs

Preliminary tool design studies are continuing in the area of assembly tooling with the following studies nearing the formal tool design stage.

- a. Optical controlled fixture bases
- b. Ablative machining attachments on the vertical lathes.

4. Master-Facility Tools

The aft compartment master facility tool is approximately 90 percent complete and has been used for coordination splash tooling for the first toroidal pilot ablative panel molding die. The base structures for the crew compartment and forward-compartment master-facility tools are being fabricated presently. A behind-schedule condition in this area is expected because of late receipt of NAA S&ID coordination tooling.

5. Pilot Ablative Panel-Molding Dies

The following tools have been completed in tool manufacturing and are ready for pilot plant operation.

- a. 18 by 24-inch flat molding die
- b. 24 by 36-inch flat molding die.

The representative toroidal molding die and the semi-conical shaped molding die for pilot operations are progressing in tool manufacturing according to schedule.

E. ADMINISTRATION AND DOCUMENTATION

During this period, the following documentation was completed and submitted to NAA S&ID:

- 1. RAD, Phase I, Biweekly Progress Report, Avco RAD-SR-62-143, Avco Report Series 201 (14 July 1962).
- 2. RAD, Monthly Weight and Balance Report, Avco RAD-SR-62-158, Avco Report Series 203 (30 July 1962).
- 3. RAD, Monthly Financial Management Report, Avco Report Series 501, Monthly Financial Management TWX Report, Avco Report Series 502
- 4. PERT Variance Report, Avco Report Series 503

~~CONFIDENTIAL~~

~~CONFIDENTIAL~~

5. RAD, Quarterly Reliability Status Report, Avco RAD-SR-62-145, Avco Report Series 205 (15 July 1962).
6. Cost Proposal for Apollo Program for NAA S&ID (13 July 1962).
7. RAD, Negative Report on Apollo Heat Shield Drawing List, Avco Report Series 202 (14 to 31 July 1962).
8. Amendment No. 1 to Revised Formal Application for Facilities in Support of Contract M2H43X-406012 (10 July 1962).
9. Submittal of Motion Picture Documentation, Avco Report Series 602,
 - a. Preparation of Materials Sample for High-Temperature Tests (10 July 1962)
 - b. Turbulent Pipe Tests of Heat-Shield Materials (26 July 1962).
10. Submittal of Still-Photo Documentation, Avco Report Series 601, Fabrication of Heat Shield Test Materials

At the present time, the PERT network is being evaluated and revisions are anticipated in several areas:

The logic of research and development activities will be revised as a result of more complete and specific definitions of R&D scope and activities. Further revisions will incorporate the interface definitions and schedules of the recent negotiations at NAA S&ID. As requested by NAA S&ID, the present network will be extended in the next report. The submittal will include all end items contracted for in lieu of the initial item delivery.

~~CONFIDENTIAL~~

II. PROBLEMS AND ACTIONS

The problems presented in this section threaten to impair the scheduled program implementation. The decisions, inputs, or other actions required to solve each problem are also presented. This section does not attempt to identify all areas requiring further definition, clarification, and/or coordination, but rather those areas requiring immediate action.

A. DESIGN

1. Heat Transfer

No action has been taken on the resolution of the difference in heating between NAA and Avco. NAA still has not defined the design-abort condition with escape rocket firing.

A discrepancy exists between the NAA radiative-heating and Avco radiative-heating calculations for trajectory 1. The NAA calculations are approximately 3 times higher than the Avco calculations. This discrepancy should be resolved as soon as possible.

Knowledge of the heat-shield composition is still not available but has been requested. The simplified injection analysis was completed on paper and examined to determine what problems exist. It is evident that it will be more sensible to wait for a full equilibrium program, rather than attempt a simplified analysis. Both approaches require additional programming. The full equilibrium program should be ready in about 3 months. The simplified approach would take 1 to 2 months, and even then it would be questionable.

2. Thermodynamic Analysis

Still outstanding are the data requested in the previous four bi-weekly progress reports. This list includes the following:

- a. Complete definition of all ascent and abort trajectories
- b. Definition of insulation, substructure, and pressure vessel geometry and thermophysical properties
- c. Definition of the drogue and main parachute deployment sequence to include descent velocities (total time) from 100,000-foot altitude to impact

~~CONFIDENTIAL~~

d. Definition of all doors, windows, and other thermal discontinuities over the entire command module

e. Definition of the blunt-face thermal environment to which the service module is attached.

3. Structural Studies

The following problems and actions in the structural study phase of the program were noted during this period:

Problem: No concrete correlation of time of abort and tumbling abort is available except the above **stated condition**.

Action: Load and time information was requested during the last reporting period.

Problem: Testing is prevented because of lack of facilities and special test equipment. Quartz lamp tests cannot be run without furnaces.

Action: Pending approval from NAA S&ID.

Problem: Definition of test completion dates cannot be made for bond-evaluation tests since remaining bonds selected for testing have not been received at Avco RAD.

Action: Testing will proceed on an availability basis.

Problem: Vibration tests cannot be performed until certain environments are better defined.

Action: Request made for information (TR-S220-T-29) and awaiting reply from NAA S&ID.

A vibration exciter has become available for a 3-day period in each of the first 2 weeks in August. A vibration survey will be performed to determine resonance modes and compare these results with the data obtained when vibrating the bare panel.

4. Engineering Design

Detail design information on all parts of the structure-heat-shield interface is urgently needed. The Design Section is using the limited information and drawings received from S&ID on 6 June. Informal information received from S&ID would indicate that numerous design changes are contemplated. Close coordination must be arranged and maintained with S&ID in order for the Design Section to meet scheduled commitments.

Information regarding procedure and format for an interface control drawing between the NAA structure and the Avco heat shield should be obtained from S&ID to give Avco time to effectively implement it.

~~CONFIDENTIAL~~

~~CONFIDENTIAL~~

MATERIALS DEVELOPMENT AND EVALUATION

1. Materials Development

The cracking of panels during postcure has now been associated with mixing on humid days. All panels made on a particular humid day (over 70 percent relative humidity) cracked during postcure. Although this one instance is not conclusive, the role of humidity is being checked to see if humidity control in the processing area is necessary.

Photomicrographs of OVERS specimens exposed to various heating conditions are now being studied to learn more about the cracking taking place in and below the char layer.

Infrared analyses of benzene and acetone extractions of postcured X5026-22 material reveals the presence of degradation products of "Harcure A." This could indicate an excess of "Harcure A" (polysebacic anhydride) in the formulation, which would correlate with weight-loss measurements. It is planned to run weight-loss studies at various ratios of anhydride to epoxy on the pure resin systems to determine the optimum quantities of anhydrides to be used.

To further check the proper proportion of the resin system, the Analytical Laboratory is to follow a typical cure cycle of the unfilled resin system on the hot stage of the infrared. It is hoped that this will show the degree of homopolymerization taking place (formation of ether group) and the degree of cross-linking with the anhydride (formations of ester groups).

An adhesive that is considered completely satisfactory has not yet been realized. Work on this problem is continuing and the additional panels prepared for NAA S&ID will reflect the adhesive appearing best at the time the assembly is made.

Design personnel have indicated that the -260°F requirement is a critical point in the structural analysis. However, no equipment is available for performing quantitative tests at this temperature. As a stop-gap measure, a testing vendor has been found who has equipment to test at very low temperatures and his facilities and competence are now under review. Use of this vendor, if qualified, will both reduce the program flexibility and increase the cost.

Considerable time has been expended in the physical test area attempting to develop techniques for performing tests in liquid nitrogen. Indications to date are that such techniques are difficult, cumbersome, and not too reliable.

~~CONFIDENTIAL~~

2. Materials Evaluation

The value of total emittance that was used to make the hot-wall correction may be in error. If it is found to be in error, the correct emittance value will be used to make the correction, and the thermochemical heats of ablation will be recalculated.

STE is required to conduct laminar shear pipe tests in the 10-megawatt facility.

The OVERS arc was down for 4 days because of unexpected trouble with the vacuum system. More careful maintenance of the vacuum system has been initiated.

The velocities that have been attainable at Avco with glass projectiles have been limited to less than 18,000 ft/sec. To obtain data at higher velocities, Armour Research Foundation of Chicago has been subcontracted to perform six impact tests into Avcoat X5026 targets at room temperature, using as projectiles 1/16-inch and 1/8-inch diameter glass spheres. These spheres will be launched at velocities greater than 20,000 ft/sec up to 22,000 ft/sec, which is their present capability. Since this contract has been let, Avco's program of projecting glass spheres has progressed so that 3/16-inch diameter spheres can now be projected at velocities up to 22,000 ft/sec.

STE is required to go to higher radiant fluxes and longer times.

Approval of STE is required to go to higher enthalpies and programmed trajectories.

C. RELIABILITY AND QUALITY ASSURANCE

1. Reliability

The problems presented in constructing the reliability math model include:

Definition of the important variables that influence the backface temperature. Development of the partial derivations that will be needed in the reliability model

Effects of certain mathematical approximations used in developing the reliability math model

Estimation of the sample sizes needed for each of the parameters has not been completely solved, although preliminary work has resulted in a temporary solution

~~CONFIDENTIAL~~

Errors introduced in making the assumption that the parameters are normally distributed random variables.

The ANOVA technique problems that are being investigated include:

If the ANOVA results in significant main effects and interactions, what are the elements of total variability that enter into the reliability calculations?

Since both the sequential randomized block design and the factorial yield ANOVA results, how is this information combined so as to give one overall reliability answer?

What is the power of these experimental designs to detect significant treatment effects, and also be capable of demonstrating the required reliability without the requirement for an excessive sample size?

D. MANUFACTURING

Because of late receipt of coordination tooling for the crew and forward compartments from NAA S&ID, a schedule delay is anticipated. To bring the program to an on-schedule condition, overtime will be required.

To start in the formal tool design stages for assembly tooling, final definition of joining ring configuration and final stabilization of interface planes between compartments is needed from NAA S&ID.

E. ADMINISTRATION AND DOCUMENTATION

The interface definitions and schedules resulting from the recent negotiations contained some differences with respect to schedule dates. It will be necessary to resolve these differences before integrating this information into the PERT network logic. It is proposed that the resulting new network logic be amended as these differences are resolved, and when complete, that time estimates be made.

~~CONFIDENTIAL~~

~~CONFIDENTIAL~~

III. FORECASTS

This section presents a forecast of the significant events anticipated during the next monthly reporting period.

A. DESIGN

1. Heat Transfer

During the next period the problem of heating in the separated region will be resolved.

The studies on the nonaxisymmetric stagnation-point heating and the use of nonsimilar solutions of the laminar boundary layer for the spherical face heating will continue during the next reporting period.

Work will also continue on the determination of the heating distributions as well as analysis of the nonequilibrium effects on the radiative heat transfer.

Subsequent reporting periods will be devoted to work on a full equilibrium program. The transport properties studies will continue at the same time.

2. Thermodynamic Analysis

During the next reporting period, time histories of the expected mass loss caused by internal decomposition of Avcoat X5026 will be completed. In addition, the heat-shield thickness requirements for trajectory 4 will be studied again using the charring ablation (digital) program.

Charring during the boost phase of the trajectory will be investigated. This study will be coupled with an analysis of the spectral property requirements for space-flight temperature control of the command module forebody.

Efforts will be directed toward integrating safety factor concepts in the re-entry and free-flight heat-shield thermal requirements.

The potential function of $N_2 + B^2 \Sigma_u^+$ will be constructed and wave functions and overlap integrals will be computed for transitions in other molecules. Progress will be made in writing the digital program for calculating radiant heating.

3. Structural Studies

Attempts will be made to calculate combined stresses using assumed load-time histories.

~~CONFIDENTIAL~~

~~CONFIDENTIAL~~

Preliminary checks will be made of the bond-stress concentration analysis.

Current work includes a study of the ablator tile attachment to the blunt end. Also a more thorough examination of the effect of the internal pressure-abort condition on the structure is being made.

The ablator panel buckling and gap study will be completed.

The bonded ablator-to-substructure ascent and re-entry stress histories will be reduced to graphs.

Investigations will be made for the stresses in two infinite viscoelastic layers of finite thickness and the applicability of the solution to the design concept.

The loads study and analysis, with emphasis on abort and tumbling abort, is continuing.

Data will be reduced to provide measured temperature gradients and tube stresses versus time.

No thermal-gradient tests are expected to be completed. Upon approval, the quartz lamp furnaces will be constructed. Tests should start approximately 2 to 3 weeks after receipt of approval.

4. Engineering Design

Comments on RAD-E70001 are being coordinated and a meeting of cognizant parties will be requested to define the specifications in the near future. Materials Engineering will begin to submit inputs for raw material specifications.

Detailed layout studies based on existing information will continue. As new information is received, it will be incorporated into the layouts to show the latest design.

Heat-shield fairing optimization studies will also continue to be investigated.

Fastener conceptual studies, tile arrangement, and detail door layout studies will continue.

B. MATERIALS DEVELOPMENT AND EVALUATION

1. Materials Development

Work on development of new formulations will continue.

~~CONFIDENTIAL~~

~~CONFIDENTIAL~~

A vacuum post cure will be evaluated.

Weight loss studies on the unfilled resin systems at various ratios of anhydride to epoxy will be initiated.

Pregelled epoxy systems using liquid and solid epoxy resins will be made up with various degrees of pregelling to obtain a system with optimum molding properties.

Further modification of DC 731 RTV and other silicone elastomers will be made to obtain optimum properties. This material will be compounded into a two-component and internal-curing type.

Silicone rubber in sheet stock, vulcanized and unvulcanized, will be tested as adhesive material in a multicomponent shield-substructure specimen.

Modification of epoxies will continue with the objective of improving strength and flexibility and lowering cure temperatures.

The structural panel will be shipped 31 July 1962 and the dynamic panel 4 August 1962.

2. Materials Evaluation

Several groups of Avcoat X5026 will be tested in the high enthalpy arc. The brightness surface temperatures will be measured with the recording pyrometer to obtain the best possible ablation temperature.

OVERS screening test samples (approximately 30) have been prepared. In addition, 18 instrumented test samples of X5026 have been prepared for test evaluation in the OVERS arc.

The program to evaluate the effect on calculated emissivities caused by deviations from the correct values of C_p and k will be continued.

Emissivity will be computed from the results of additional tests on the OVERS arc. Except for comparing measured and calculated surface temperatures and internal temperatures, it is doubtful that little more can be learned from the calculations of the existing data. Several calculations have been submitted to the computer in an attempt to reduce the oscillation in output from the 958 program during the first part of the cooling period. An attempt will be made to explain why values of emissivities calculated from the tests were in error.

A further effort will be made to smooth out oscillations in the emissivities calculated by program 958 by smoothing values of emissivity directly. A linear relation will be employed fitting the curve by means of a least-square technique through 10 points.

~~CONFIDENTIAL~~

~~CONFIDENTIAL~~

A simple computer program will be written so that values of emissivity and rms error can be computed by machine directly from the output of program 958. At present this is done by hand calculation.

More values of effective thermal diffusivities will be computed for the specimens examined. Values for the slopes of the temperature histories, the temperature-distribution history, and effective thermal diffusivity will be reported for plate 9, sample 20. Effective specific heats and thermal conductivities as functions of temperature will be calculated employing program 958 and 1166C and program 1105.

The forecast for the coming period is continued testing of Avcoat X5026 formulations.

The scheduled series of tests outlined in the last progress report should be completed within the next reporting period. The re-entry heating calculations should also be completed.

During the next period, the transmittance of arc-exposed samples will be determined. Two sets of Avcoat X5026 and Avcoat X5019 have been scheduled for complete measurement and data reduction by program 1275.

A small amount of work will be undertaken during the coming period to establish a standard of measure (quartz, optical, and diffuse) for the purpose of apparatus standardization and monitoring for normal aging of apparatus components.

C. RELIABILITY AND QUALITY ASSURANCE

1. Reliability

A supporting investigation of a possible association between nondestructive test data vs material property data is continuing.

A supporting investigation of randomization techniques for material sample selection in determining final property estimates of Apollo heat-shield material is also continuing.

Support of the design program for optimum bonding and/or fastener agents for the Apollo heat shield is still underway.

2. Quality Assurance

The vendor-capability survey of suppliers of raw materials to be used on the Apollo heat shield is scheduled to start about 1 August 1962.

~~CONFIDENTIAL~~

D. MANUFACTURING

1. Tool Engineering and Tool Design

Tool design on the pilot ablative molding dies will continue as per schedule.

Assembly tool design, both in the study and formal stages, will continue, although in a behind-schedule condition, until final engineering design information on joining rings and interface-station planes is received from NAA S&ID.

2. Tool Manufacturing

During the next period, the following items of tooling will start, or continue, per schedule.

- a. Pilot ablative panel molding dies
- b. Tooling patterns for the assembly tool-proving program.

The following items will be started in the next period, on a behind-schedule basis, and overtime will be necessary to return to an on-schedule condition.

- a. Master facility tool--crew compartment.
- b. Master facility tool--forward compartment.

3. Status of NAA S&ID-Supplied Coordination Tooling

Coordination tooling for the aft compartment has been received in Tool Manufacturing in good order and has been utilized in the construction of the male master facility tool for Avco use. The coordination tooling for the forward compartment and crew compartment has not yet been received from NAA S&ID. Promise dates for the receipt of these items of tooling from NAA S&ID indicate a schedule slippage. To return to an on-schedule condition after this late receipt, overtime will be necessary.

4. Facilities

Availability of production equipment is being studied and proper paper work is being formulated to expedite purchase when the facilities funding is made available.

~~CONFIDENTIAL~~

E. ADMINISTRATION AND DOCUMENTATION

The forecast documentation to be submitted to NAA S&ID during the coming month falls into general categories of progress submittals and revised documentation in accordance with recent negotiations. The progress reports are as follows:

1. PERT variance reports
2. Monthly financial management reports
3. Subcontractor report
4. Monthly progress report
5. Weight and balance report
6. Clarification has been requested regarding the qualification status list.
7. Continued still- and motion-picture coverage.

~~CONFIDENTIAL~~

~~CONFIDENTIAL~~

IV. ANALYSIS

A. DESIGN

1. Heat Transfer

A report covering the preliminary aerodynamic heating analyses has been completed.¹ This report covers all of the analytical work done on the Apollo program up to this date and includes a description of the various techniques that have been used in the analysis. These methods have also been generally justified in this report by comparison with available experimental data.

A comparison of the latest heating calculations on trajectory 1 indicates that the agreement between the analytical estimates of NAA and Avco is much better than the earlier NAA results. However, the agreement of both estimates with Avco shock tube data in the stagnation region is poor.

Comparisons between experimental and theoretical heating distributions are shown in figure 2. The data on this figure represent Avco theoretical heating, revised NAA theoretical heating, and Avco shock tube heating.

Variations in the recovery enthalpy over the body have been incorporated into the test data corrections utilizing perfect gas relationships.

An exploratory study of the necessity and/or feasibility of using the nonsimilar solution of the laminar boundary layer equations² (as opposed to a similarity solution) for the determination of the convective heat rates along streamlines on the spherical face has been initiated.

A numerical comparison of similar and nonsimilar results for various streamwise pressure gradients will be made. No results are available yet.

The heating of an axisymmetric stagnation point has been well defined through the following relation

$$q_s = C_1 \left(\frac{dU}{ds} \right)^{1/2}$$

An axisymmetric stagnation point is characterized by equal velocity gradients in all directions about the stagnation point. However, a three-dimensional stagnation point may have unequal velocity gradients in all directions. Since only one value of heating exists at a three-dimensional stagnation point, it appears that the above equation is also applicable to a three-dimensional stagnation point, providing a proper value of the velocity gradient can be found. A mean velocity gradient will be computed in a manner so as to account for the variation in the velocity gradient about a three-dimensional stagnation

¹Gustafson, R., N. Thyson, Preliminary Aerodynamic Heating Analysis for the Apollo Command Module, Avco RAD-TM-62-65 (31 July 1962). Confidential

²Pallone, A., Non-similar Solutions of the Compressible Laminar Boundary Layer Equations with Applications to the Upstream Transpiration Cooling Problem, J. Aerospace Sci., 28, No. 6 (June 1961), pp. 449-456.

~~CONFIDENTIAL~~

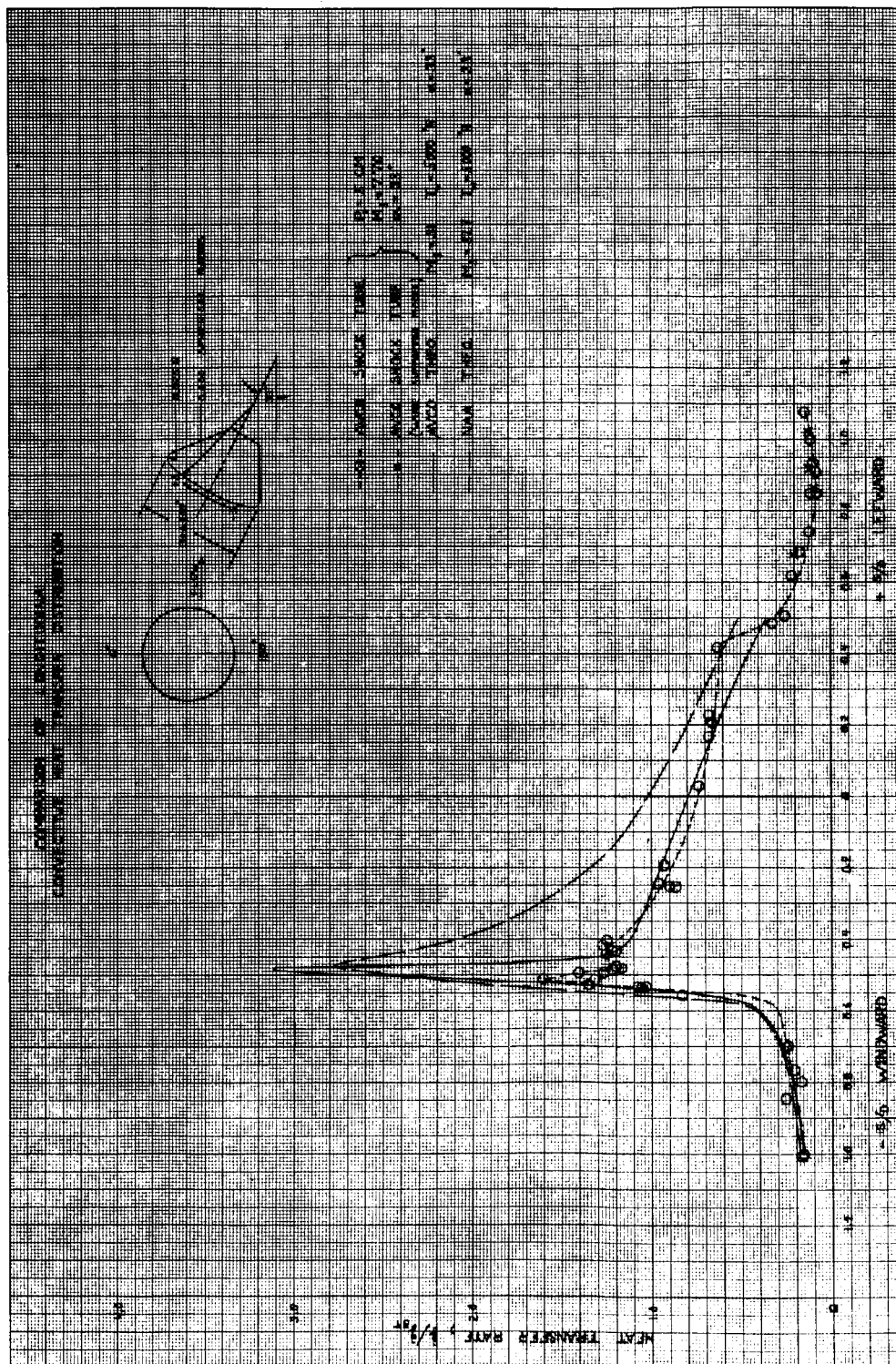


Figure 2 COMPARISON OF LONGITUDINAL CONVECTIVE
HEAT TRANSFER DISTRIBUTION

point. It will be assumed that the velocity gradient in any direction may be expressed in terms of an equivalent sphere in that direction through the usual velocity gradient expression

$$\left(\frac{dU}{dS}\right)_{\phi} = C_2 \left(\frac{1}{R_{\text{sphere}}}\right)_{\phi}$$

The equivalent sphere in any direction about the stagnation point is given by

$$(R_{\text{sphere}})_{\phi} = \frac{(S_{\text{sonic pt.}})_{\phi}}{45^{\circ}}$$

A mean velocity gradient is then computed as follows

$$\frac{\overline{dU}}{dS} = \frac{\int_0^{360^{\circ}} \left(\frac{dU}{dS}\right)_{\phi} d\phi}{360^{\circ}}$$

This mean value for the velocity gradient is then used in the axisymmetric heating equation.

It should be noted that the above method is dependent upon knowing the following:

- a. Location of stagnation point on the body
- b. Location of sonic line on the body.

However, it appears that a modified Newtonian analysis can be used to give the stagnation point location and sonic line location on a body.

With the mean velocity gradient, $\frac{\overline{dU}}{dS}$ defined for a three-dimensional stagnation point, a mean sphere radius can be defined as follows:

$$\overline{R}_{\text{sphere}} = C_2 / \frac{\overline{dU}}{dS}$$

By using this equivalent sphere radius, a shock standoff distance can be computed at the stagnation point.

Preliminary heating and shock standoff-distance calculations at the stagnation point appear to give satisfactory results for very limited experimental results on the Apollo shape. The validity of using the above method is currently being investigated so as to put it on a more theoretical basis. In addition to this theoretical investigation, more experimental data are also being obtained.

~~CONFIDENTIAL~~

Comparisons between the NAA radiative heating calculations and the Avco radiative heating calculations are presented in figures 3 to 7. The Avco radiative heating calculations have been based on conservative methods as noted in previous progress reports. Therefore, the large discrepancy between NAA and Avco calculations is not explainable at the present time.

The determination of species radiation from the boundary-layer gases is dependent upon the chemical composition. The important radiating bonds for air have been established, and clean air boundary-layer calculations are now routine. With ablated species present, the calculations are not routine since many more species are present and the actual composition is not known.

A full thermochemical-equilibrium boundary-layer analysis with multicomponent injection is currently being studied and programmed for digital computation. This program will couple the boundary-layer solution with a thermochemical solution. The results will include the composition and temperature profiles for the laminar boundary layer.

In typical boundary-layers with foreign gas injection many species are present. For the Teflon cases previously studied, there was a total of 37. Clearly the computations needed to include all species would be prohibitive. To overcome this problem, only five injected species and five air species will be considered at one time. The five injected species will be selected on the basis of partial pressures. With the 10 species considered the sum of the partial pressures will exceed a given percentage of the total pressure (for example, 95 percent).

The 10 species considered will all be in chemical equilibrium throughout the boundary layer. For purposes of radiation studies, the 10 species present may not be important. This will be overcome by considering the computed properties at several points in the boundary layer as input for pure thermochemical calculations using all species. A profile of the important radiative species can be constructed by this technique.

The experimentally determined heat-transfer rate distributions about the body at a 33-degree angle of attack along the windward-leeward plane and the plane perpendicular to it are shown in figures 2 and 8 respectively. The data obtained along the lee portion of the body using the wire-models are included in figure 2. The trends and results previously reported are supported by the new data.

The blunt face data obtained at enthalpy levels of H/RT_0 of 240 to 510 at shock tube initial pressures of 0.025 and 0.005 cm Hg are shown in figures 9 and 10 respectively, where the ratio of the measured heat transfer rate at a 33-degree angle of attack to the zero-degree stagnation value is plotted as a function of nondimensional body distance. Included in the figures is the curve faired

~~CONFIDENTIAL~~



Figure 3 RADIATIVE HEAT TRANSFER, TRAJECTORY 1, POINT 1

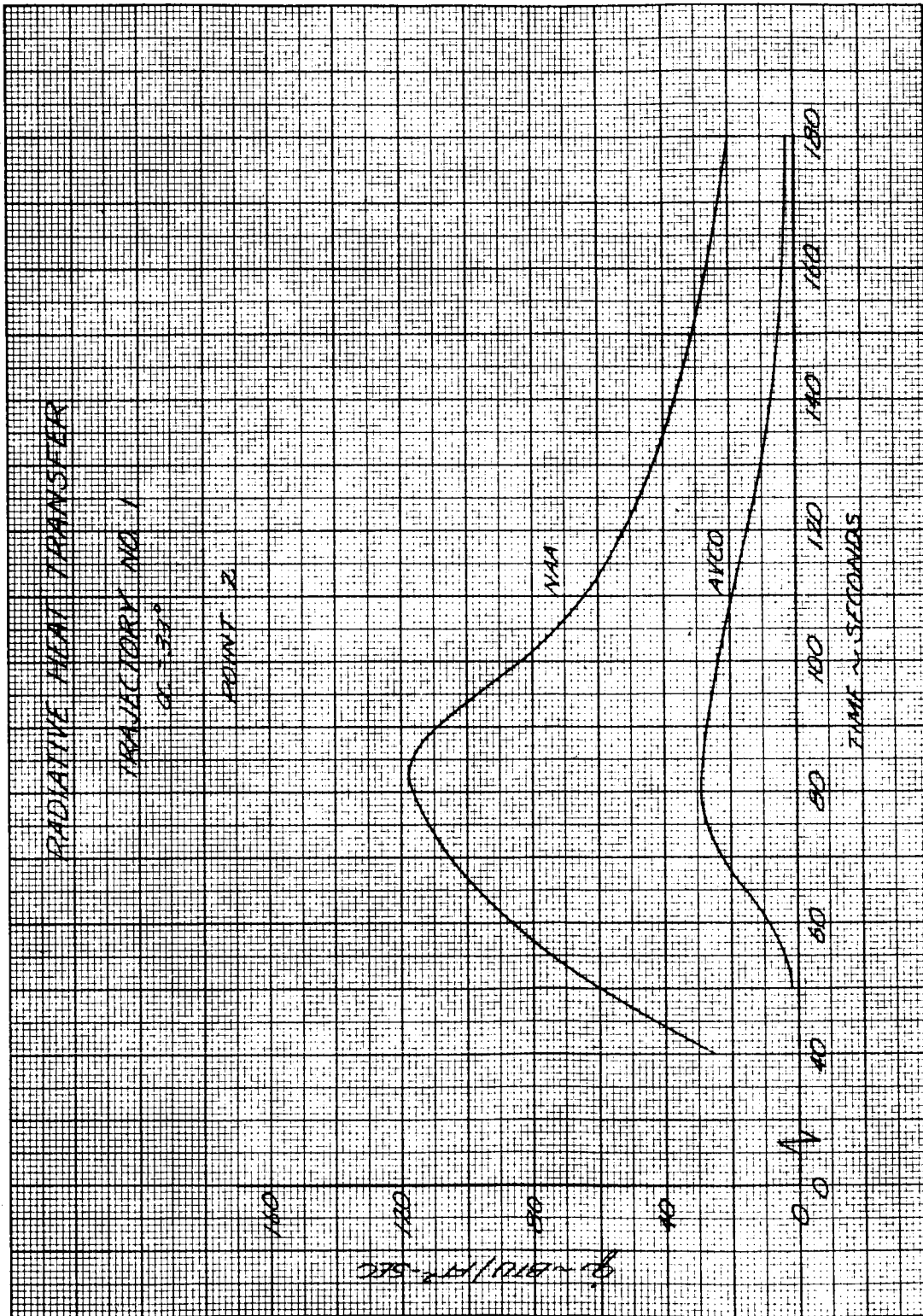


Figure 4 RADIATIVE HEAT TRANSFER, TRAJECTORY 1, POINT 2

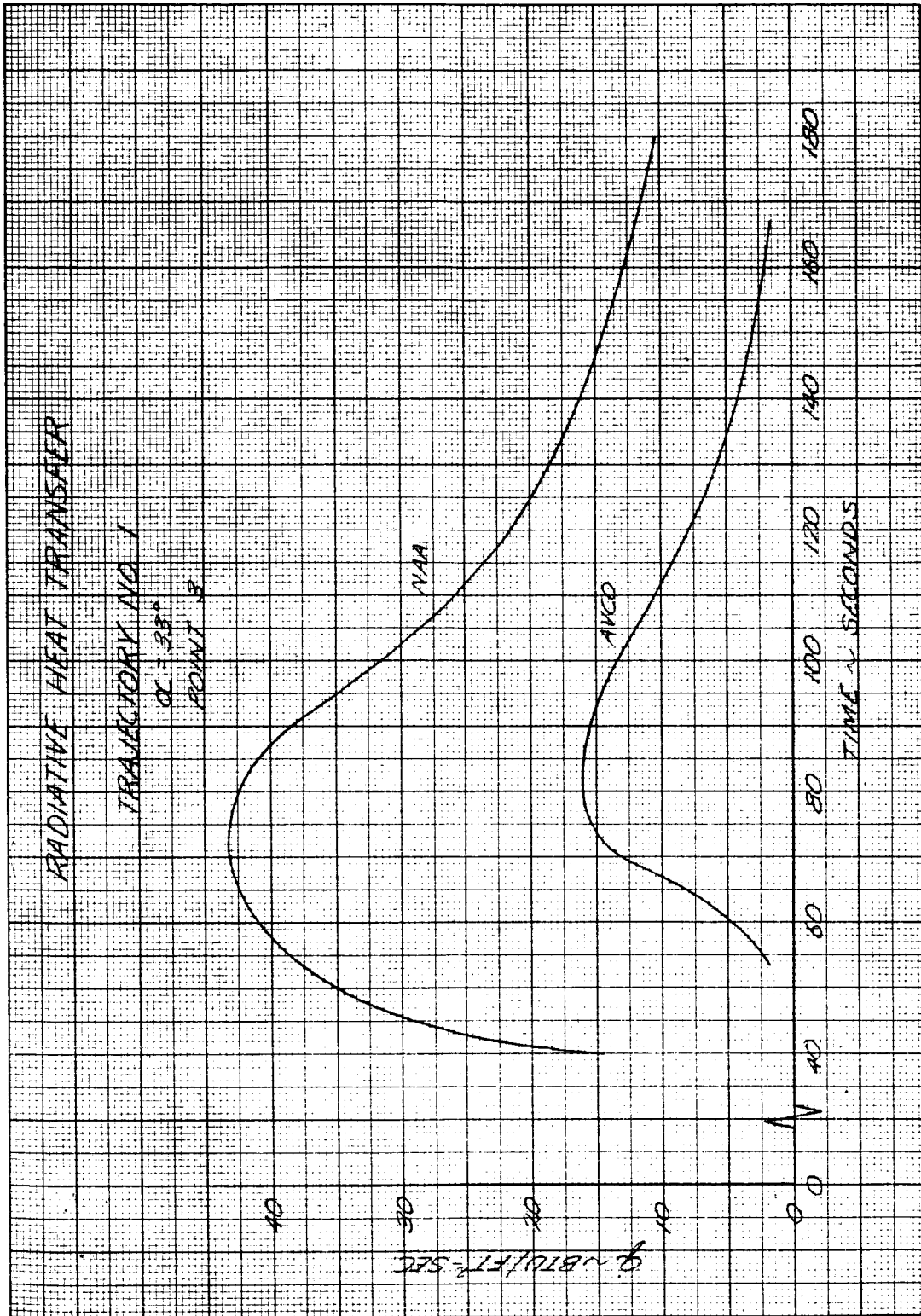


Figure 5 RADIATIVE HEAT TRANSFER, TRAJECTORY 1, POINT 3

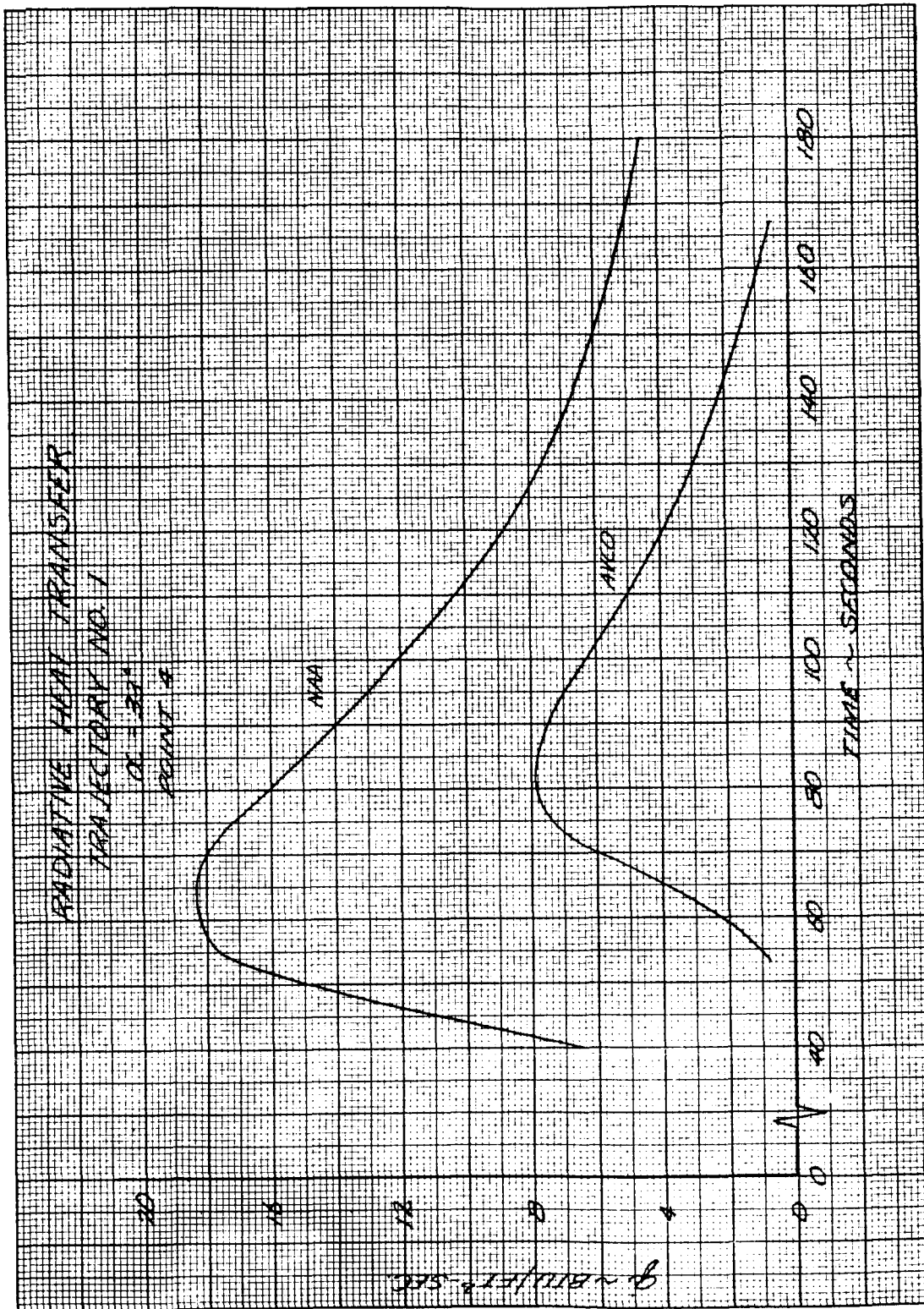


Figure 6 RADIATIVE HEAT TRANSFER, TRAJECTORY 1, POINT 4

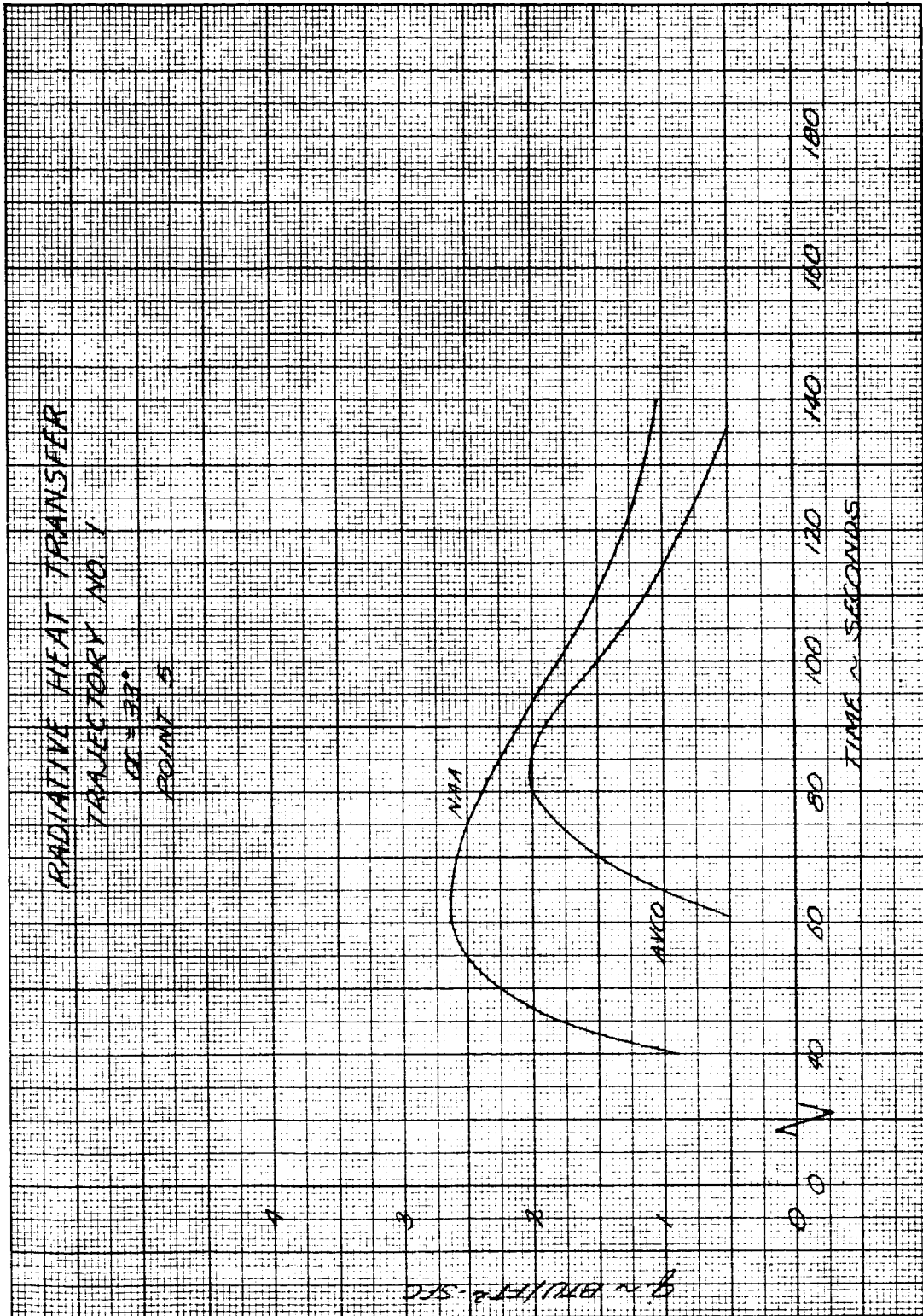


Figure 7 RADIATIVE HEAT TRANSFER, TRAJECTORY 1, POINT 5

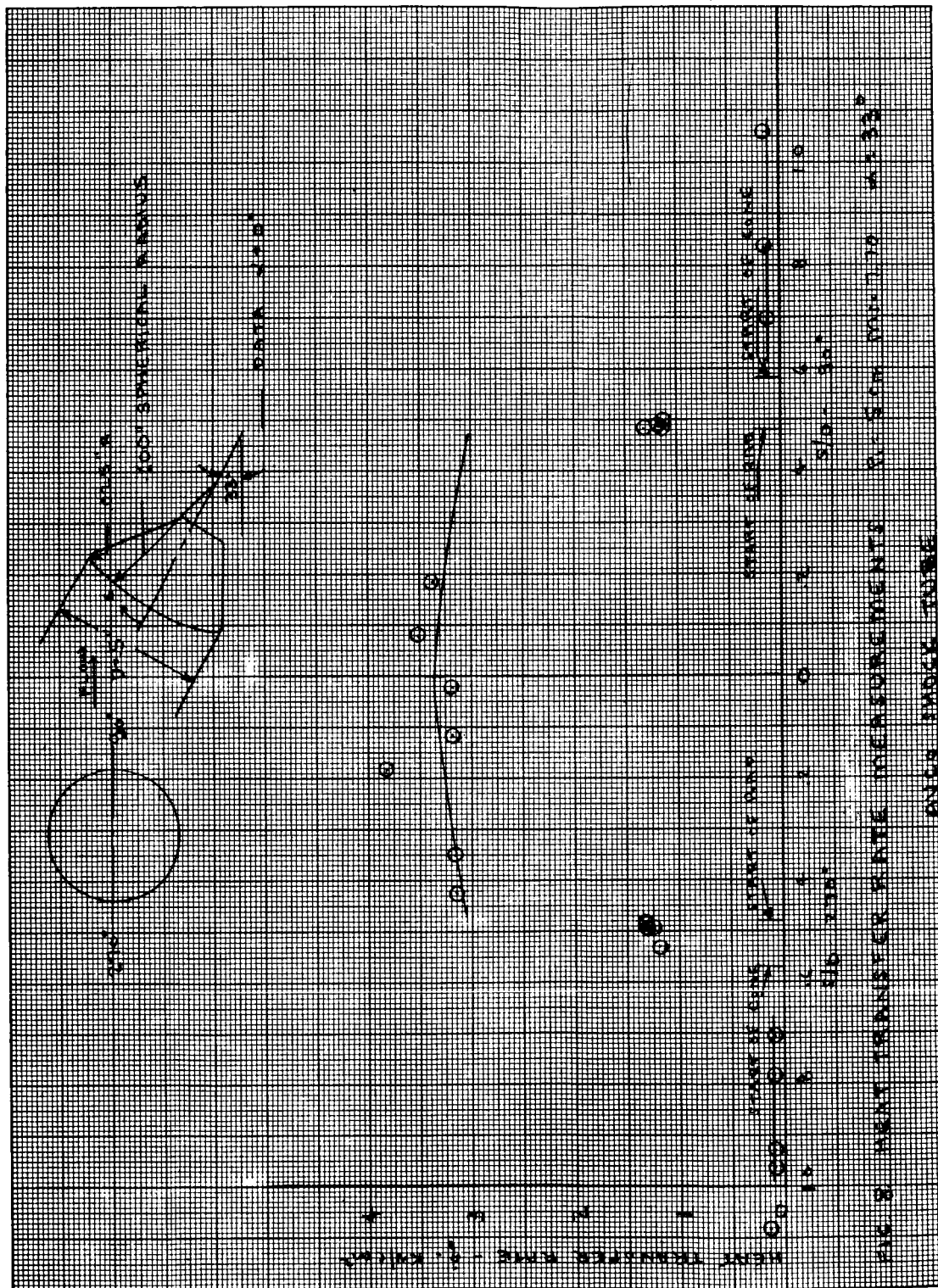


Figure 8 HEAT-TRANSFER RATE MEASUREMENTS

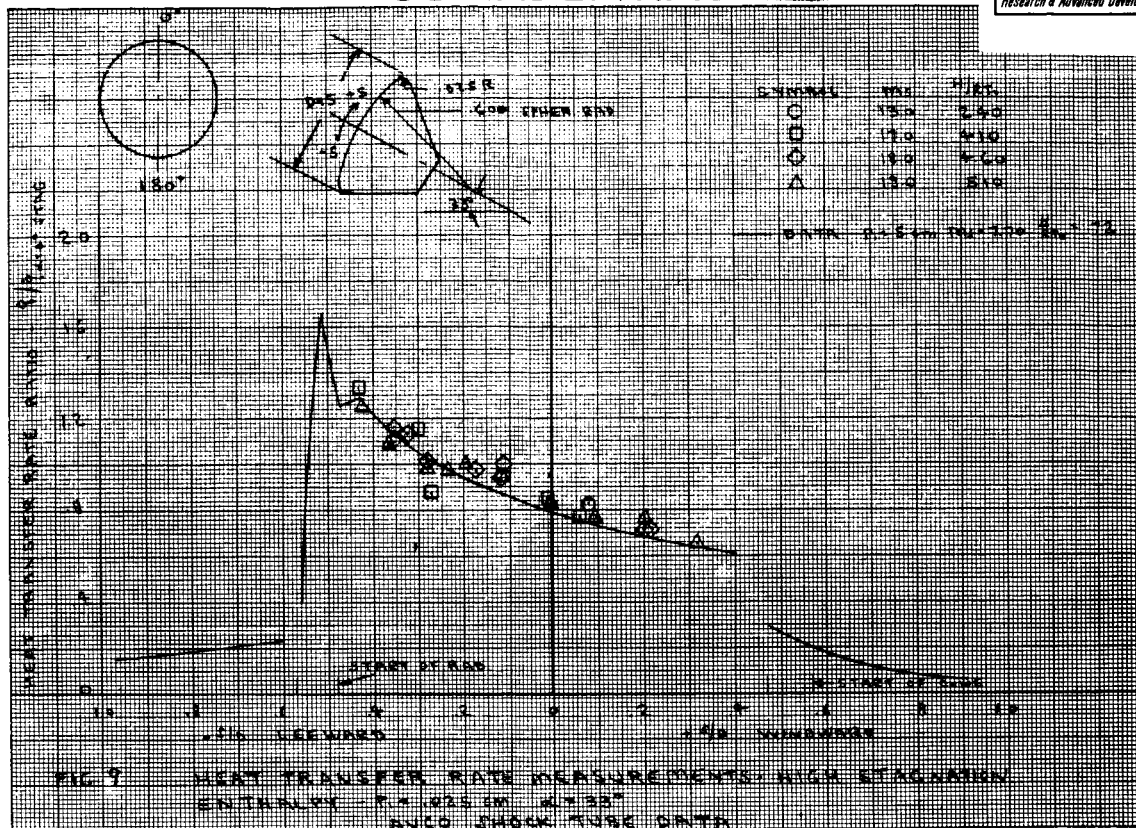


Figure 9 HEAT-TRANSFER RATE MEASUREMENTS - HIGH-STAGNATION
ENTHALPY ($p_1 = 0.025$ cm, $\alpha = 33^\circ$)

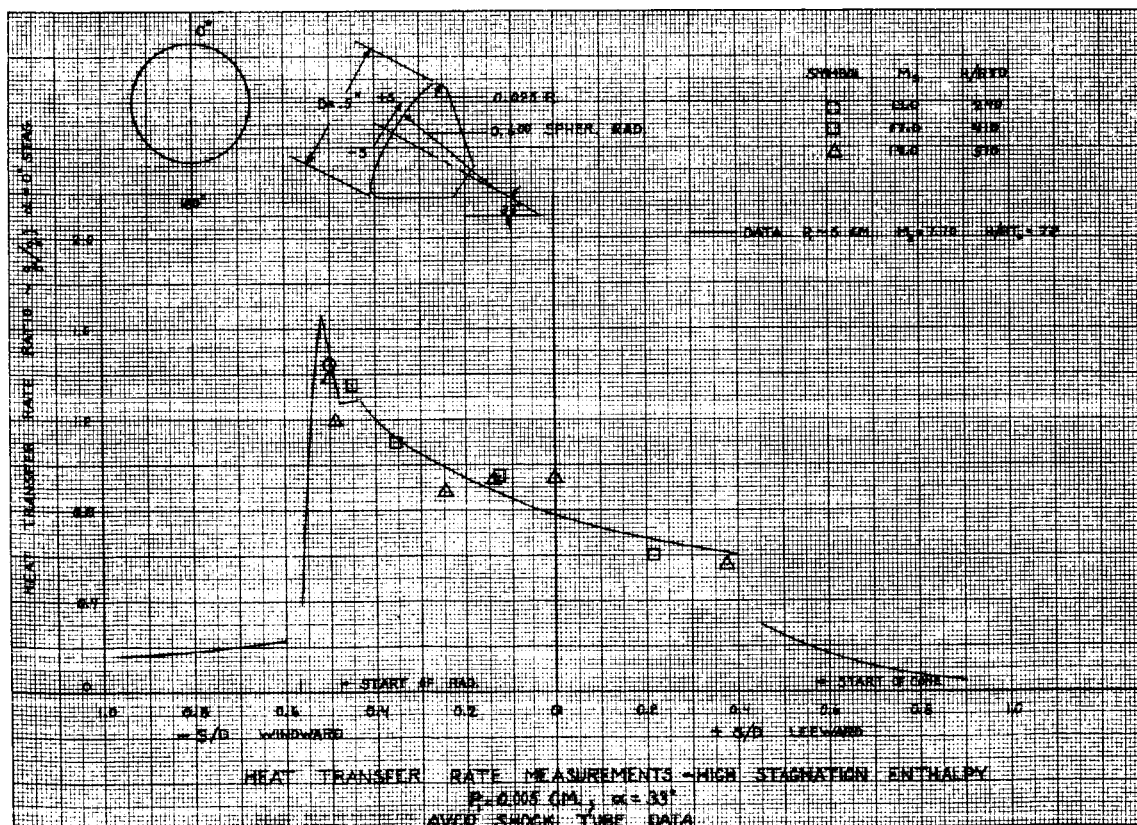


Figure 10 HEAT-TRANSFER RATE MEASUREMENTS - HIGH-STAGNATION
ENTHALPY ($p_1 = 0.005$ cm, $\alpha = 33^\circ$)

~~CONFIDENTIAL~~

through the $H/RT_0 = 72$ data. As can be seen, the high enthalpy data yield results which are essentially the same as the low enthalpy data.

2. Thermodynamic Analysis

The thermodynamic space environment program (program 1258) is operational and available for design analysis. This program makes it possible to evaluate the transient temperature history of a vehicle in space flight. The program is versatile and can handle a wide variety of inner and outer boundary conditions. For example, the outer surface of the vehicle may be subjected to the following heat sources: (a) the sun, (b) sunlight reflected from the earth, (c) long-wave radiation from the earth, and (d) free-molecular flow. The interior surface may be considered either adiabatic or subjected to a radiative and/or convective heat source. These heat sources which constitute the thermal environment during space flight are assumed to determine the temperatures in a one-dimensional plane normal to the vehicle surface. The effect on temperature caused by heat flowing parallel to the surface is neglected.

The external radiative heat sources are considered to be a function of the vehicle altitude, orbital position, and inclination of the orbit with respect to the earth-sun line. The shape of the vehicle may be either a cylindrical or conical body, with freedom of rotation about its longitudinal axis. It is assumed that the orbit is circular and the longitudinal axis of the vehicle remains parallel to the surface of the earth.

The numerical solution for the transient temperatures of the heat shield is based upon the weighted average of an implicit and explicit system of difference equations (Ref. 3). The solution applies to a composite solid, limited to six materials with constant thermal properties. The convective and radiative boundary conditions at the interior surface are considered to be both time and temperature-dependent.

The analysis of charring Avcoat X5026 has been completed for trajectory 1. This analysis, in contrast to the "thickness loss" Program 640 Analysis, indicates weight loss as a function of re-entry time. Predictions of the weight loss are shown in figure 11 for a range of design backface temperatures of 400° to 600°F and total cold-wall heat flux from 5000 to 42,900 Btu/ft². Based on the currently employed materials properties for the charring plastic X5026 and for a design structure temperature, limit of 600°F, the weight loss is 55 to 58 percent of the required heat-shield weight. For temperature limits in excess of 700°F, the weight loss would be 61 percent, since the material is essentially completely charred. In this fully charred condition the heat shield is no longer capable of absorbing large additional quantities of heat. For structure-temperature design limits of less than 400°F, the actual (not percent) weight loss becomes relatively insensitive to the required heat-shield weight for a fixed-vehicle location. For the range of heating and

³Richmyer, R.D., "Difference Methods for Metal-Value Problems" (New York, N.Y.: Interscience Publisher, 1957).

~~CONFIDENTIAL~~

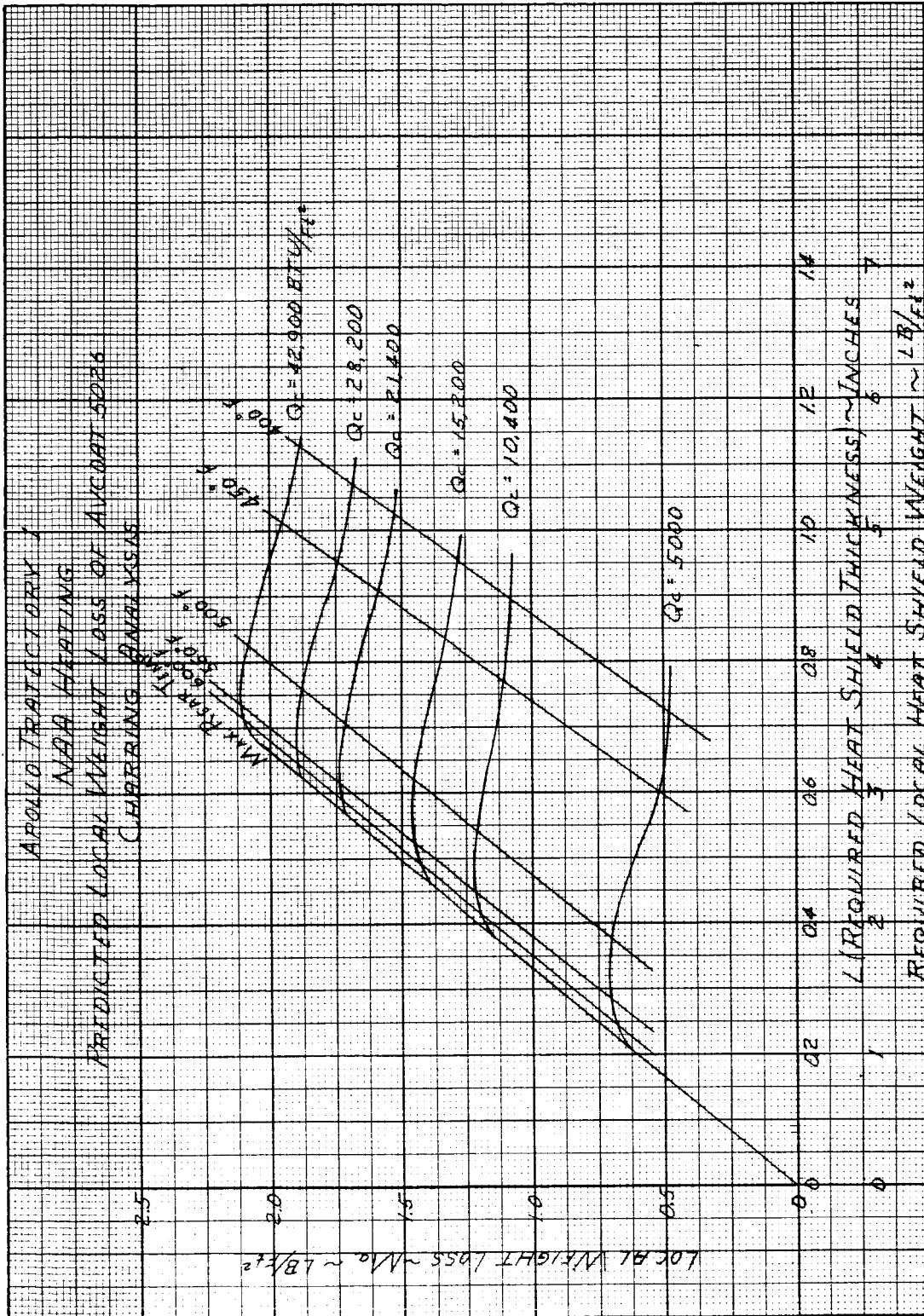


Figure 11 APOLLO TRAJECTORY 1, NAA HEATING, PREDICTED LOCAL WEIGHT LOSS OF AVCOAT X5026, CHARRING ANALYSIS

~~CONFIDENTIAL~~

design temperatures indicated in figure 11, the weight loss varies from 10 to 35 percent for 400°F, to 61 percent weight loss for temperatures over 700°F.

As confidence in the charring plastic analysis increases (in particular, as additional test data are incorporated into the analysis), it may be possible to revise the design analysis concept from one in which the "safe" 640 calculations are used to one in which the more realistic 951 results are employed.

A preliminary thermal analysis of the windward and mid-plane meridians for the "patched" boost and abort trajectory (nominal Saturn boost followed by abort on trajectory 5) indicates no particular temperature problems for either the pressure vessel or the substructure. A follow-on analysis of the leeward meridians will be conducted to establish the thermal safety of the entire forebody. Typical time-temperature histories and gradients for Avcoat X 5026 are shown in figures 12 and 13.

Figure 14 shows the results of our analysis to evaluate the internal air-conditioning system's additional heating or cooling capability to handle heat leaks through the crew-compartment heat shield for the maximum heating and lunar-residence conditions. Plotted are the additional capacity versus the thermal conductance of the wall.

It can be seen that as the wall conductance increases the cooling or heating capability increases. For true evacuated insulation (containing no thermal shorts), the added capacity is very small (less than 100 Btu/hr).

For more realistic conditions (for example where the thermal shorts increase the effective conductance to about the equivalent of unevacuated Q felt), the load will be about 2000 Btu/hr for locating during lunar residence or 1000 Btu/hr for cooling during space flight, providing the vehicle has a cone-on view of the sun. A more desirable situation, that is, a semi-shaded vehicle aspect in space will tend to reduce the cooling requirements of the air-conditioning system.

The composite structure for this analysis was comprised of 0.26-inch Avcoat X5026 plus 0.5-unit stainless-steel honeycomb plus 1.5-inch Q-felt insulation plus the pressure vessel.

Analysis of safety factor requirements centered around the selection of suitable criteria to which reasonable and reliable factors may be logically applied. Currently, the concepts of individual factors on aerodynamic heating, individual thermophysical and ablation properties, and design structure temperature are being evaluated for overall design significance.

Figure 15, for example, shows the change in overall heat-shield weight for a corresponding change in $\sqrt{pk/cp}$, a suitable safety criterion for heat-shield systems which function strictly as radiators.

~~CONFIDENTIAL~~

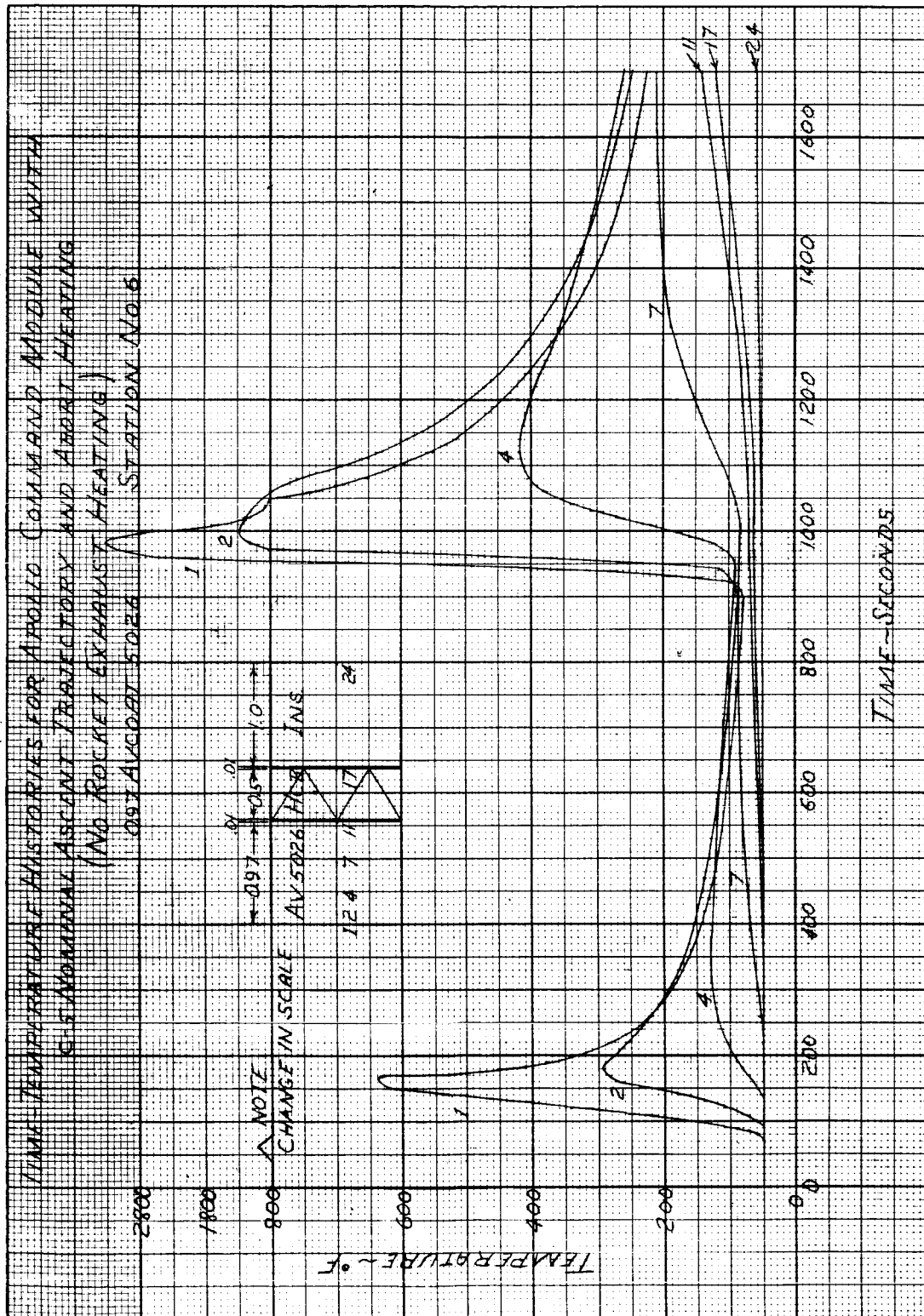


Figure 12 TIME-TEMPERATURE HISTORIES FOR APOLLO COMMAND MODULE WITH C-5 NOMINAL ASCENT TRAJECTORY AND ABORT HEATING

~~CONFIDENTIAL~~

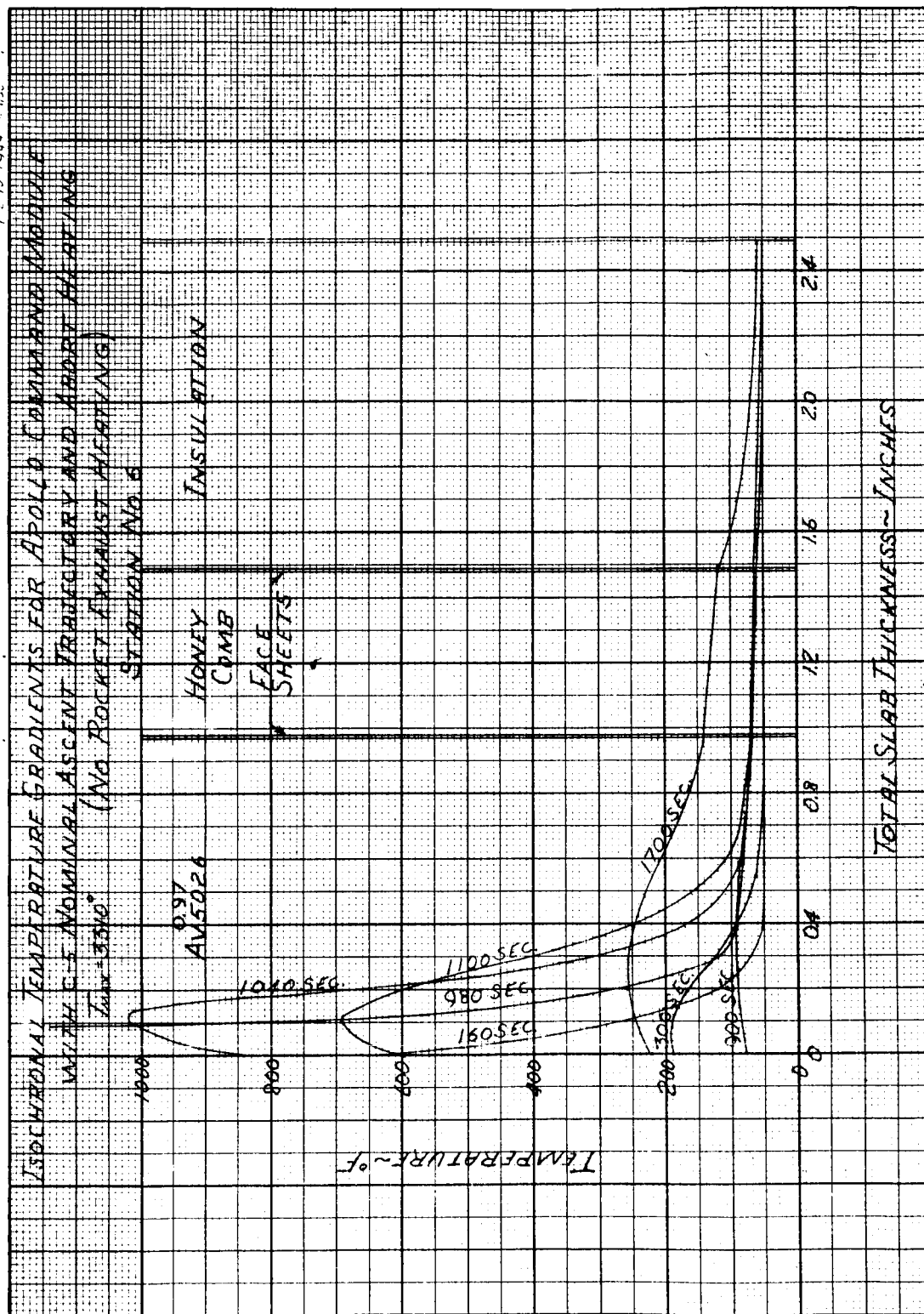


Figure 13 ISOCHRONAL TEMPERATURE GRADIENTS FOR APOLLO COMMAND MODULE WITH C-5 NOMINAL ASCENT TRAJECTORY AND ABORT HEATING

~~CONFIDENTIAL~~

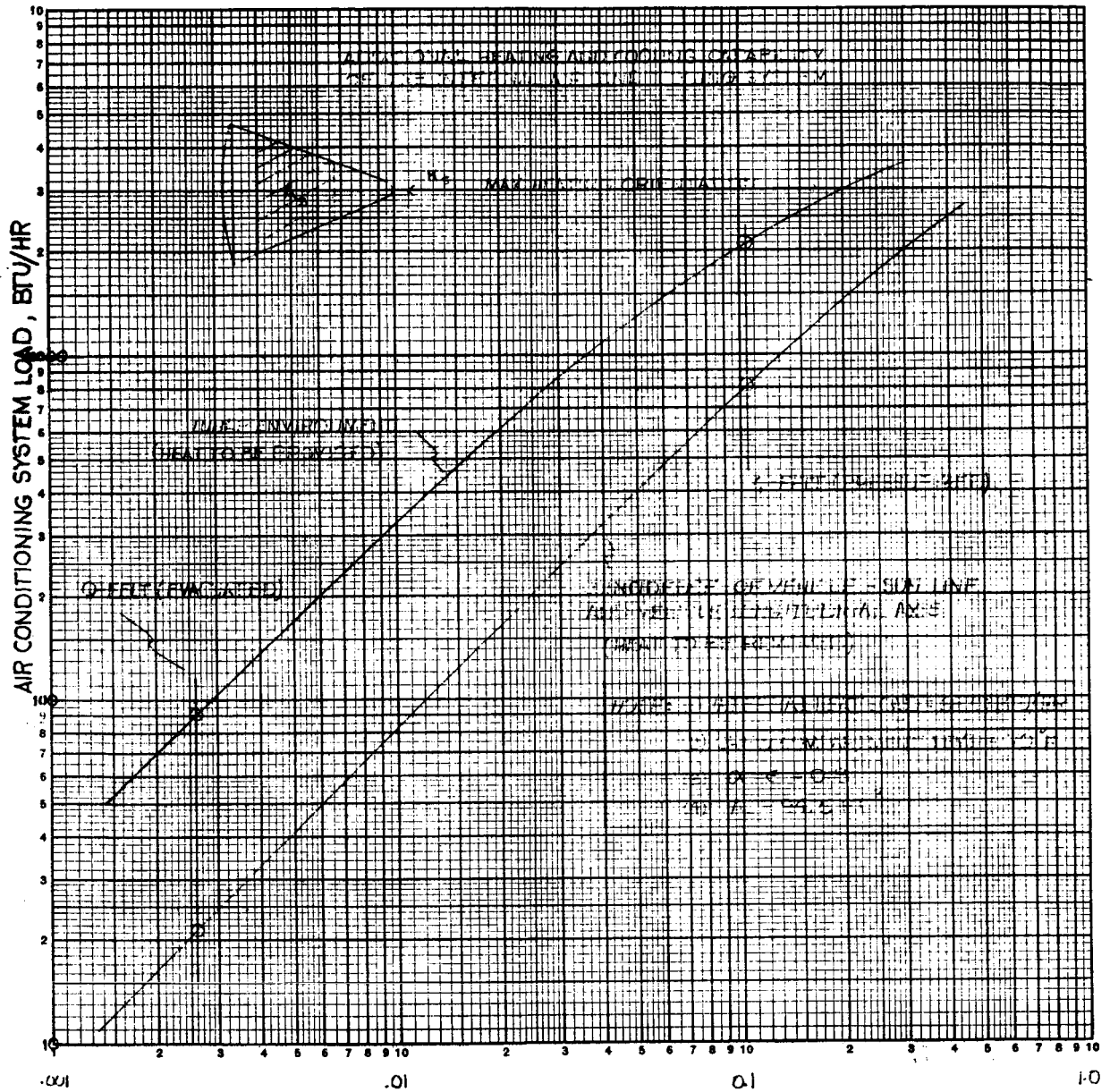


Figure 14 ADDITIONAL HEATING AND COOLING CAPABILITY OF THE
INTERNAL AIR CONDITIONING SYSTEM

~~CONFIDENTIAL~~

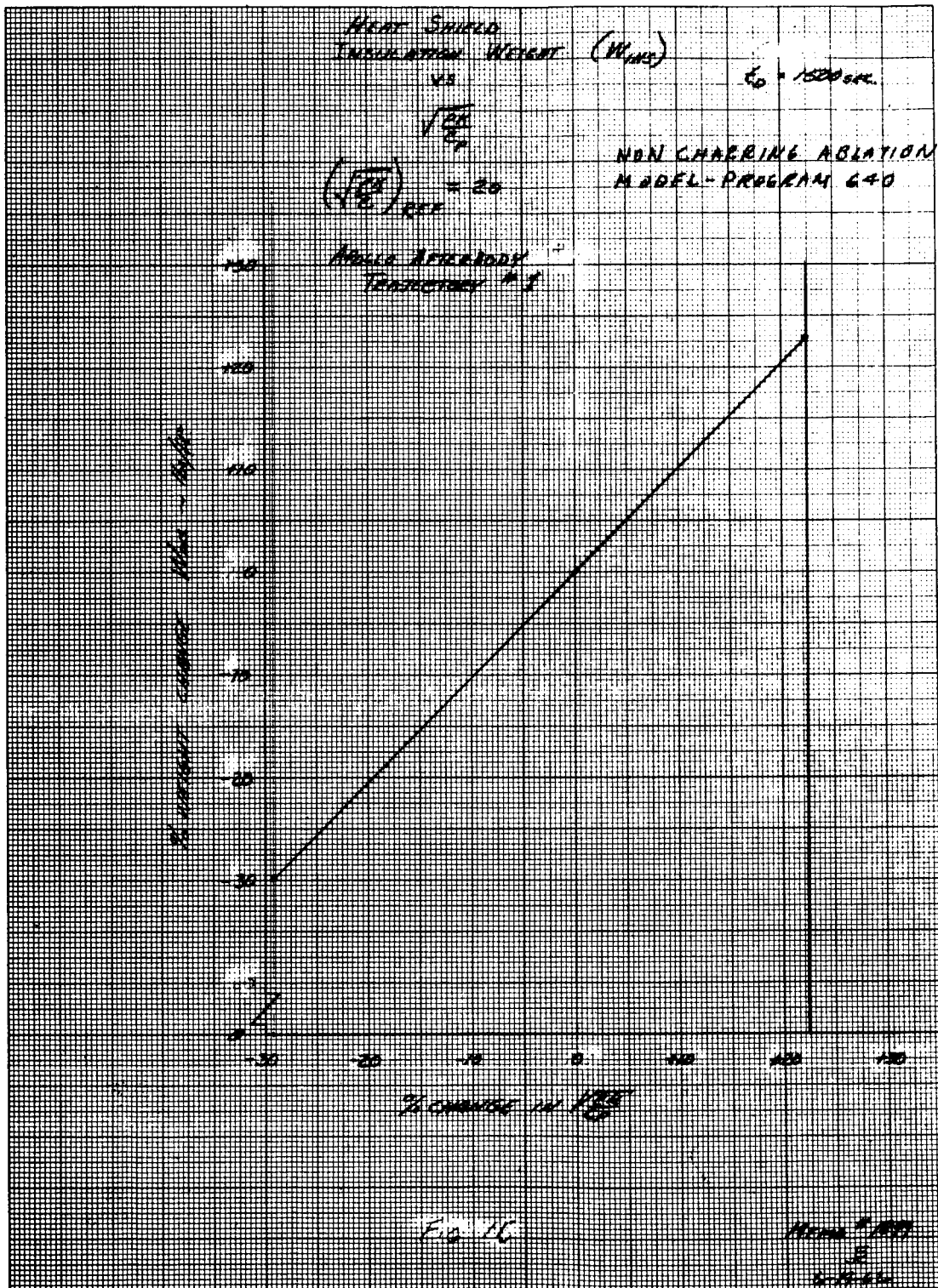


Figure 15 HEAT SHIELD INSULATION WEIGHT (W_{INS}) VERSUS $\sqrt{\frac{\rho k}{C_p}}$

~~CONFIDENTIAL~~

~~CONFIDENTIAL~~

Figure 16 is a plot of the change in weight per square foot associated with a change in design structure temperature. These curves consider both a charring and noncharring ablation analysis. The curve labeled "charring ablation model" exhibits a rather pronounced change in slope for structure temperatures greater than 500°F. As discussed previously, the fully charred condition is attained at about 500° to 600°F under the (material properties) condition of the charring plastic analysis. It therefore appears that extreme caution must be used in attempting a charring plastic design for structure temperatures greater than 500°F. The noncharring analysis is much less sensitive in this temperature range.

One-dimensional thermal analysis indicates that a limited number of exposed fasteners would be acceptable on the leeward side of the command module. Several metals and fiberglass have been examined. Basically, these materials tend to behave as heat sinks thereby reducing the local structure temperatures in the vicinity of the fastener. Figure 17 compares temperature for several fasteners at a depth corresponding to the outer face sheet of the stainless-steel substructure under trajectory 1 heating conditions.

Figures 18 and 19 present similar data for the mid-plane meridian for trajectories 1 and 4, respectively.

The maximum temperature of recessed heat shield fasteners as a function of their depth from the heat-shield surface was evaluated. This one-dimensional analysis was accomplished for three values of integrated heating covering the complete boost through re-entry sequence. The type of fastener selected for analysis was dictated by the overall heat-shield thickness. The results of this study are indicated in figure 20. Figure 21 indicates the depression of temperature caused by the inclusion of the fastener by comparing the maximum fastener temperature to the undisturbed temperature at the corresponding depth. Perfect thermal contact is assumed.

The potential energy function for the $x^2 \Sigma_g^+$ electronic state is given in figure 22. Figure 23 illustrates a typical result of the analog computer work being performed under subcontract. Shown here is the wave function of the 10th vibrational level in the $B^2 \pi$ electronic state of the NO molecule. The ordinate to this curve gives the amplitude of the function in arbitrary units, the abscissa gives the internuclear separation in units of $(r - r_e)$ where r_e is the value of r corresponding to the minimum of the potential energy function. The square of this function is shown in figure 24. When the integral of figure 24 is normalized to unity, the scale factor by which the ordinates of figure 23 must be multiplied in order to obtain the normalized wave function may be obtained. The overlap integrals, which are proportional to the transition probabilities, are obtained by integrating the product of two such wave functions, one in a particular vibrational level of an upper electronic state, the other in a different vibrational level in a lower electronic state. The square of the overlap integrals gives the Franck-Condon factors.

~~CONFIDENTIAL~~

~~CONFIDENTIAL~~

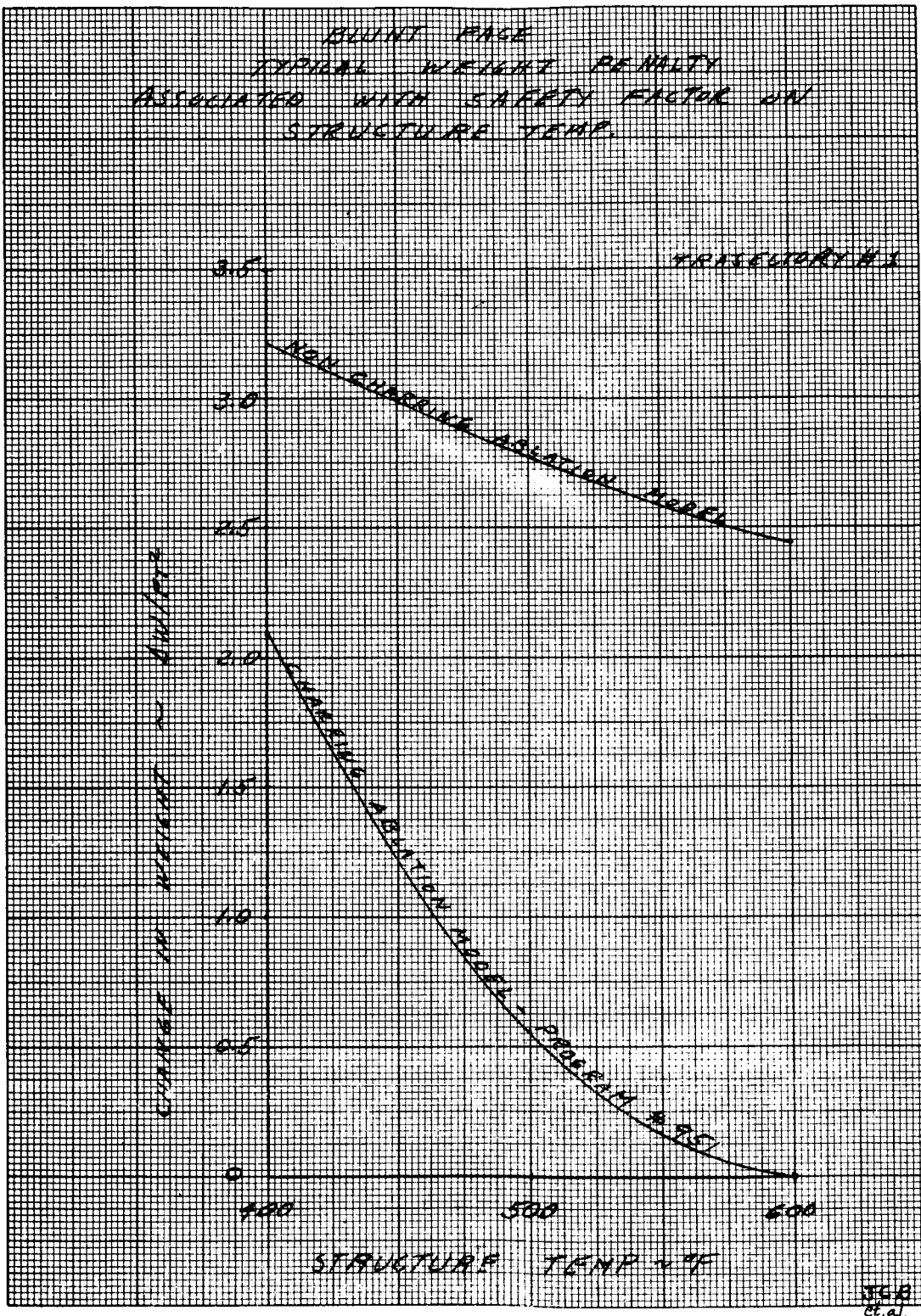


Figure 16 BLUNT FACE - TYPICAL WEIGHT PENALTY ASSOCIATED WITH SAFETY FACTOR ON STRUCTURE TEMPERATURE

~~CONFIDENTIAL~~

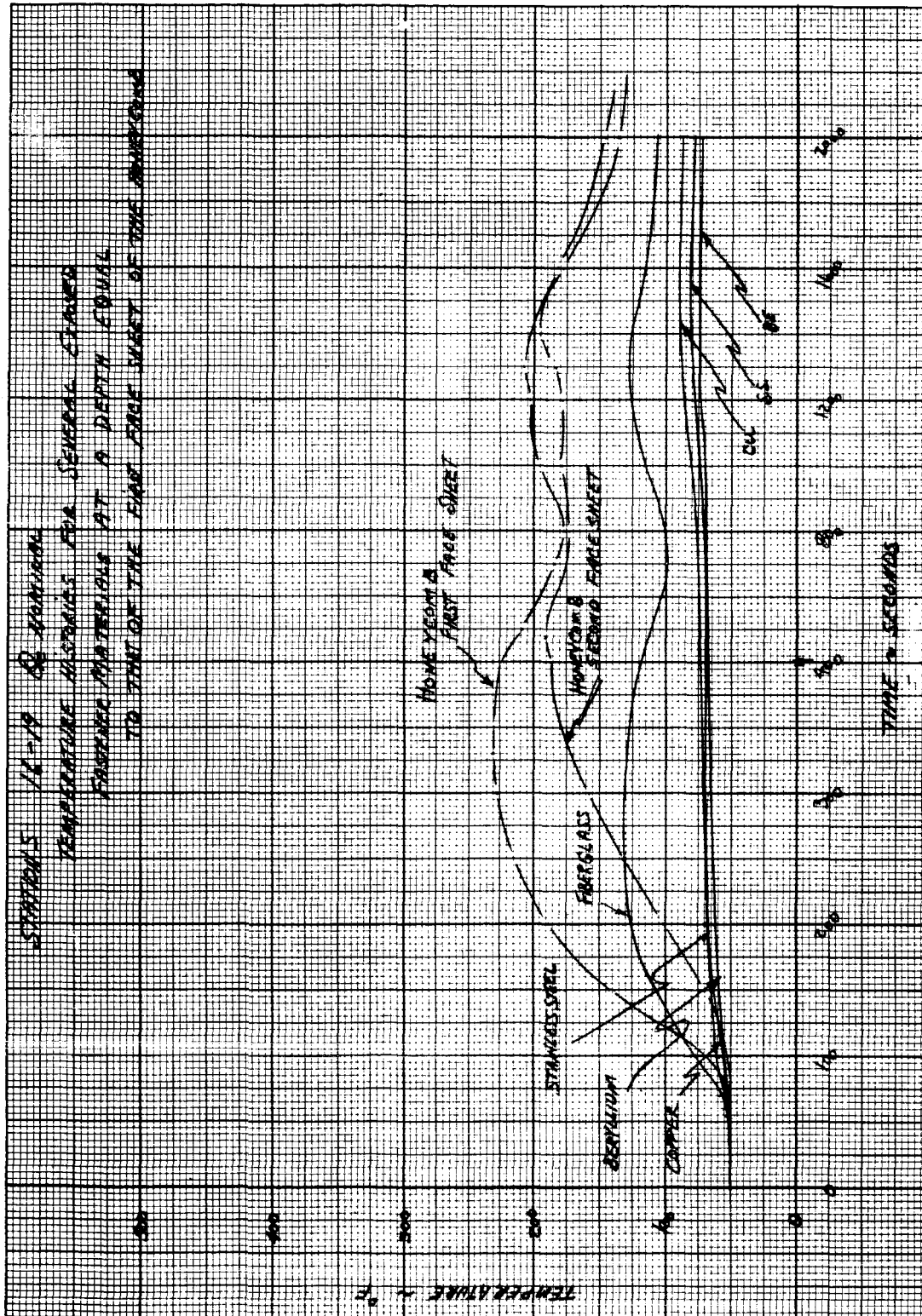


Figure 17 TEMPERATURE HISTORIES FOR SEVERAL EXPOSED FASTENER MATERIALS AT A DEPTH EQUAL TO THAT OF THE FIRST FACE SHEET OF THE HONEYCOMB - STATIONS 16 - 19

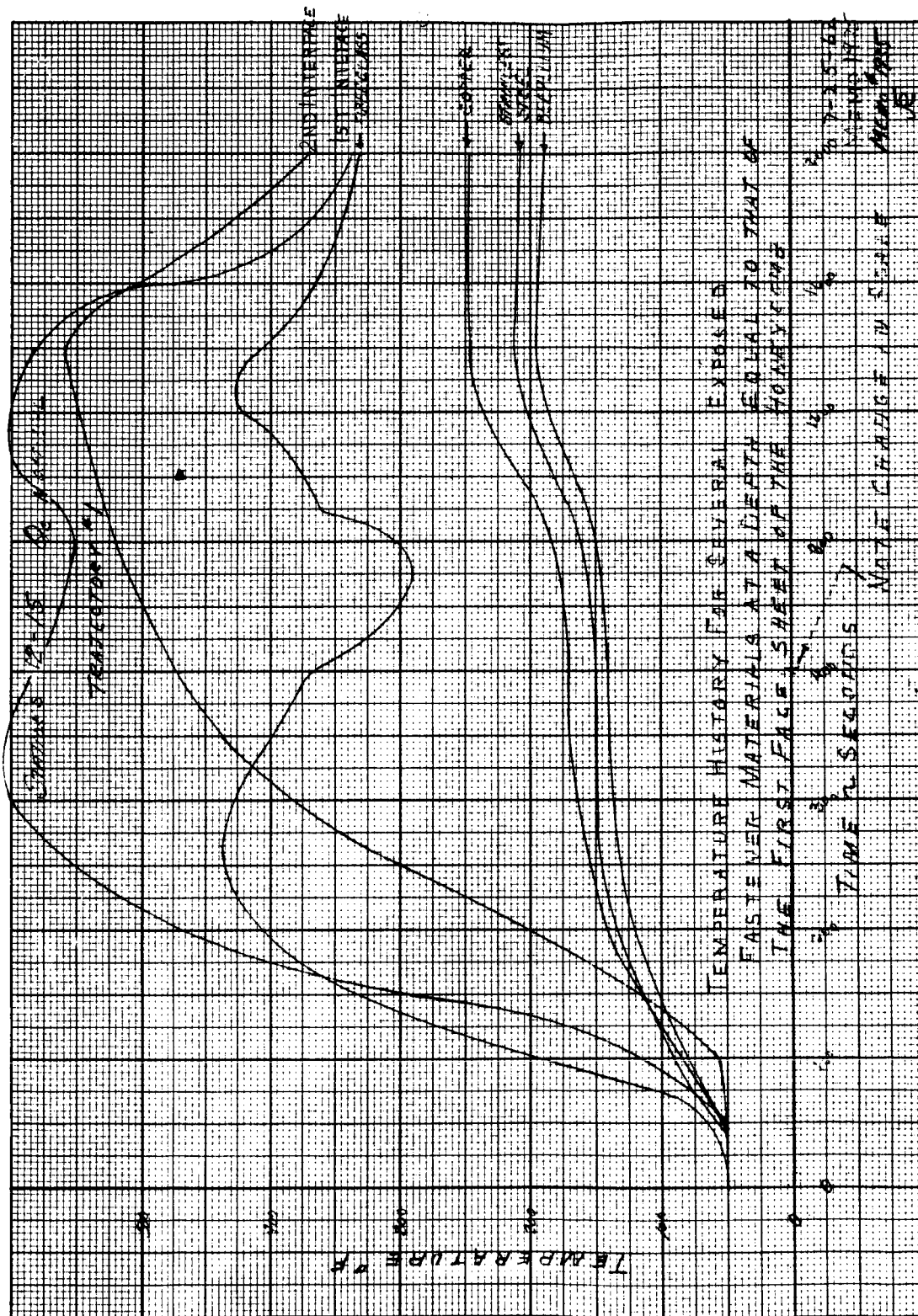


Figure 18 TEMPERATURE HISTORIES FOR SEVERAL EXPOSED FASTENER MATERIALS AT A DEPTH EQUAL TO THAT OF THE FIRST FACE SHEET OF THE HONEYCOMB - STATIONS 12-15, TRAJECTORY 1

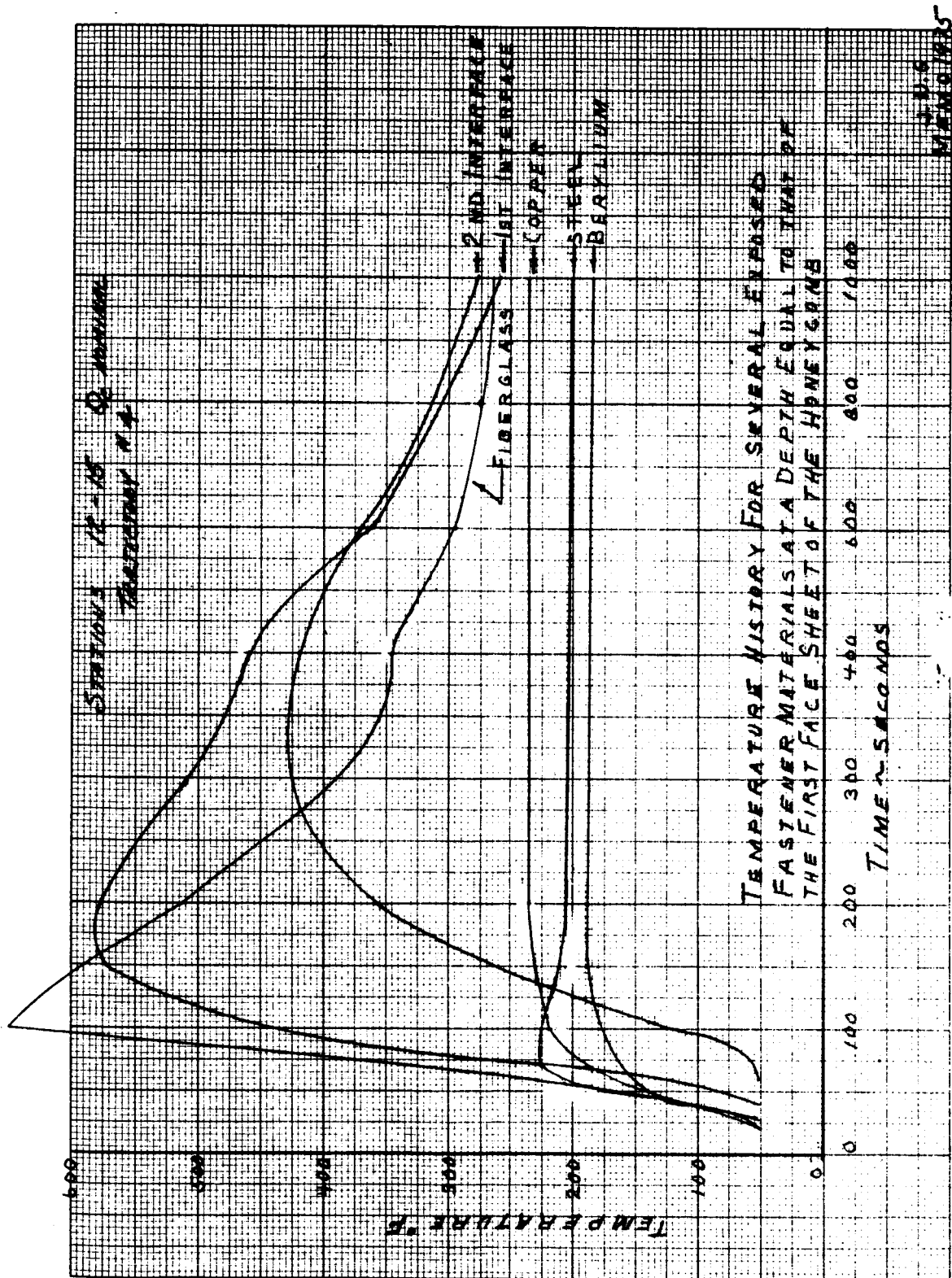


Figure 19 TEMPERATURE HISTORIES FOR SEVERAL EXPOSED FASTENER MATERIALS AT A DEPTH EQUAL TO THAT OF THE FIRST FACE SHEET OF THE HONEYCOMB - STATIONS 12-15, TRAJECTORY 4

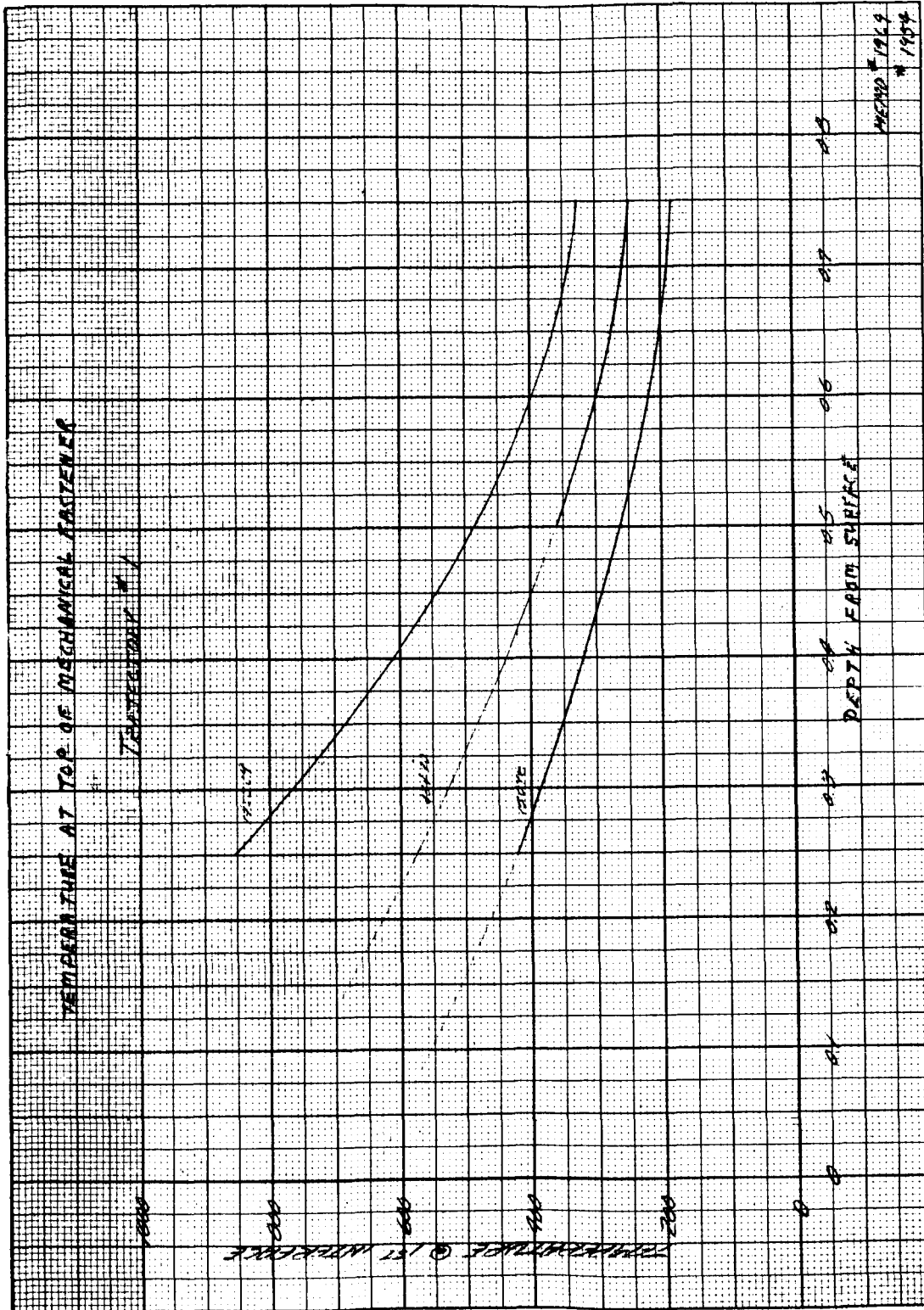


Figure 20 TEMPERATURE AT FIRST INTERFACE VERSUS DEPTH FROM SURFACE

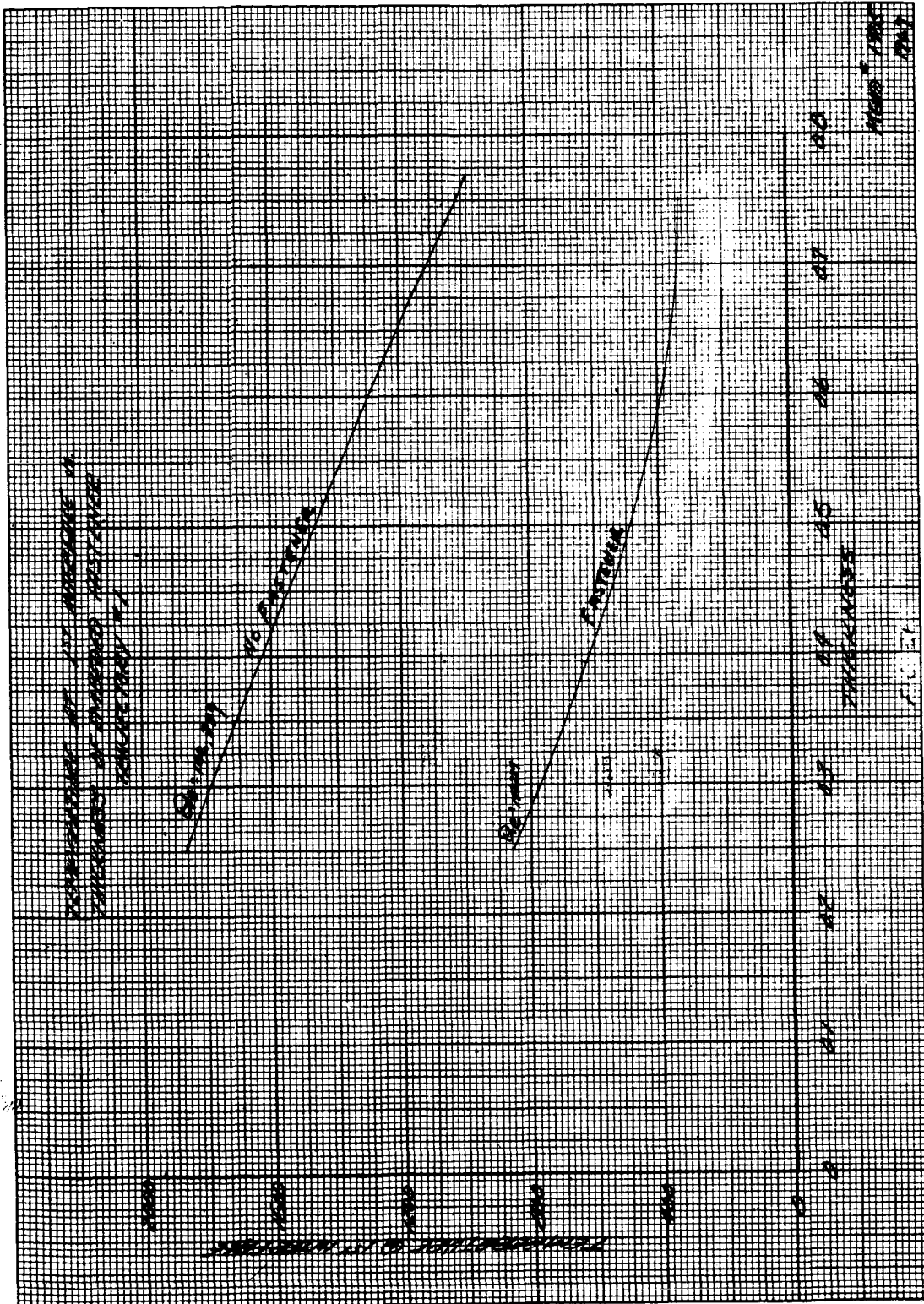


Figure 21 TEMPERATURE AT FIRST INTERFACE VERSUS THICKNESS OF
EMBEDDED FASTENER, TRAJECTORY 1

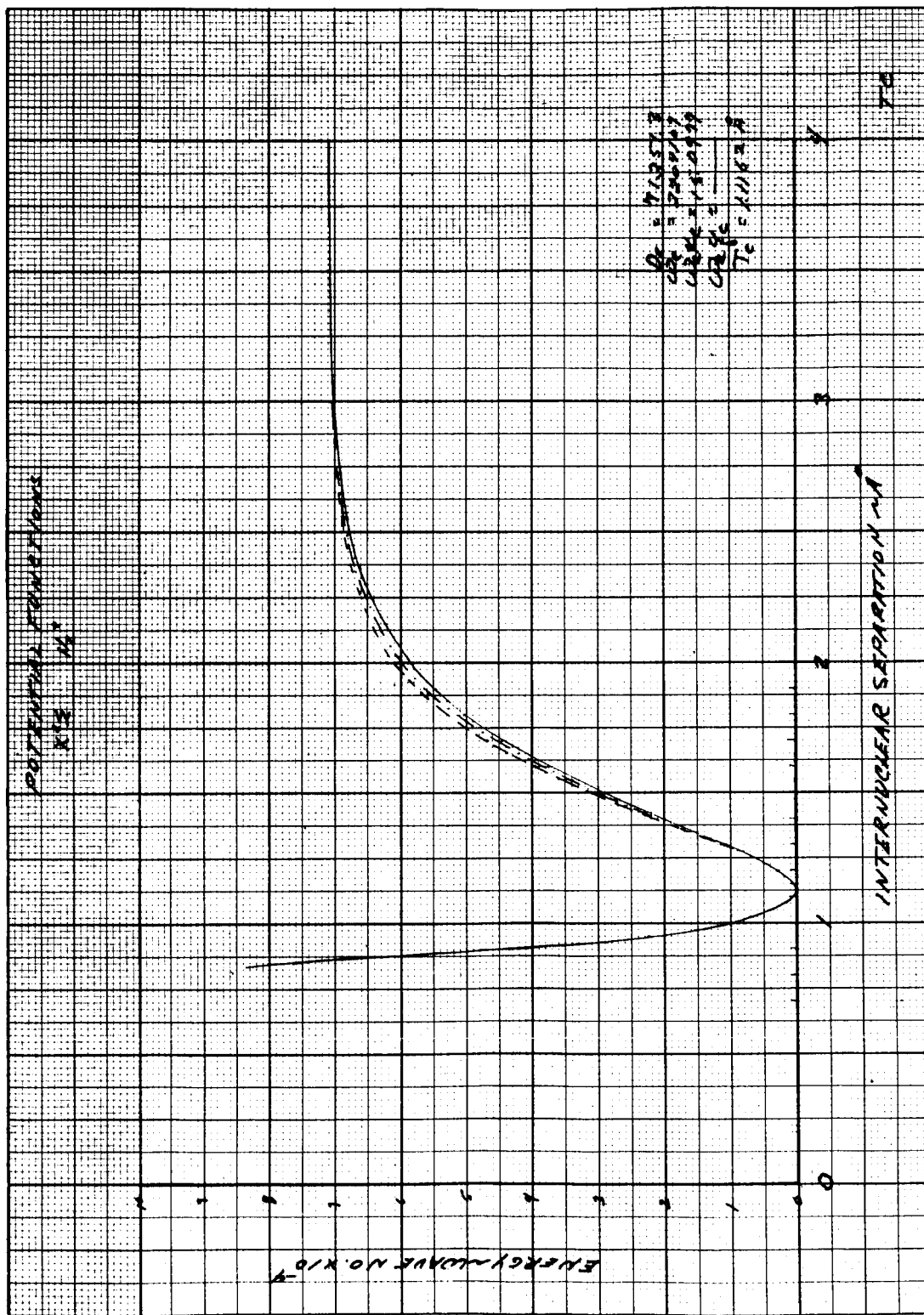


Figure 22 ENERGY - WAVE NO. X 10⁻⁴ VERSUS INTERNUCLEAR SEPARATION - Å

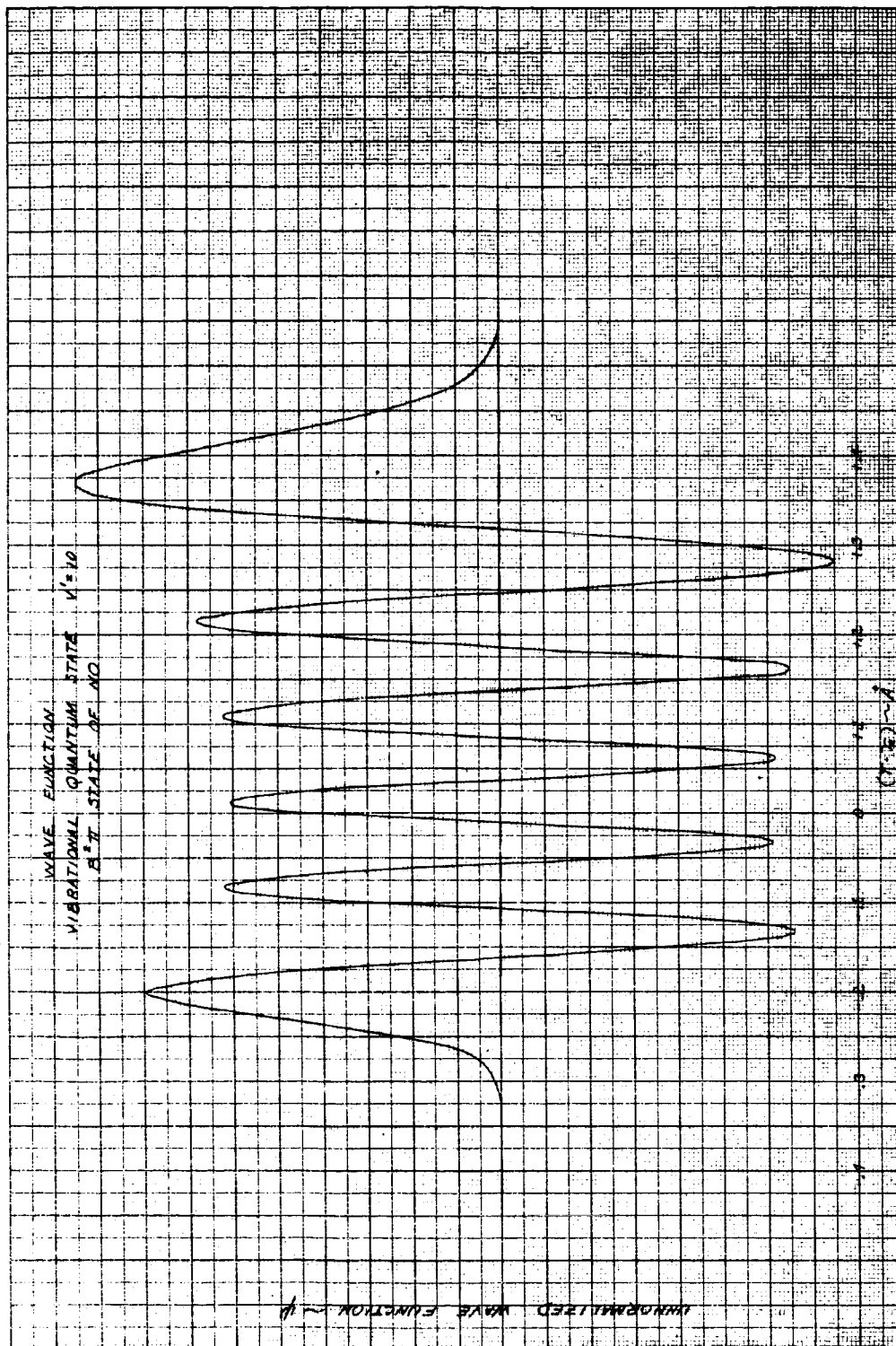


Figure 23 WAVE FUNCTION - VIBRATIONAL QUANTUM STATE, $v' = 10$,
 $B^2 \pi$ STATE OF NO (NO. 1)

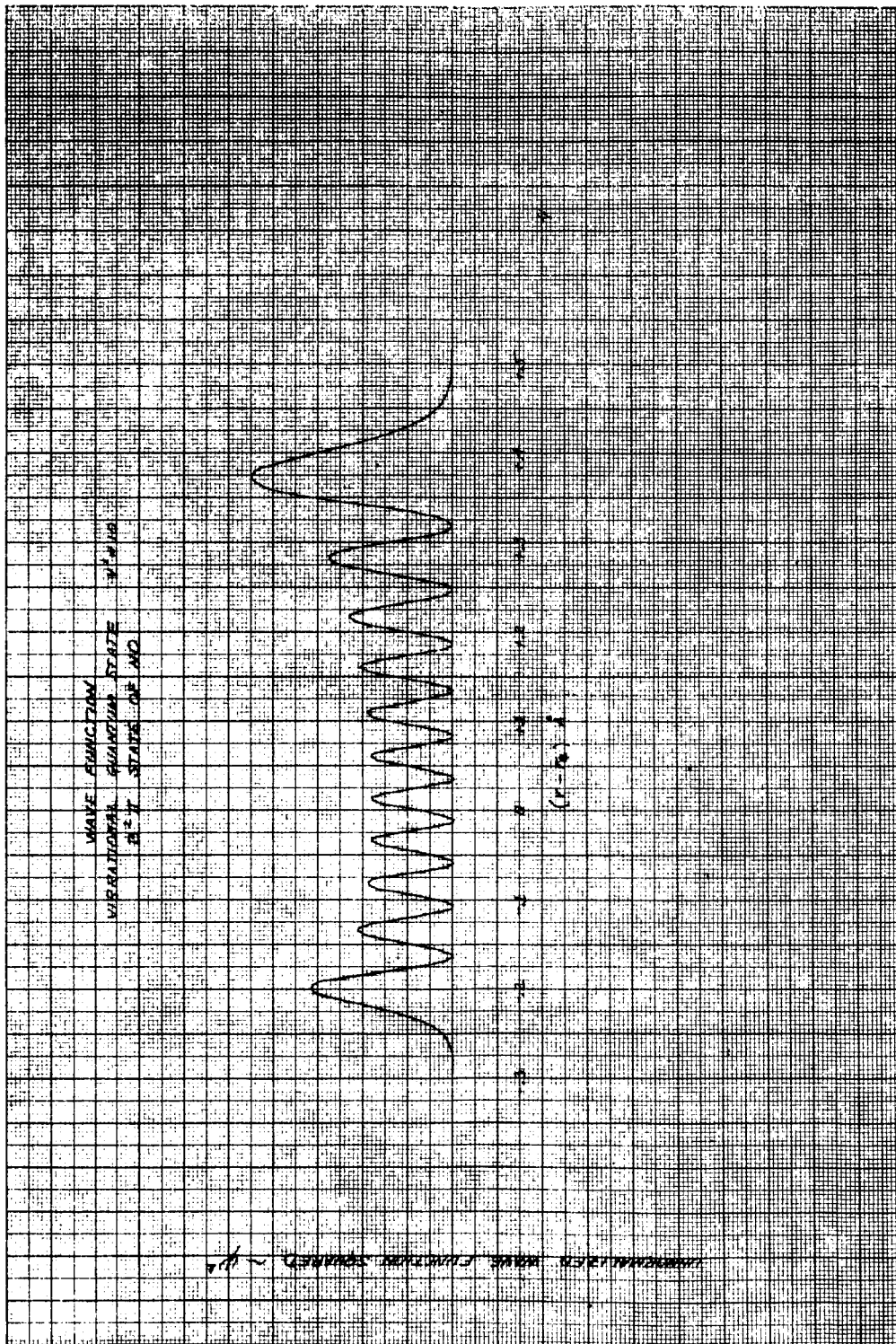


Figure 24 WAVE FUNCTION - VIBRATIONAL QUANTUM STATE, $v' = 10$,
 $B^2 \pi$ STATE OF NO (NO. 2)

~~CONFIDENTIAL~~

Table II gives an excerpt of values obtained for the Franck-Condon factors of the NO- β bands for the first five quantum levels in the upper ($B^2\pi$) and lower ($X^2\pi_{1/2}$) electronic states. The complete list of values extends out to $v'' = 36$ (i. e., the 37th vibrational level of the $X^2\pi_{1/2}$ electronic state) and down to $v' = 12$ (i. e., the 12th vibrational level in the $B^2\pi$ electronic state). Similarly, for the NO- γ bands, Franck-Condon factors have been obtained out to $v'' = 36$ ($X^2\pi_{1/2}$) and down to $v' = 12$ ($A^3\Sigma^+$). For the N_2 molecule, Franck-Condon factors have been computed out to $v'' = 33$ (i. e., the 34th vibrational level in the $X'\Sigma_g^+$ electronic state) and down to $v' = 27$ in the $A^3\Sigma_u^+$ state (i. e., to the 28th vibrational level in this state). Likewise, Franck-Condon factors have been obtained out to $v'' = 33$ in $X^1\Sigma_g^+$ and down to $v' = 12$ in $B^3\Pi_g$.

Figures 25, 26 and 27 summarize the work to date on obtaining accurate potential functions for the various electronic states of NO, N_2 , and O_2 . Each of these states is, of course, filled with vibrational and rotational energy levels, and transitions between levels give rise to the emission spectrum of the molecule and thus contribute to the spectral distribution of the total radiant heat input. These potential functions are based on the values of spectroscopic constants obtained from the most recent experimental data available. Data for N_2^+ and CN are still being processed.

The following is a description of the method developed for interim calculations of the total radiant heating at the stagnation point of the vehicle.

Under certain conditions of velocity, altitude, and nose radius, the radiant heating to a hypersonic re-entering vehicle becomes the dominant mode of heating. At present, a detailed program is being developed to compute the spectral radiant intensity.

Most radiant heating has been calculated using the semi-infinite plane parallel layer approximation of Kivel et al⁴ which results in the following equation.

$$\dot{q}_r = \frac{1}{2} \left(\frac{\epsilon}{L} \right) \delta \sigma T_S^4 \quad (1)$$

where:

$\frac{\epsilon}{L}$ is the emissivity per unit length

δ is the shock detachment distance

~~CONFIDENTIAL~~

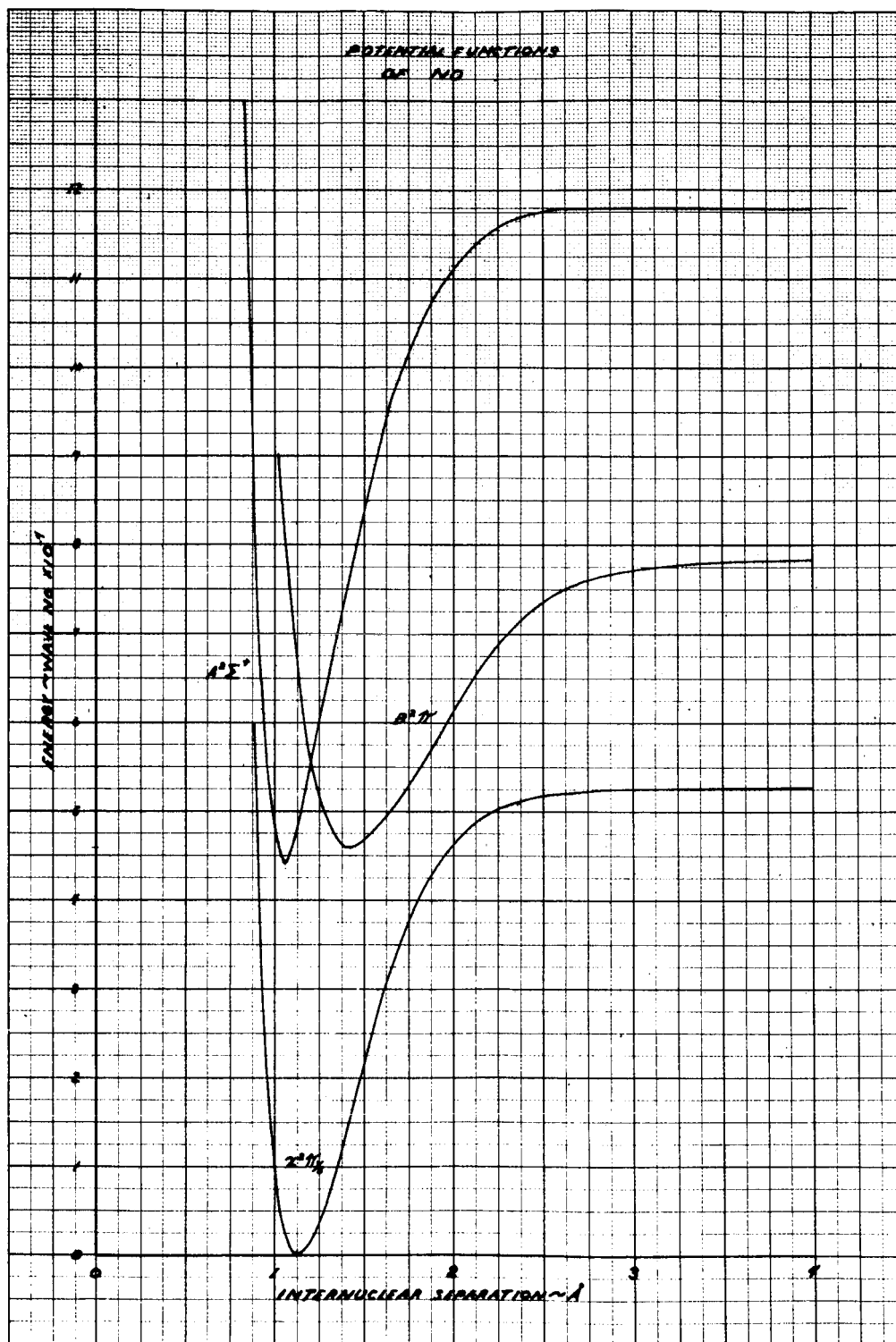


Figure 25 POTENTIAL FUNCTIONS OF NO

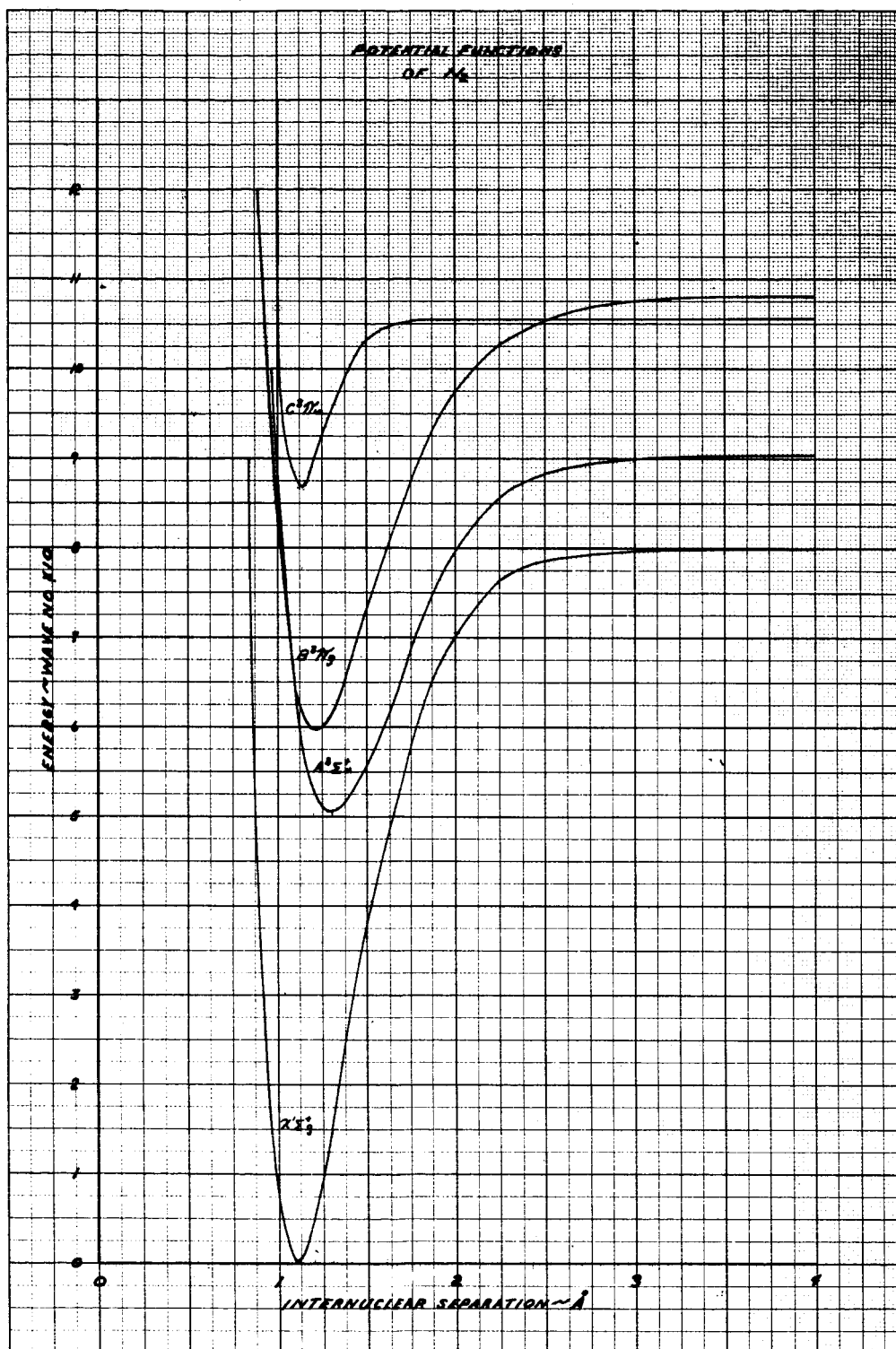


Figure 26 POTENTIAL FUNCTIONS OF N_2

~~CONFIDENTIAL~~

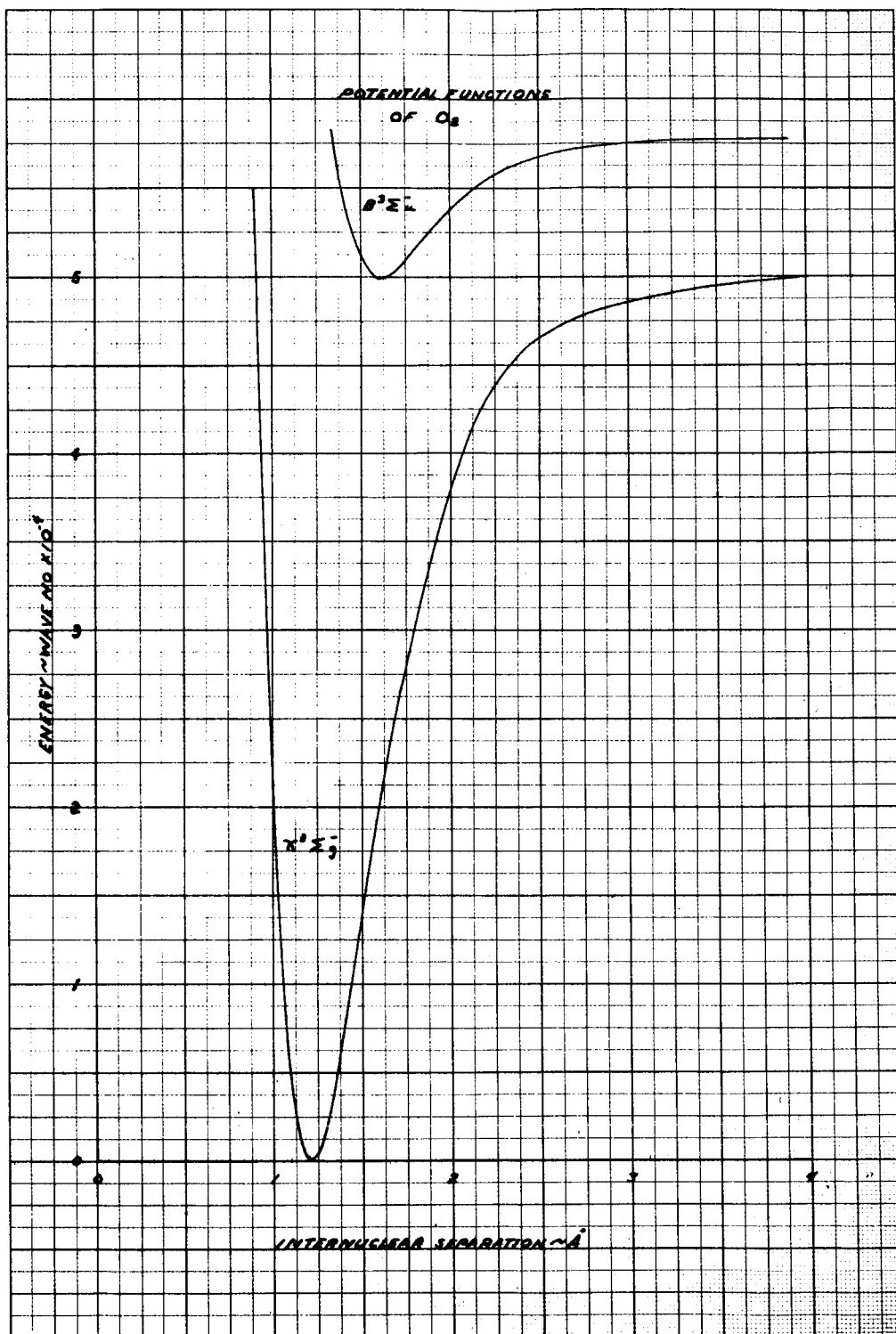


Figure 27 POTENTIAL FUNCTIONS OF O_2

~~CONFIDENTIAL~~

~~CONFIDENTIAL~~

σ is the Stefan-Boltzmann constant

T_S is the gas stagnation temperature.

Values of ϵ/L for various temperatures between 1000° and 18,000°K and pressure ratios (ρ/ρ_0) between 10^{-6} and 10 have been computed by Kivel et al⁴ and Meyerott⁵. In the calculations by Meyerott, the radiation from atoms which are included in the calculations of Kivel et al⁴ are excluded. Also, Meyerott et al⁵ use higher oscillator strengths. Noteworthy is that the oscillator strength for O₂, used by Meyerott, is an order of magnitude greater than that used by Kivel. This higher oscillator strength seems well justified since the radiative measurements of Kivel were made in emission, thus neglecting the transitions from the lower electronic state to the continuum of the upper electronic state. Thomas⁶ has fitted an empirical curve to the results of references 4 and 5 of the following form:

$$\frac{\epsilon}{L} = a_1 (\rho/\rho_0)^{a_2} (T/10^4)^{a_3} \quad (2)$$

Erdoes⁷ has also used an empirical fit of the form $\left(\frac{\epsilon}{L}\right) \sigma T^4 = BT^4$ which lies near the values of reference 5. All the above suffer from the following:

- (a) The shock geometry is not taken into account
- (b) Equation 1 is valid only for an optically thin layer, i. e. , $\tau < 1$
- (c) The transitions between higher quantum numbers which will become important at temperatures greater than 8000°K are not taken into account
- (d) The temperature throughout the shock is assumed to be a constant.

The following equations that have been developed and programmed for the Philco 2000 eliminate the first two objections.

⁴Kivel, B., and K. Bailey, Tables of Radiation From High Temperature Air, Avco Everett Research Report 21 (October 1959).

⁵Meyerott, R.E., J. Sokoloff, and R.A. Nicholls, Absorption Coefficients of Air, Geophysics Research Paper 68, AFCRC, Bedford, Mass. (1960).

⁶Thomas, P.D., Air Emissivity and Shock Layer Radiation, J. Aerospace Sci., 29 (April 1962).

⁷Erdoes, J., Equilibrium Radiative Heating, Avco RAD TR/TA-62-83 (2 May 1962).

~~CONFIDENTIAL~~


$$\dot{q}_r = (1 - \omega) \frac{B}{\lambda} \int_{\theta=0}^{2\pi} \int_{\phi=0}^{\pi/2} \int_{r=0}^{\rho} e^{-r/\lambda} \sin \phi \cos \phi dr d\phi d\theta \quad (3)$$

- 70 -

where:

$$B = \frac{\sigma T^4}{\pi}$$

ρ is a function of the angle ϕ

λ is the radiation mean free path defined as

$$\lambda = \frac{\int I_{BB} d\omega}{\int E d\omega} \quad (4)$$

where:

E is the flux radiated per unit volume

$$\int E d\omega = \frac{EA_S}{V}$$

E is the radiative power

A_S is the surface area of the radiating volume V .

Since the empirical equation of reference 6 is to be used, the proper geometry for A_S and V is that of a semi-infinite layer.

Thus:

$$\int E d\omega = \frac{E 2A}{AL} = \frac{2 \epsilon \sigma T^4}{L}$$

Then:

$$\lambda = \frac{\int I_{BB} d\omega}{2 \left(\frac{\epsilon}{2}\right) \sigma T^4} = \frac{4 \sigma T^4}{2 \left(\frac{\epsilon}{L}\right) \sigma T^4} \quad \lambda = \frac{2}{\left(\frac{\epsilon}{L}\right)} \quad (5)$$

The first two integrations of equation (3) yield

$$\dot{q}_r = (1 - \omega) 2 \sigma T_S^4 \int_{\mu=0}^1 \left\{ 1 - e^{-\rho/\lambda} \right\} \mu d\mu \quad (6)$$

Where:

ω is the diffuse reflectivity

$$\mu = \cos \phi$$

The parameter ρ can be written in terms of μ , the nose radius R , and the shock detachment distance δ .

$$\rho = -R\mu + \{R^2\mu^2 + 2R\delta + \delta^2\}^{1/2} \quad (7)$$

There are a number of hypotheses relating the shock detachment distances to a combination of the nose radius R and the shock density ratios (ρ_2/ρ_∞). See, for example, L'Hommedieu⁹. These may be fitted to an equation of the form

$$\delta = \frac{R}{a_4 \{ \rho_2/\rho_\infty - \beta \}} \quad (8)$$

Combining equations (2), (5), (7) and (8) in equation (6) yields:

$$\dot{q}_r = (1 - \omega) \sigma T_S^4 \left\{ 1 - 2 \int_{\mu=0}^1 \exp \left[Y \{ \mu - (\mu^2 + K)^{1/2} \} \right] \mu d\mu \right\} \quad (9)$$

where:

$$Y = \frac{R (\rho_2/\rho_\infty)^{a_2} \left(\frac{T}{10^4} \right)^{a_3}}{a_1}$$

and

$$K = (2k + 1)/k^2$$

$$k = a_4 [(\rho_2/\rho_\infty) - \beta]$$

A comparison of the different methods employed to compute the equilibrium radiative heat transfer is shown in Table III. The term \dot{q}_r was computed using equation (9); \dot{q}_{r2} was computed using equation (1) and the method of Erdos⁷; and \dot{q}_{r3} was computed using equations (1) and (2). The comparisons are made as a function of varying nose radii. The environment of the vehicle is as follows:

⁹L'Hommedieu, J., Shock Detachment Distance During Re-entry, Avco RAD TR/TA-62-92, (28 May 1962).

~~CONFIDENTIAL~~

TABLE II

EXCERPT FROM MATRIX OF FRANCK-CONDON FACTORS:
NO-BANDS

$\nu' \backslash \nu''$	0	1	2	3	4	5
0	0.0000	0.0001	0.0010	0.0043	0.0170	0.0416
1	0.0001	0.0011	0.0064	0.0235	0.0507	0.0971
2	0.0004	0.0037	0.0182	0.0483	0.0853	0.0918
3	0.0011	0.0086	0.0378	0.0760	0.0835	0.0380
4	0.0028	0.0170	0.0540	0.0761	0.0434	0.0013
5	0.0052	0.0324	0.0689	0.0571	0.0060	0.0125

TABLE III

DIFFERENT METHODS USED TO COMPUTE THE
EQUILIBRIUM RADIATIVE HEAT TRANSFER

R (ft)	\dot{q}_r (Btu/ft ² -sec)	\dot{q}_{r_2} (Btu/ft ² -sec)	\dot{q}_{r_3} (Btu/ft ² -sec)
1	8.9	27.3	5.7
5	44.6	136.4	28.6
10	89.1	273.5	57.5
15	133.7	411.8	86.6
20	178.2	547.2	115.1
25	222.6	682.6	143.6
30	267.0	818.9	172.3
35	311.4	956.2	201.2
40	355.7	1098.0	231.0

~~CONFIDENTIAL~~

~~CONFIDENTIAL~~

$$T_S = 19,450.0 \text{ } ^\circ\text{R}$$

$$\rho_2/\rho_0 = 3.86 \times 10^{-3}$$

$$\rho_\infty/\rho_0 = 1.466 \times 10^{-4}$$

The hypothesis of Hayes and Probstein was used to find the constants in equation (8).

3. Structural Studies

On the basis of the information presently available, some very high stress concentration factors may be expected at the corners of a rectangular cutout, particularly if the corners are sharp or if the stress field is unfavorably oriented. Since these results are part of a preliminary study no curves or numbers will be available until the analysis is complete.

The bond-stress concentration analyses at cutouts considers a combined plate bending and a "pseudo" two-dimensional elasticity analysis in the cutout region. Finite-difference techniques are currently being considered for the rectangular cutouts (with rounded corners if necessary) and possibly a closed-form solution for circular cutouts. If the latter is obtainable, it will readily allow a check on finite-difference convergence.

The concentrations due to plate bending analysis will consider the effect of a "thermal moment" distributed along the boundary cutout. The two-dimensional plane stress analysis will consider that the boundary at the cutout is stress-free at every point rather than considering zero-resultant statistical conditions.

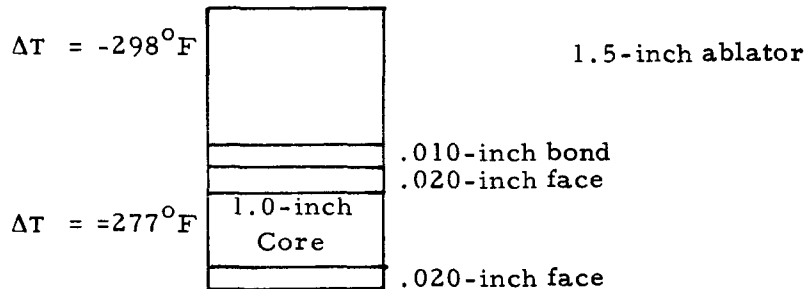
The free-edge bond analyses consider that for rigid bonds the free boundary of the tile controls the bond stress state rather than the bond elasticity. The method initially considers a stipulation, with application to plate corners considered as previously. (Re-evaluation of this problem will be considered later.) The analytic technique is to consider the rigidly bonded strip as a problem in two-dimensional elasticity. It is a mixed boundary-value problem. A stress-free boundary is prescribed along three edges and a zero-displacement condition is prescribed along the fourth boundary. Proper equations have been derived to investigate this problem. If the bond is considered flexible, the bond and tile strip will be considered as the structure with a zero-displacement condition between the bond and the substructure. The solution to this problem would require many nose mesh points to define the laminate properly, since thickness and elastic properties will vary significantly between the materials. A variable mesh will be required and an investigation will be necessary to determine effects of large variation in mesh size on both accuracy and computational difficulties.

~~CONFIDENTIAL~~

~~CONFIDENTIAL~~

The results of a parametric study to determine bond-stress requirements in the steady-state cold environment (-260°F) are presented in figure 29. The study consisted of variations of geometry and ablator and bond mechanical properties run on the 640S digital program similar to the studies previously reported for ablators X5026 and X5019. The assumed geometry and ablator properties (Fig. 29) were chosen to indicate extreme bond requirements found in the study. However it is felt these requirements are only slightly greater than actual vehicle requirements.

The estimated multiplier $\eta = 4.0$ is obtained as follows: A shear lag solution of the following case:



Zero stress temperature = 70°F gives a **max** shear stress at the corner of:

$$\tau_{\max} = 25,200 \text{ psi}$$

assuming the shear allowable to be 60 percent of the tensile allowable requires:

$$\sigma_{\text{ult}} = 42,000 \text{ psi}$$

or a factor of about 4.0 based on the mean bond α and $\nu = 0.3$.

Thin shell digital program runs have been made on the blunt end substructure to define effects of the toroidal corner rigidity. Partial results are presented in figures 30 through 36. Five toroidal shells of varying stiffness were investigated as shown in figure 37. An ultimate external pressure of 20 psi was assumed to be reacted at the pad circle. The resulting meridional stresses in the outer skin is given for each case (Figs. 38 through 42). Some resulting deflections are given for case 1.0 and 1.4 (Figs. 30 through 36). Complete results and evaluation of results will be presented in future reports.

Thermal gradients measured in Avcoat X5026 (run 2947) are given in figure 43.

~~CONFIDENTIAL~~

~~CONFIDENTIAL~~

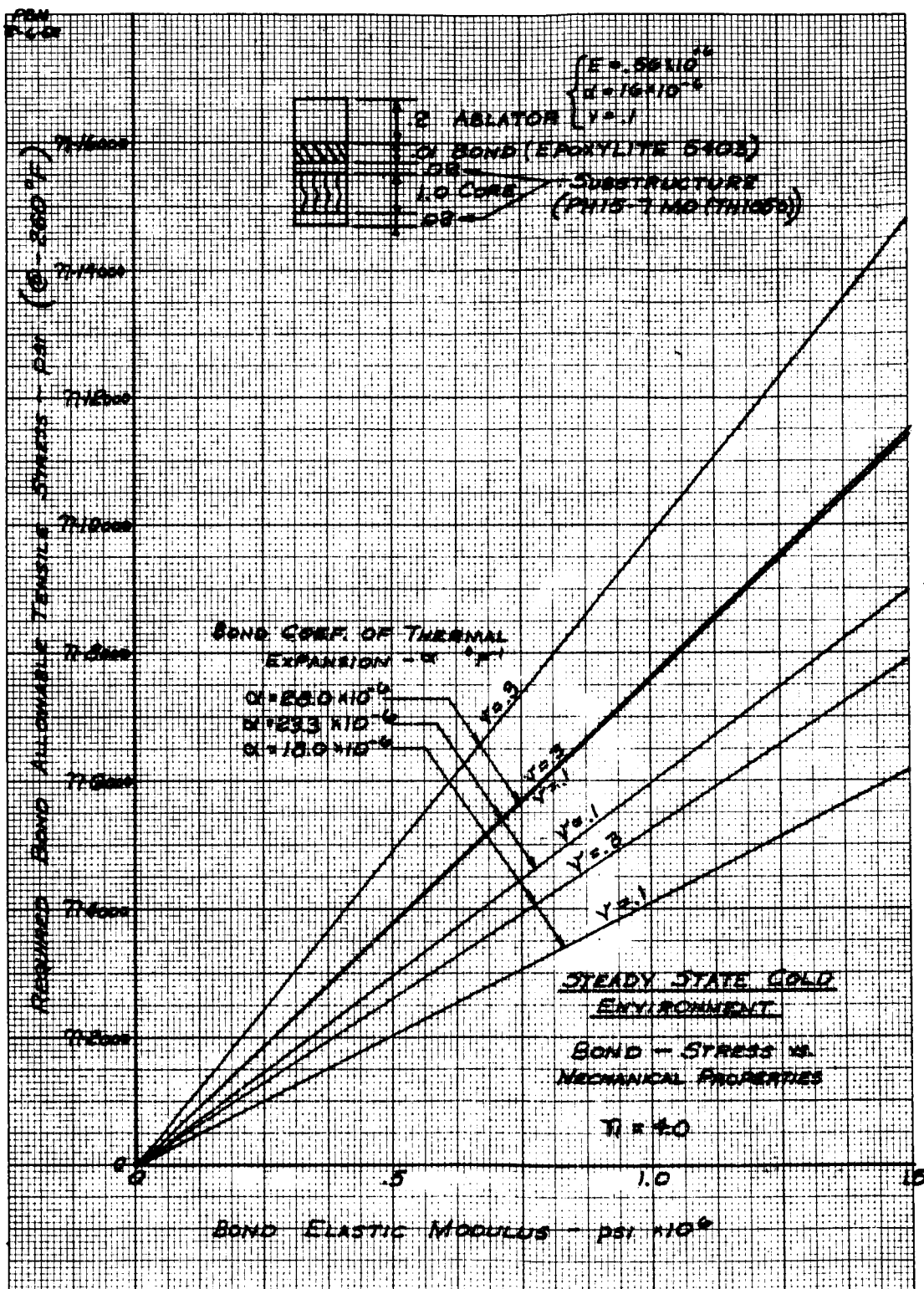


Figure 29 REQUIRED BOND ALLOWABLE TENSILE STRESS VERSUS BOND ELASTIC MODULES

~~CONFIDENTIAL~~

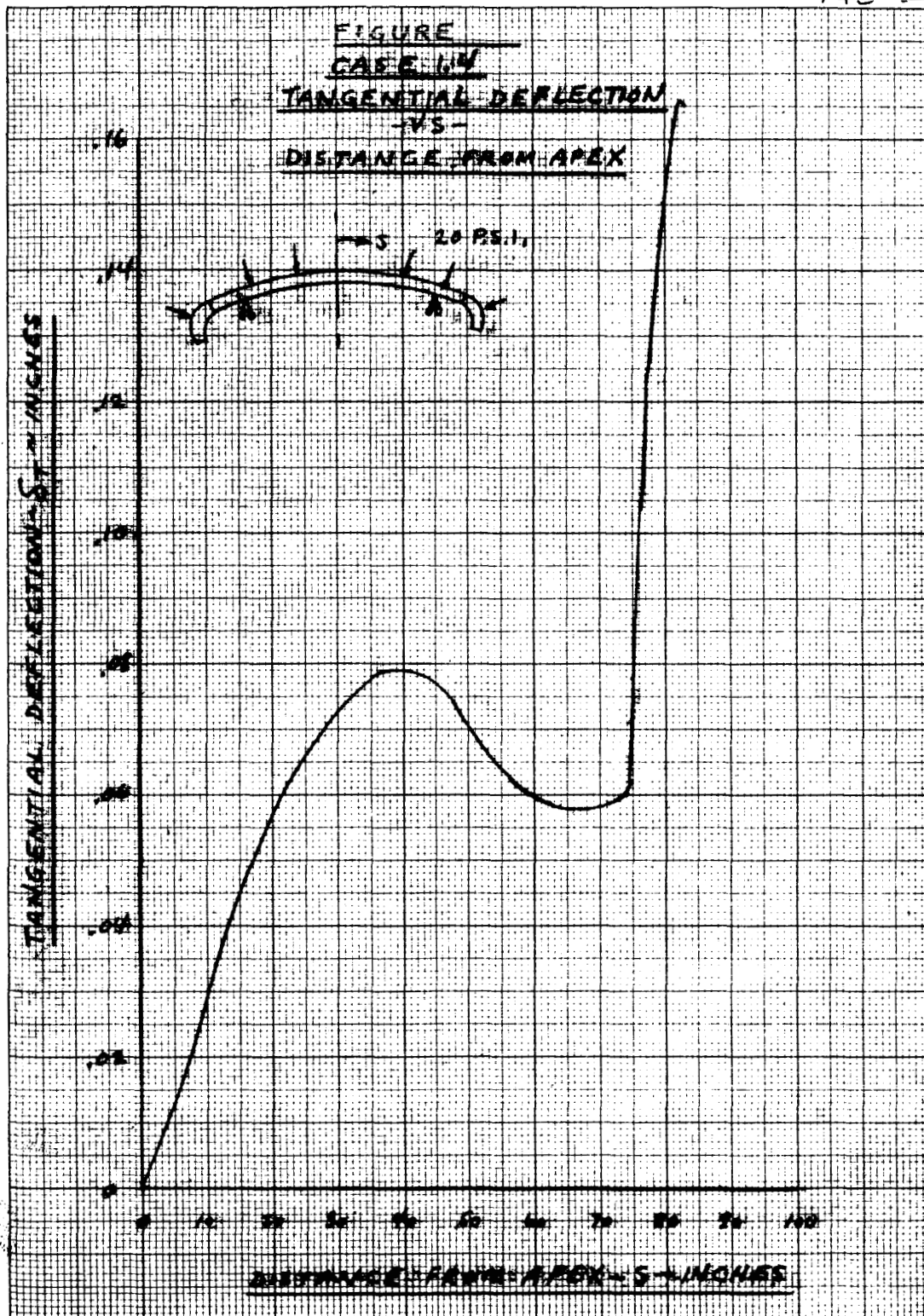


Figure 30 TANGENTIAL DEFLECTION VERSUS DISTANCE FROM APEX-
CASE 1.4

~~CONFIDENTIAL~~

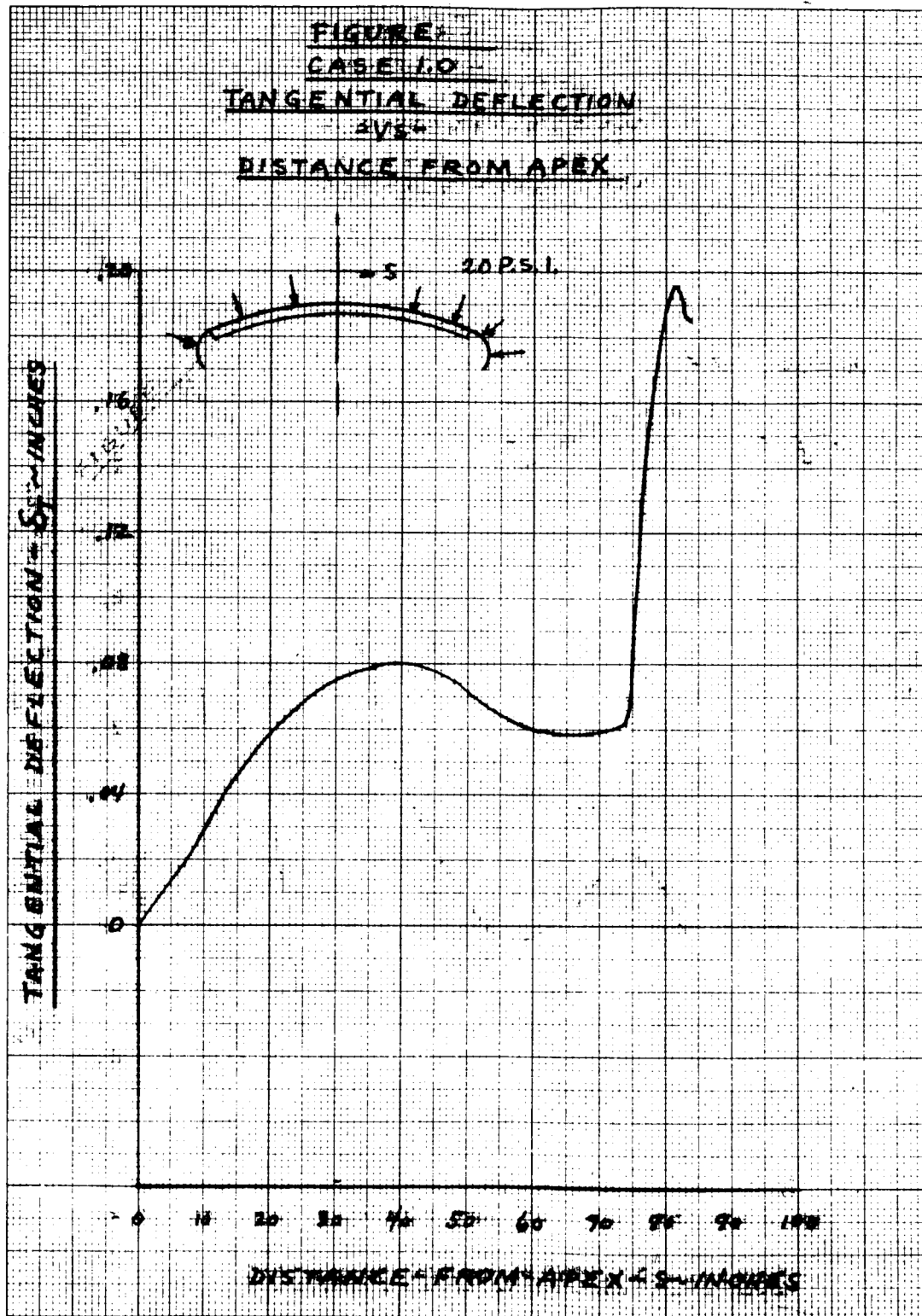


Figure 31 TANGENTIAL DEFLECTION VERSUS DISTANCE FROM APEX-
CASE 1.0

~~CONFIDENTIAL~~

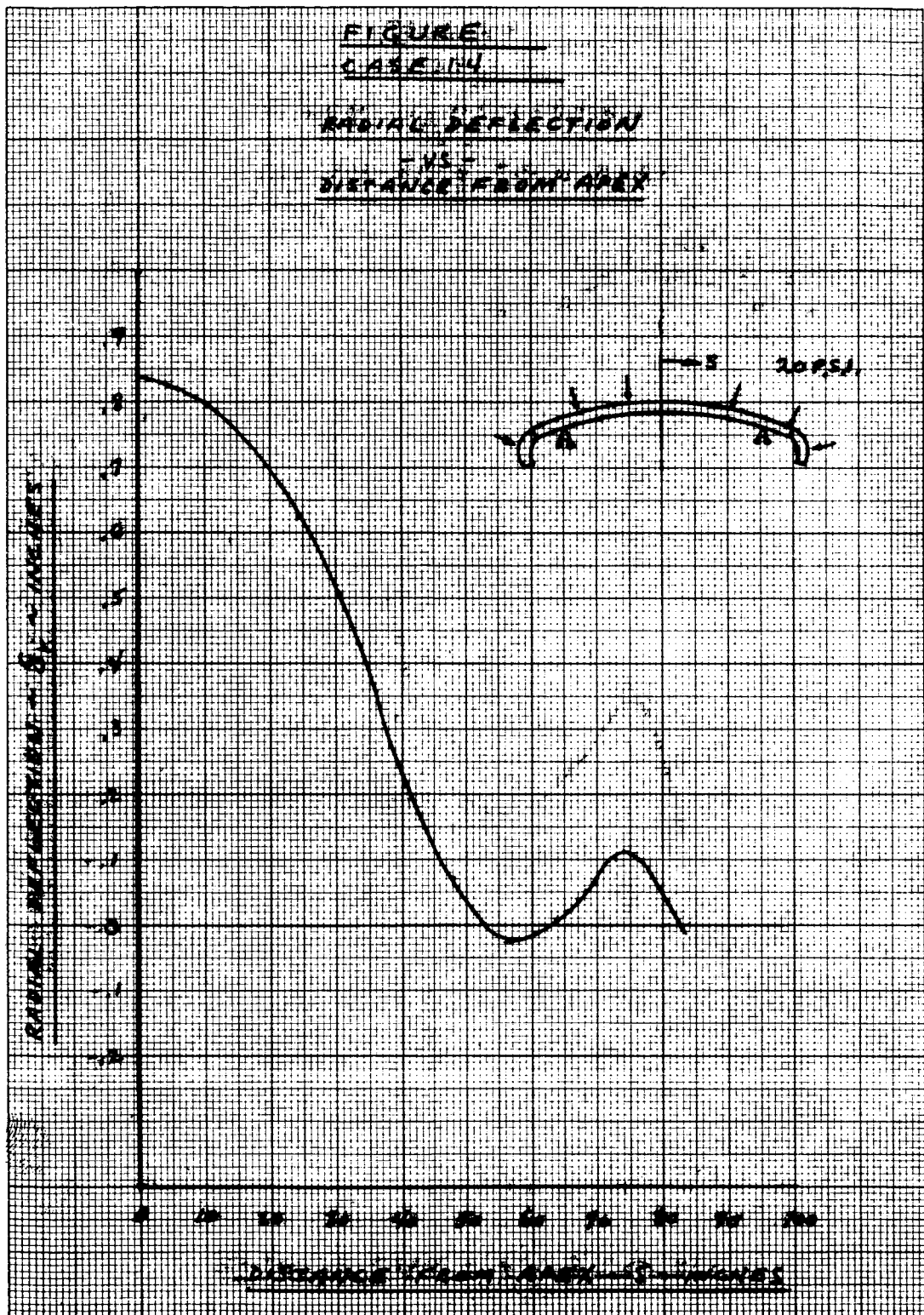


Figure 32 RADIAL DEFLECTION VERSUS DISTANCE FROM APEX- CASE 1.4

~~CONFIDENTIAL~~

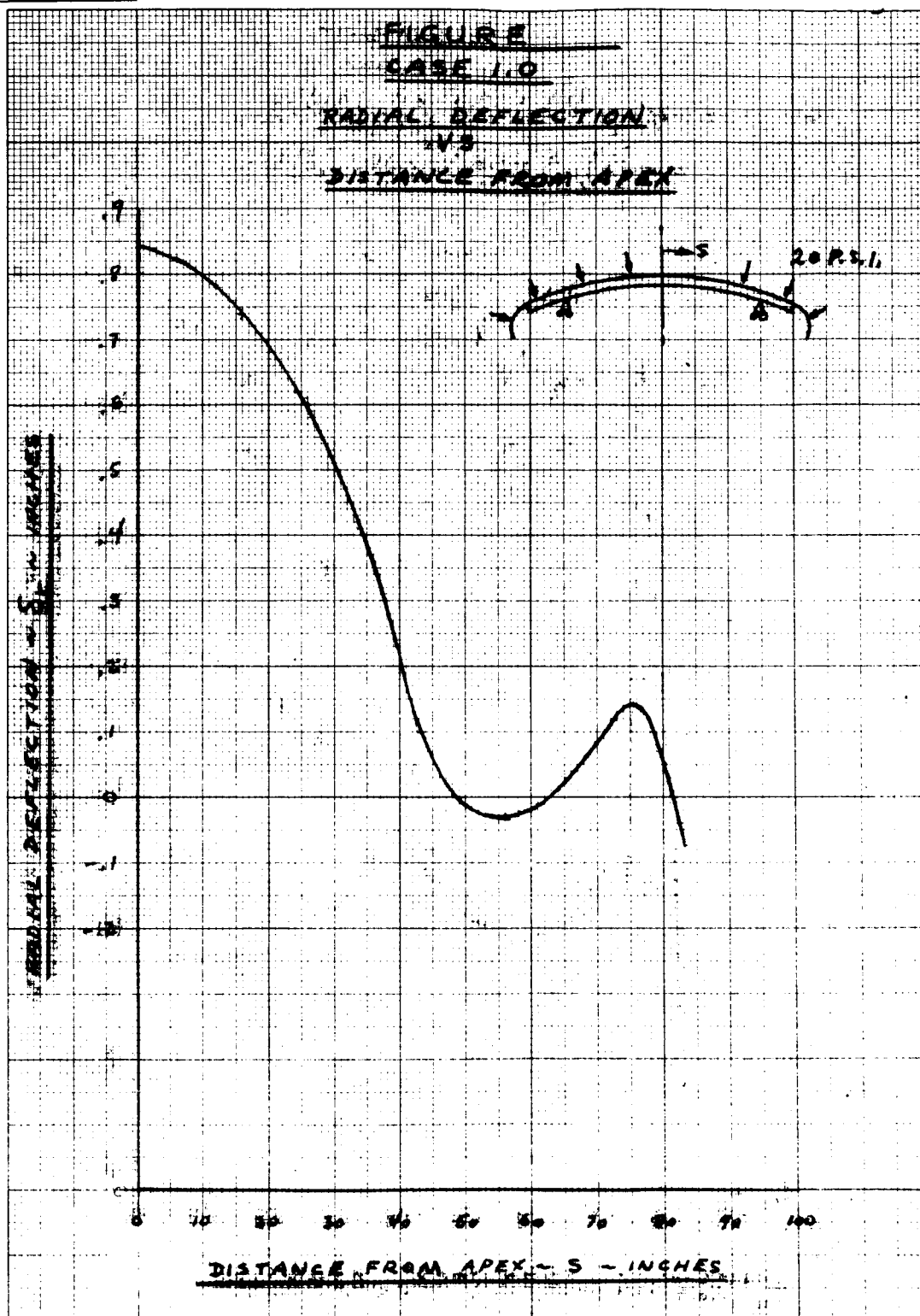


Figure 33 RADIAL DEFLECTION VERSUS DISTANCE FROM APEX - CASE 1.0

~~CONFIDENTIAL~~

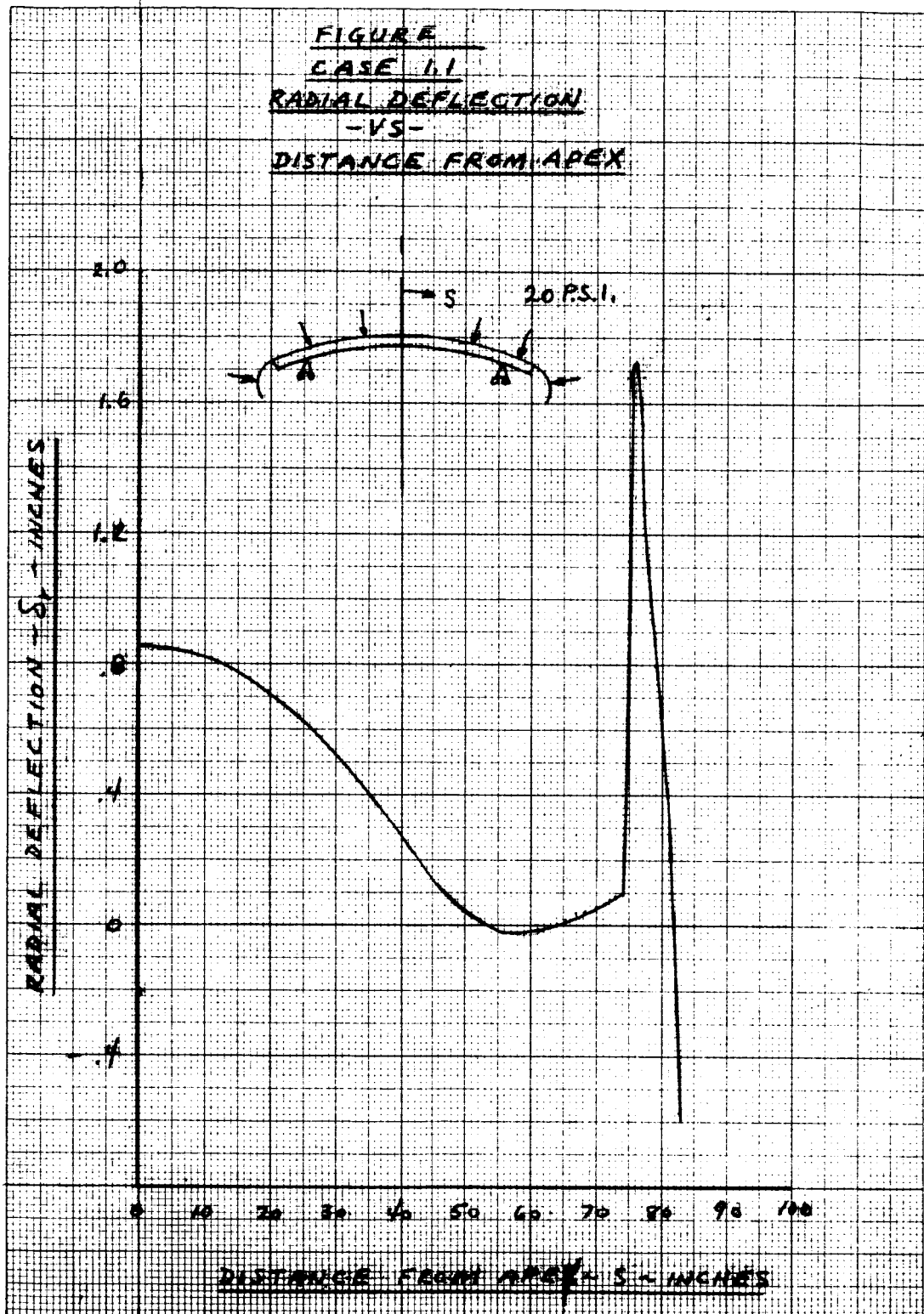


Figure 34 RADIAL DEFLECTION VERSUS DISTANCE FROM APEX - CASE 1.1

~~CONFIDENTIAL~~

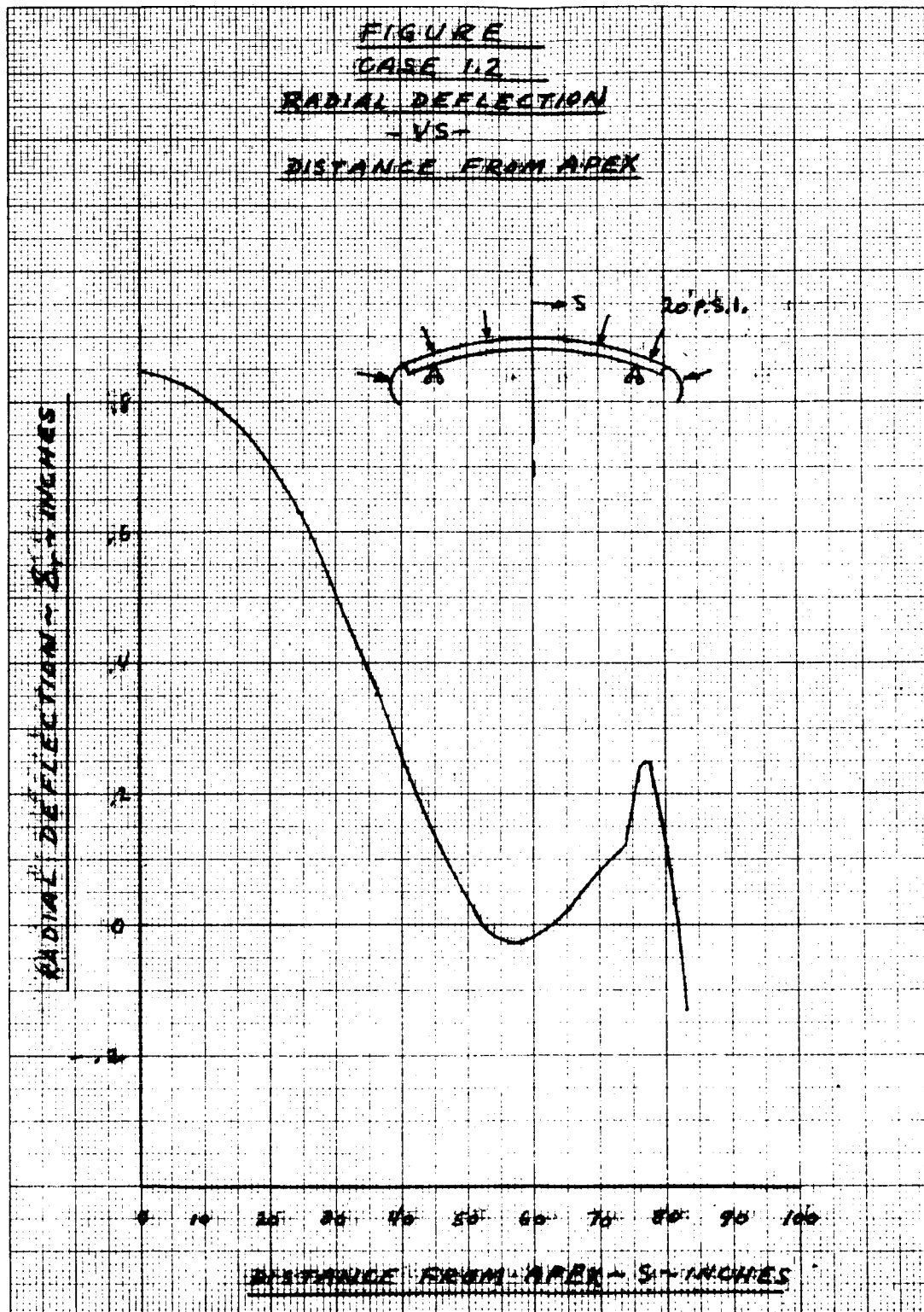


Figure 35 RADIAL DEFLECTION VERSUS DISTANCE FROM APEX - CASE 1.2

~~CONFIDENTIAL~~

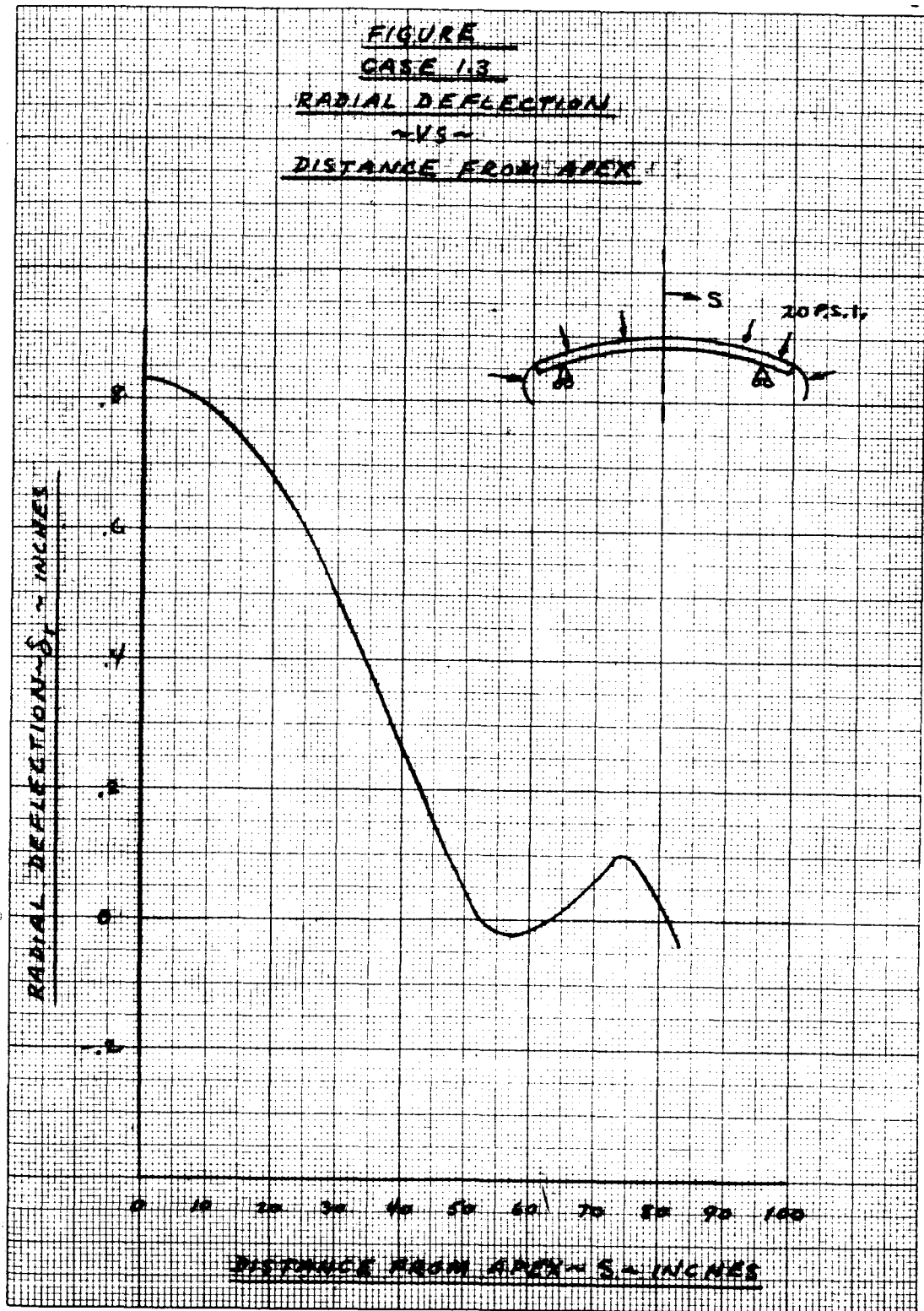
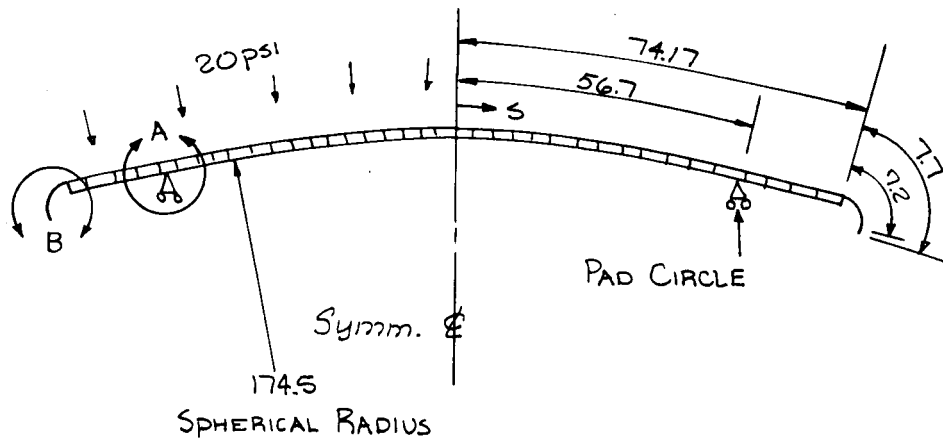
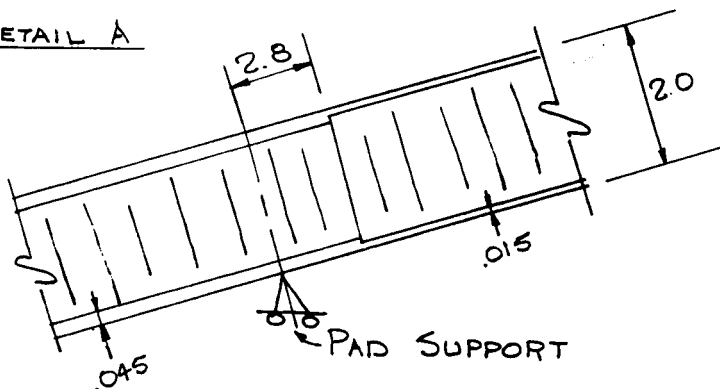


Figure 36 RADIAL DEFLECTION VERSUS DISTANCE FROM APEX - CASE 1.3

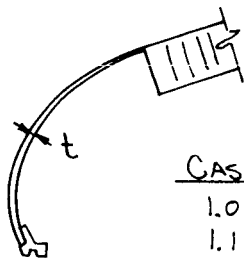
MODEL NO.		TITLE:	ANAL. BY	
PARA. NO.			DATE	
DWG. NO.			CHKD. BY	
LOADS ARE			REV. NO.	



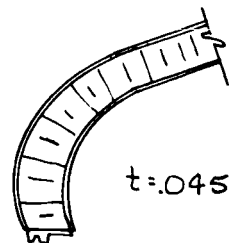
DETAIL A



DETAIL B



CASE	t
1.0	.126
1.1	.010
1.2	.050
1.3	.500



CASE 1.4

Figure 37 TOROIDAL SHELLS OF VARYING STIFFNESS

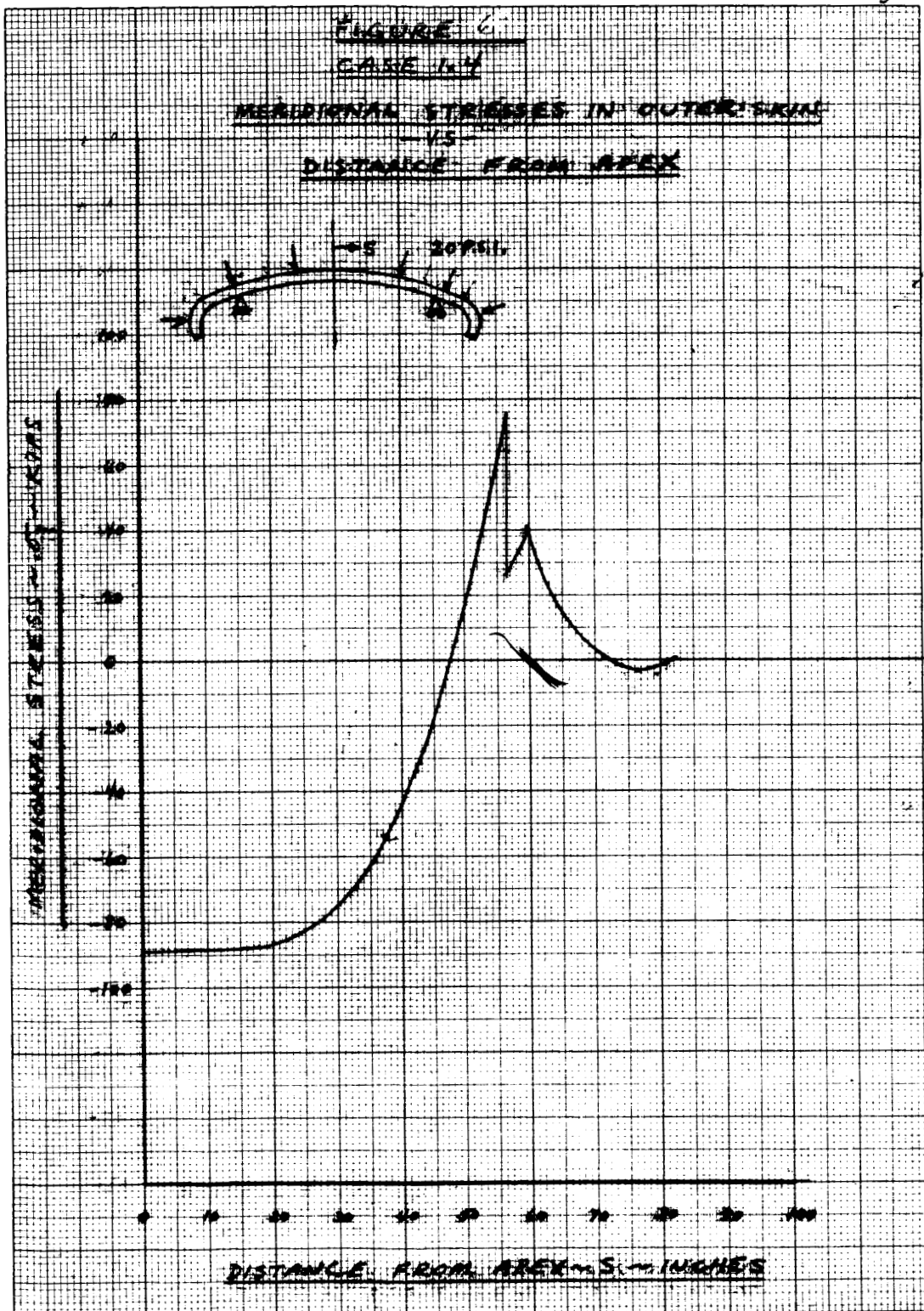


Figure 38 MERIDIONAL STRESSES IN OUTER SKIN VERSUS DISTANCE FROM APEX - CASE 1.4

~~CONFIDENTIAL~~

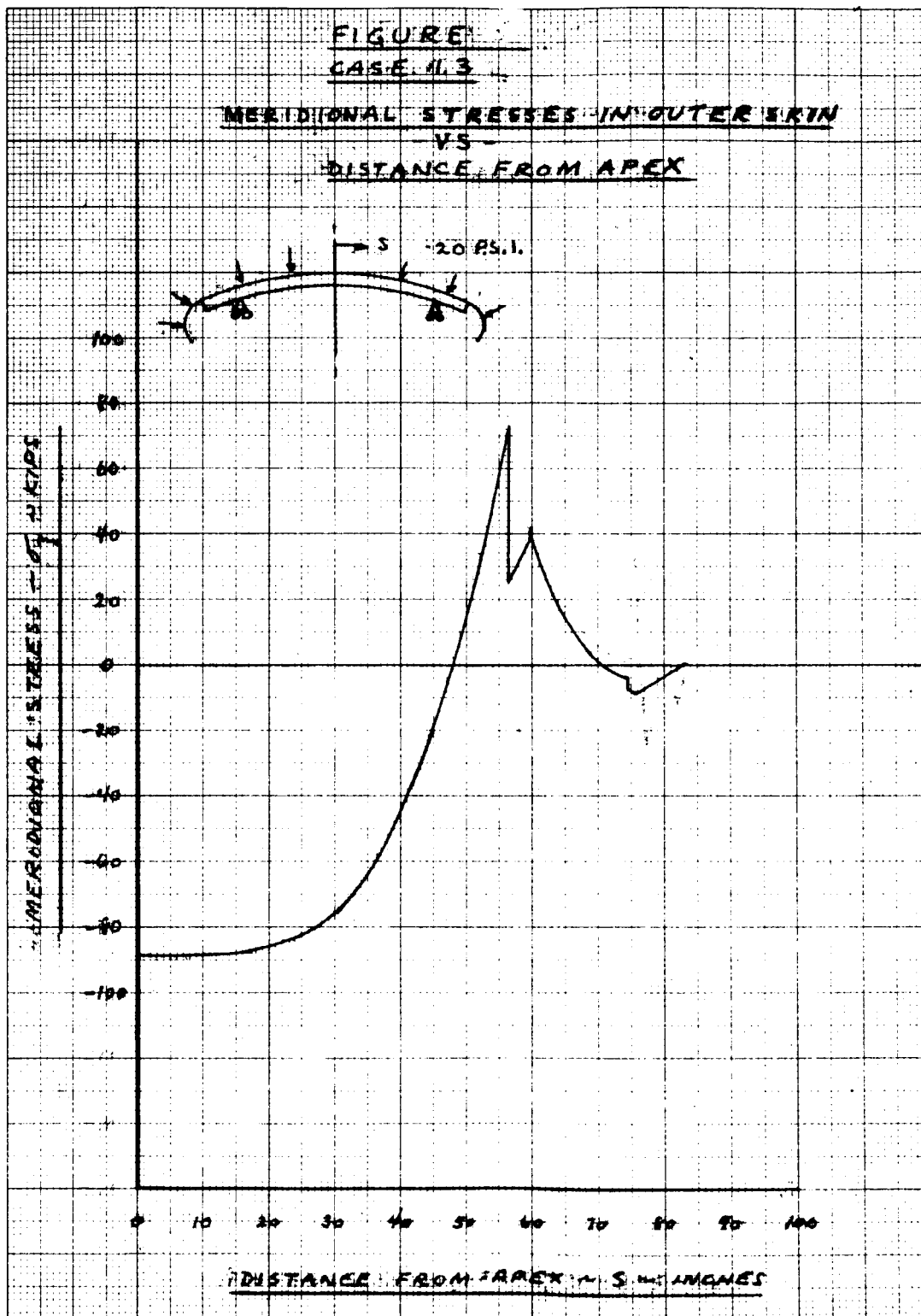


Figure 39 MERIDIONAL STRESSES IN OUTER SKIN VERSUS DISTANCE FROM APEX - CASE 1.3

~~CONFIDENTIAL~~

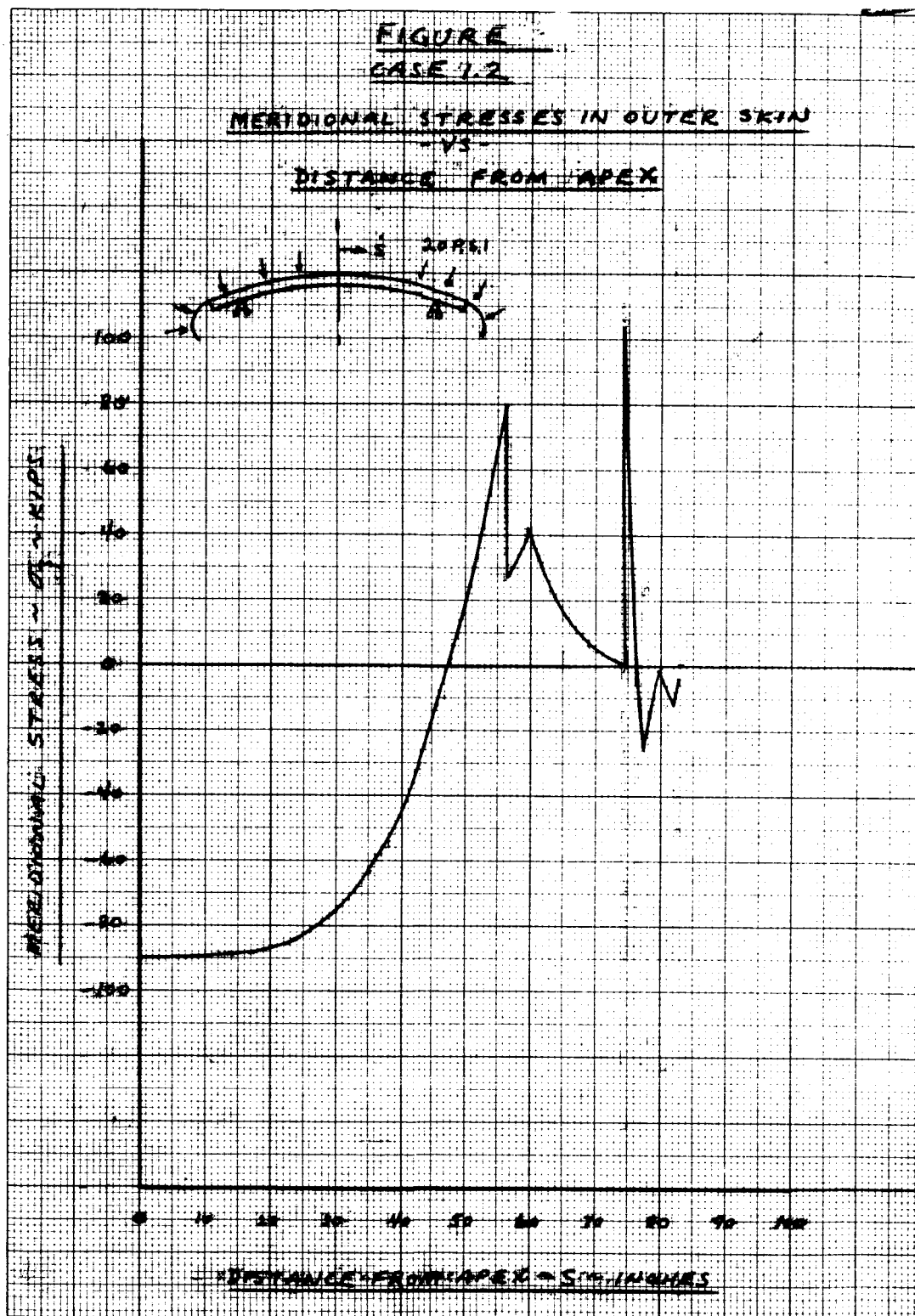


Figure 40 MERIDIONAL STRESSES IN OUTER SKIN VERSUS DISTANCE FROM APEX - CASE 1.2

~~CONFIDENTIAL~~

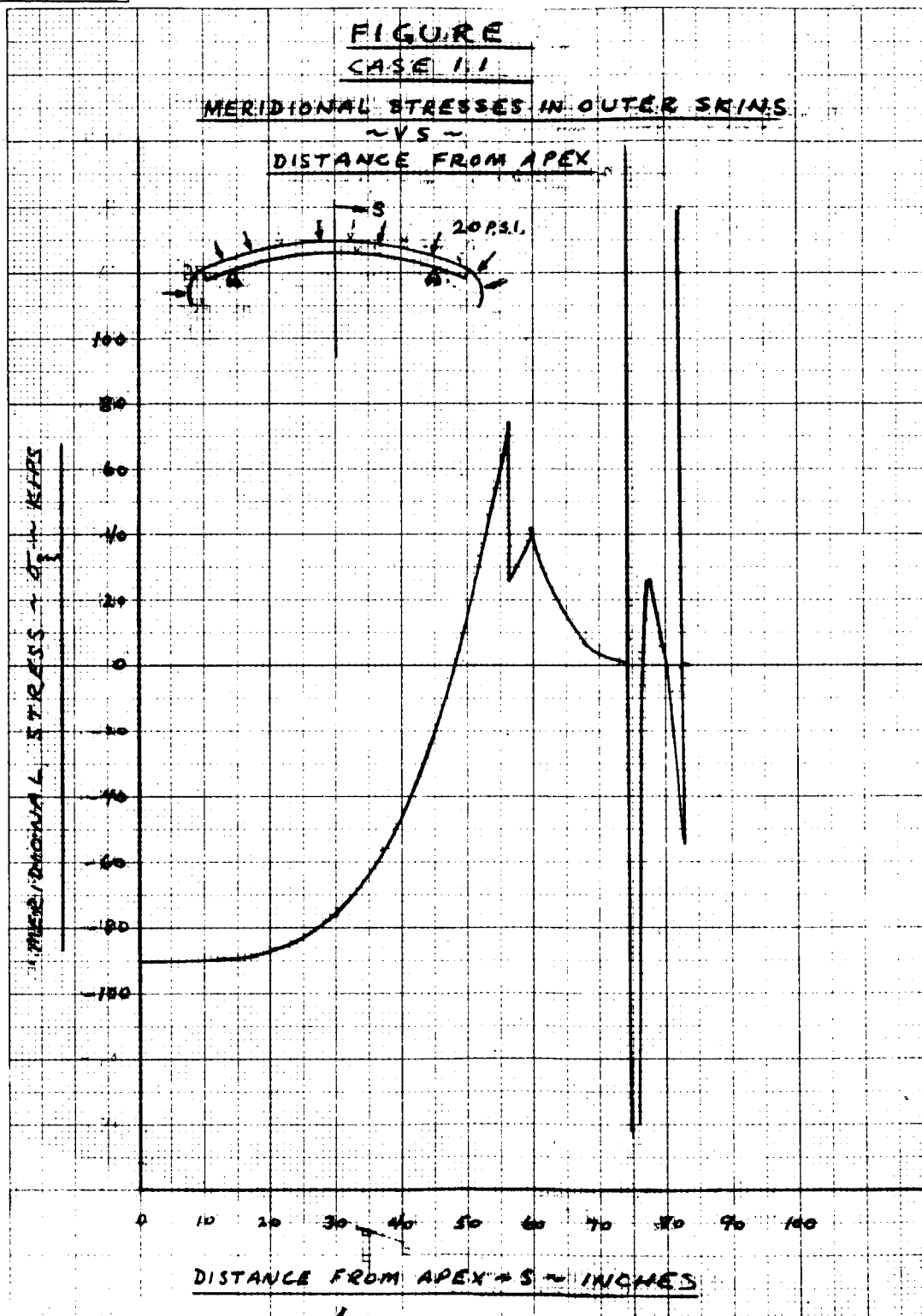


Figure 41 MERIDIONAL STRESSES IN OUTER SKIN VERSUS DISTANCE FROM APEX - CASE 1.1

~~CONFIDENTIAL~~

~~CONFIDENTIAL~~

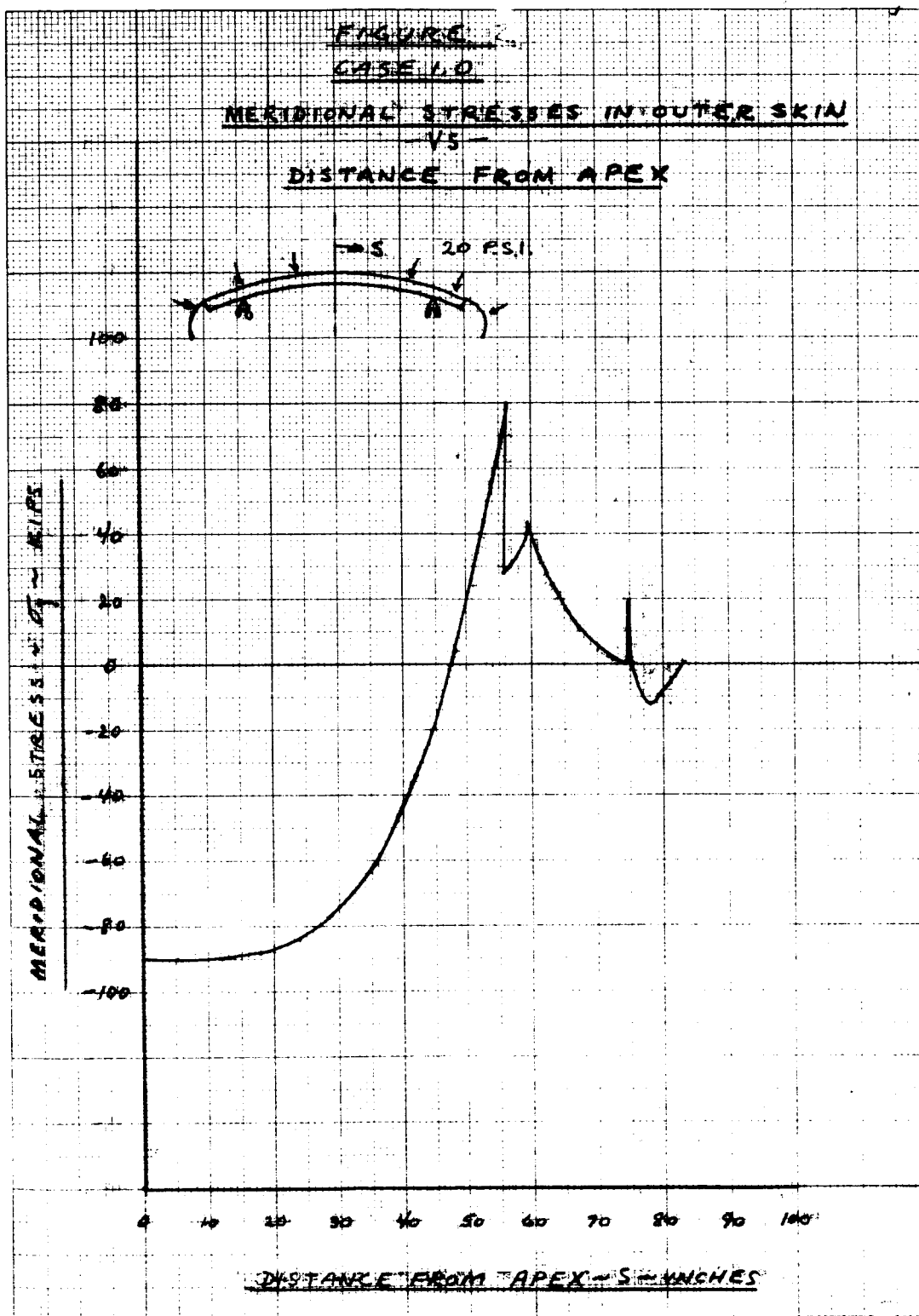


Figure 42 MERIDIONAL STRESSES IN OUTER SKIN VERSUS DISTANCE FROM APEX - CASE 1.0

~~CONFIDENTIAL~~

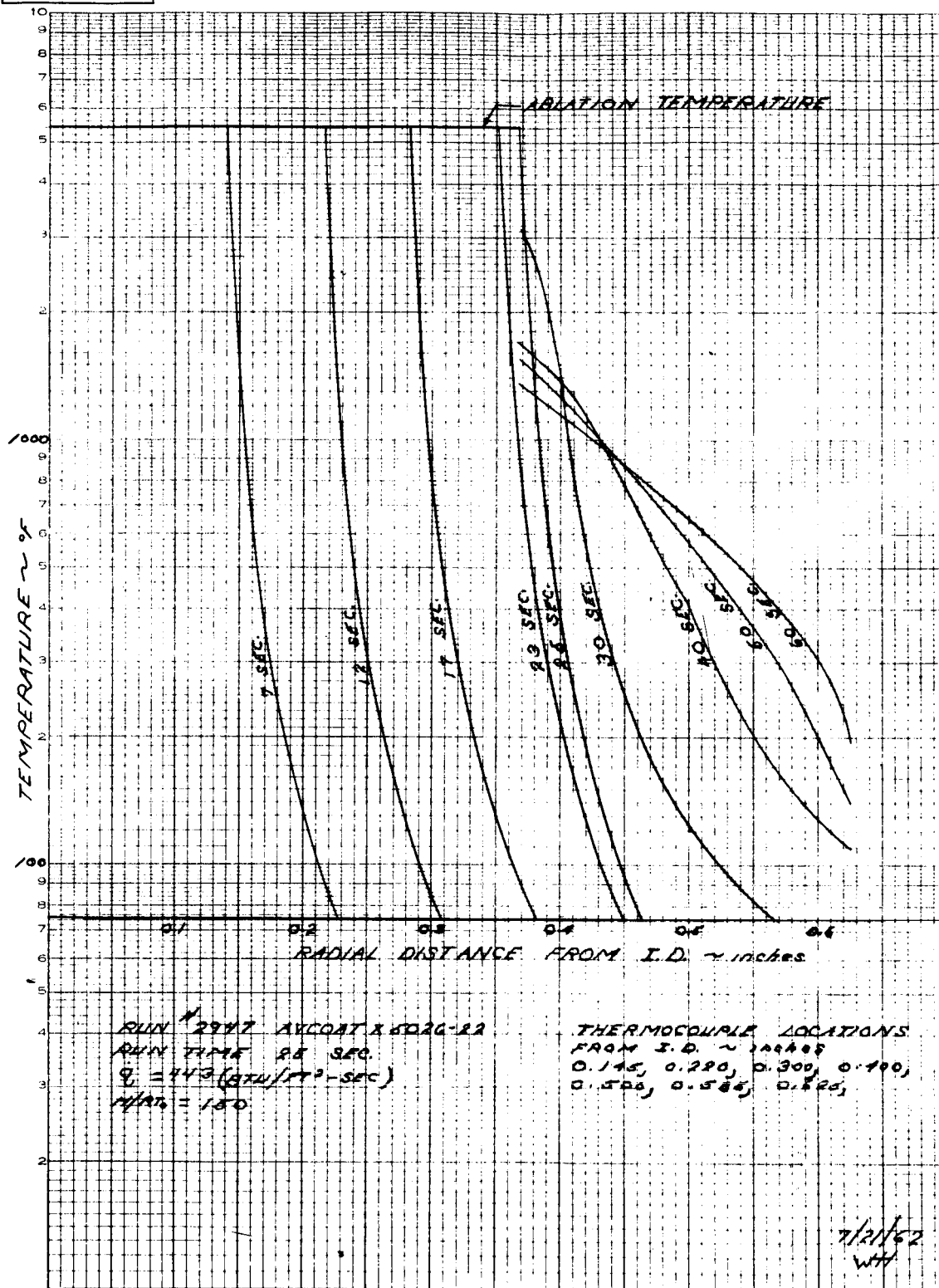


Figure 43 AVCOAT X5026 THERMAL GRADIENTS - RUN 2947

~~CONFIDENTIAL~~

Temperature-time histories for the various tests completed to date are being reduced from oscillograph recordings. No final plots are available at the present time.

Typical test specimens are shown in figures 44 and 45. Temperature gradients for runs 2963 (Avcoat X5026) and 2953 (Avcoat X5026) are shown in figure 46 and 47. Running conditions for the arc are shown on the figures. The problem of radiation effects on thermocouple installations had been recognized.¹⁰ A suitable additive must be found to block radiation without increasing ablation. All future tests planned for Avcoat 5019 tubes are suspended until the Materials Department has completed the evaluation of such additives.

4. Engineering Design

Layouts have been prepared showing proposed solutions to the following problem areas:

- a. Tile arrangements
- b. Typical access-door detail
- c. Typical rocket-motor aperture detail
- d. Details for reference fasteners
- e. Tile joints and gaps
- f. H/S Geometry

As soon as additional design or test information becomes available, this information will be evaluated and the layouts will be revised accordingly.

¹⁰RAD, Radiation Properties of Samos Materials before Ultraviolet or Thermal Degradation, Avco RAD-17-TM-60-63 (15 June 1960).

~~CONFIDENTIAL~~



Figure 44 TURBULENT TUBE SPECIMEN OF AVCOAT X5026

~~CONFIDENTIAL~~

AVCO
Research & Advanced Development

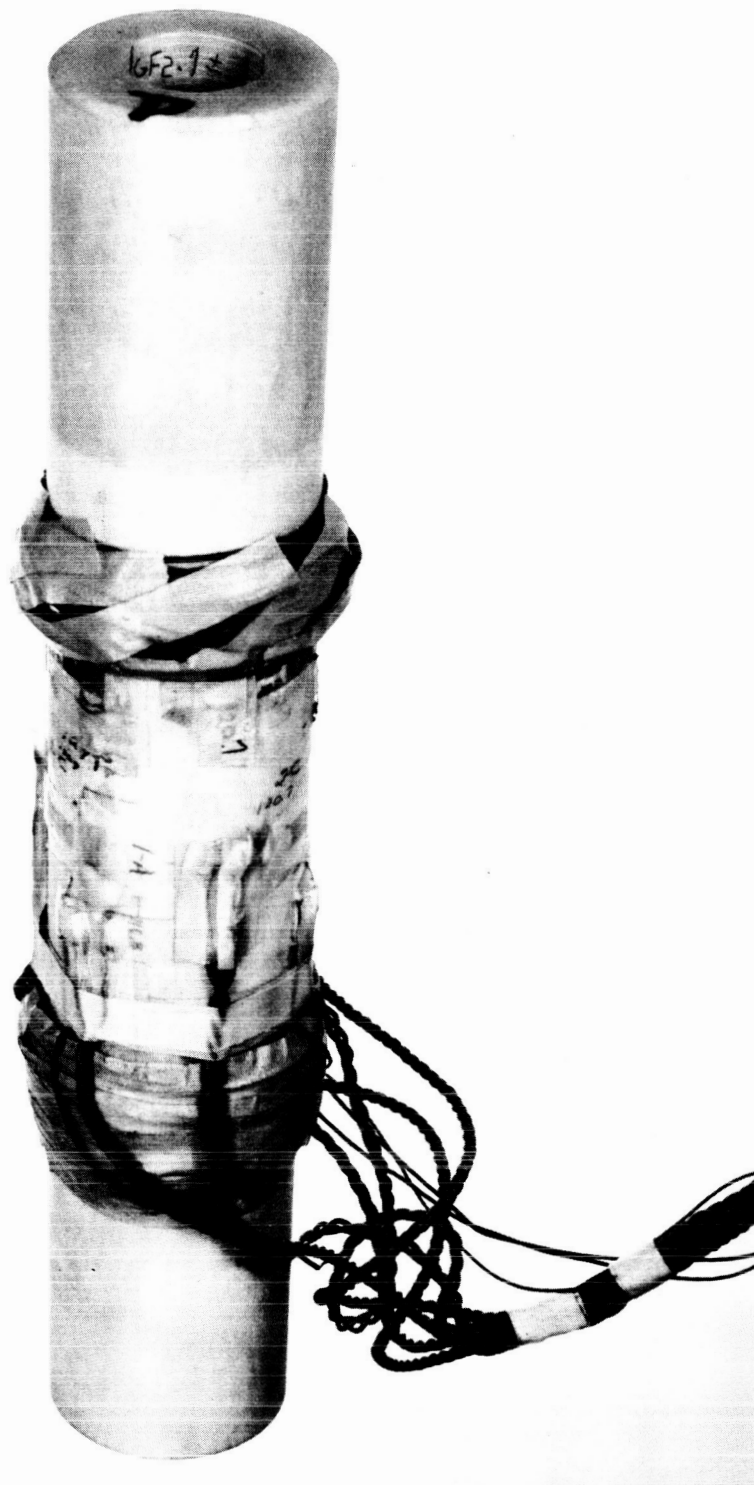


Figure 45 TURBULENT TUBE SPECIMEN OF AVCOAT X5019

~~CONFIDENTIAL~~

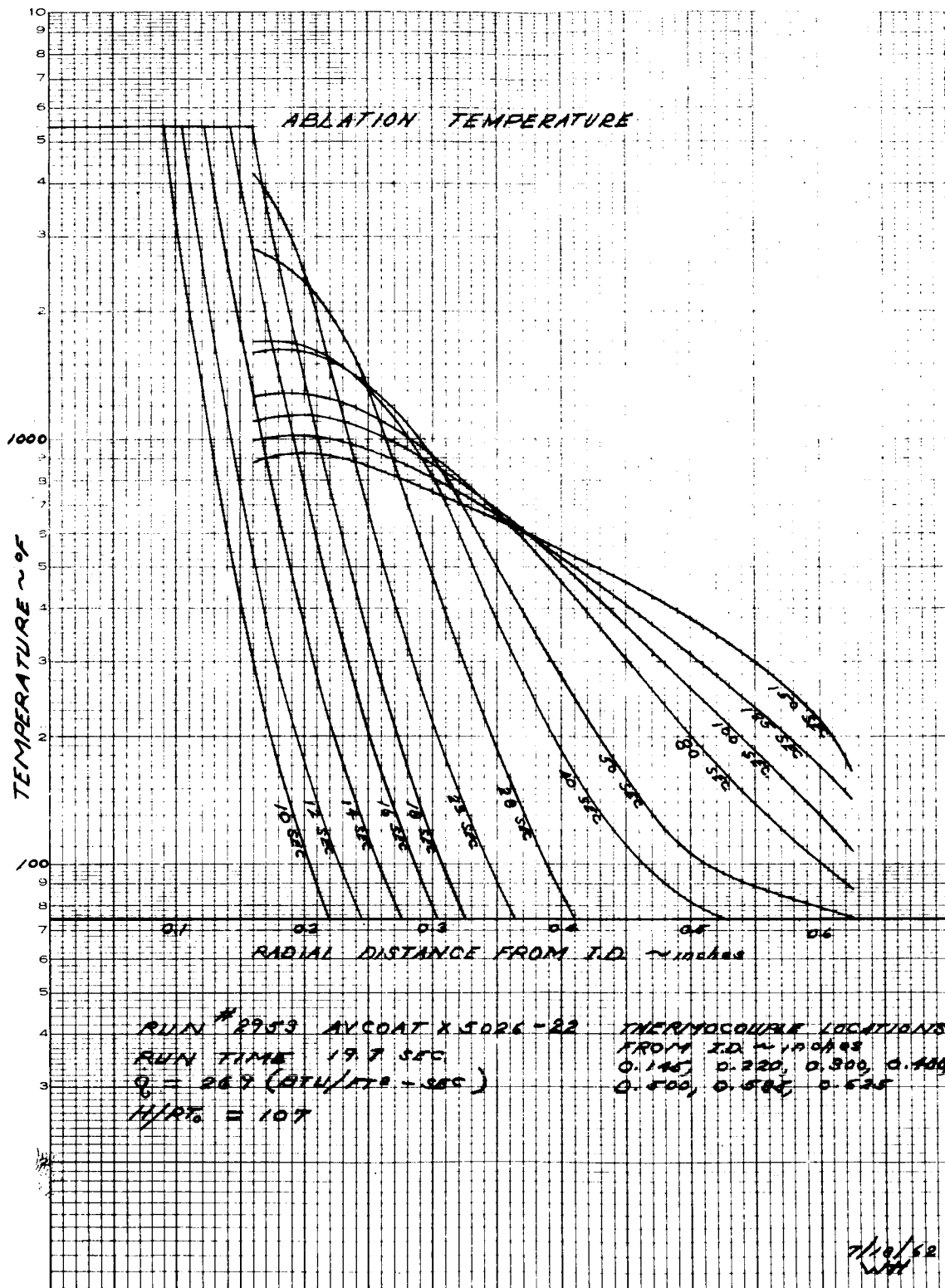


Figure 46 AVCOAT X5026 THERMAL GRADIENTS - RUN 2953

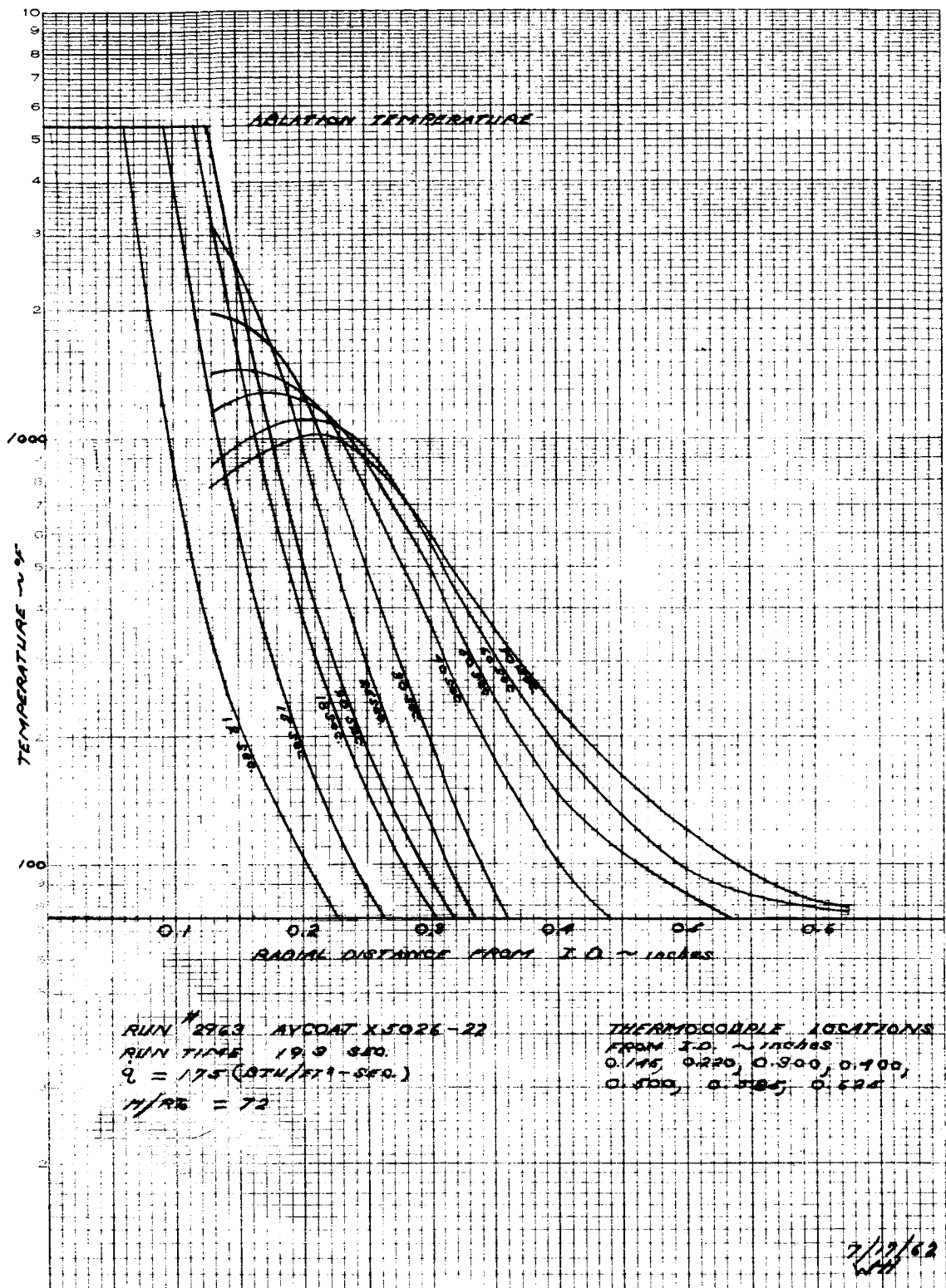


Figure 47 AVCOAT X5026 THERMAL GRADIENTS - RUN 2963

B. MATERIALS DEVELOPMENT AND EVALUATION

1. Materials Development

a. Weight Loss Studies

<u>Panel No.</u>	<u>Formulation No.</u>	<u>Postcure Period</u>	<u>Percent Volatiles</u>
133	X5026-22	None	3.86
75	X5026-22	Standard	2.07
133	X5026-22	Standard plus 16 hrs. at 350° F	1.35

Weight loss measurements were carried out on a 40-gram sample of ground material at 175°C and 20 mm Hg.

b. Benzene and Acetone Extractions of X5026-22 Material

<u>Panel No.</u>	<u>Postcure</u>	<u>Percent Weight Loss</u>	
		<u>Benzene</u>	<u>Acetone</u>
75	Standard	1.30	2.03

Extractions were carried out on approximately 30 grams of ground sample for 6 hours in a Soxhlet extraction apparatus.

The weight loss in acetone agrees quite well with the weight loss in heat and vacuum. Infrared analysis of the extractions indicated the presence of degradation products of polysebacic anhydride. Further analysis will be made.

c. Dry-blended Specimens (Glass and Silica Microballoons)

The dry-blended specimens made up using the glass and silica microballoons all had high densities compared both to the phenolic microballoon formulations and to their theoretical densities. Specimens molded at 125 psi showed densities between 15 and 20 percent higher than theoretical. At a molding pressure of 180 psi, phenolic microballoon formulations gave densities less than, or equal to, theoretical. This indicates that the silica and glass balloons are fragile and break very easily resulting in higher densities. Density comparisons are as follows:

Disc No.	Balloon Type and Content	Theoretical Density (gm/cc)	Actual Density (gm/cc)	Molding Pressure (psi)
DB-3	Phenolic, 30%	0.570	0.487	90
DB-4	Phenolic, 30%	0.570	0.580	180
DB-9	Glass, 30%	0.860	1.008	125
DB-11	Silica, 30%	0.667	0.958	125

d. Dry-blended Specimens (Chopped Glass)

Dry-blended specimens were fabricated containing 30- and 40-percent, 1/4-inch chopped glass by weight with a constant phenolic microballoon content. Molding at 125 psi, the 30 percent fiber specimen had a density of 0.686, and the 40-percent fiber specimen had a density of 0.552.

The 40-percent fiber specimen appeared to be excessively dry resulting in the low density. The 30-percent fiber specimen did not appear to be fiber rich and showed satisfactory balance of constituents.

e. Gellation

Gellation of the standard 5026-22 resin system was accomplished at 250°F. After immediate cooling, the material was ground into powdered form with dry ice in the Waring blender. This work demonstrated the feasibility of taking the standard X5026-22 resin system and converting it by gellation for use in a dry-blended formulation.

Table IV shows the effect of adding a low-viscosity epoxy resin diluent to three of the current high-viscosity resin systems being studied for Avcoat X5019. This material is seen to be an effective viscosity-reducing agent. This should be of material value in assisting the uniform impregnation of the felt. Its effect on ablation performance must be evaluated, however.

TABLE IV

EFFECT OF DILUENT ON HIGH-VISCOSITY RESINS

Ratio of Resins to Added Diluent	Viscosity at 25°C (cps)		
	75/25	50/50	25/75
Resin I - charring epoxy	36,400	2,090	265
Resin II - flexible system	6,090	1,250	260
Resin III - flexible system	7,106	4,130	350

~~CONFIDENTIAL~~

2. Results of Physical Tests

TABLE V

TENSILE STRENGTH OF MODIFIED DC-731 AS A FUNCTION OF
BORAX CONCENTRATION AND CURE TEMPERATURE

Concentration of Borax ($\frac{\text{g Borax}}{\text{g 731}}$)	Conditions of Heat-Treatment		Ultimate Tensile Strength (psi)
	Time (hr)	Temperature (°F)	
0.0388	1.0	at 140	201
0.0070	1.0	140	249
0.0338	0.5	140	176
0.0676	0.5	140	225
0.0338	1.0	120	219
0.0676	1.0	120	228
0.0338	0.5	120	52
0.0676	0.5	120	176
Controls (no borax), two specimens:			195
			229

TABLE VI

TENSILE STRENGTH (SINGLE LAP SHEAR) OF DC-601 BONDED
TO PRIMED PH 15-7 MO STAINLESS STEEL

Specimen Number	Test Temperature (°F)	Ultimate Shear Strength (psi)
3004	76	210
3005	77	220
3006	76	208
3007	76	170 avg.
3008	-100	1180
3009	-100	1010
3010	No test	-
3011	-100	1210 avg.
	Temperature to failure at 20 psi	Load (psi)
3012	695 °F	20
3013	650	20
3014	665	20
3015	702	20

~~CONFIDENTIAL~~

~~CONFIDENTIAL~~

As shown in figure 48, there is no apparent correlation of moisture absorption with interconnected porosity. Engineering curves of tensile properties of X5026-22 have been completed and are included as figure 49. It therefore is assumed that one or more of the components in X5026-29 is hygroscopic. Identification of this component or components will be attempted. As is shown by the graph, the moisture expansion coefficient is significant and exhibits no tendency to decrease even after long periods of time. Table VII gives an analysis of microballoons.

TABLE VII
ANALYSIS OF MICROBALLOONS

Sample	Volatiles	Sinkers	Density
	3 hrs. (16 hrs.) 350°F		
Phenolic, Lot C303E			
Bag 2	5.45 (7.09)	3.05	0.256
Bag 10	2.37 (4.51)	2.86	0.252
Bag 22	5.39	4.05	0.250
Phenolic, Lot C 350P			
Bag 22	4.89	3.04	0.248
Phenolic			
Dried 305°F/10mm. Hg.	1.71	3.00	0.249
Urea, Lot G 144			
Bag 9 (open)	10.75	0.00	0.277
Eccospheres	moisture, 220°F		
R	0.018	27.5	0.4952
SI	1.825	6.1	0.2467

~~CONFIDENTIAL~~

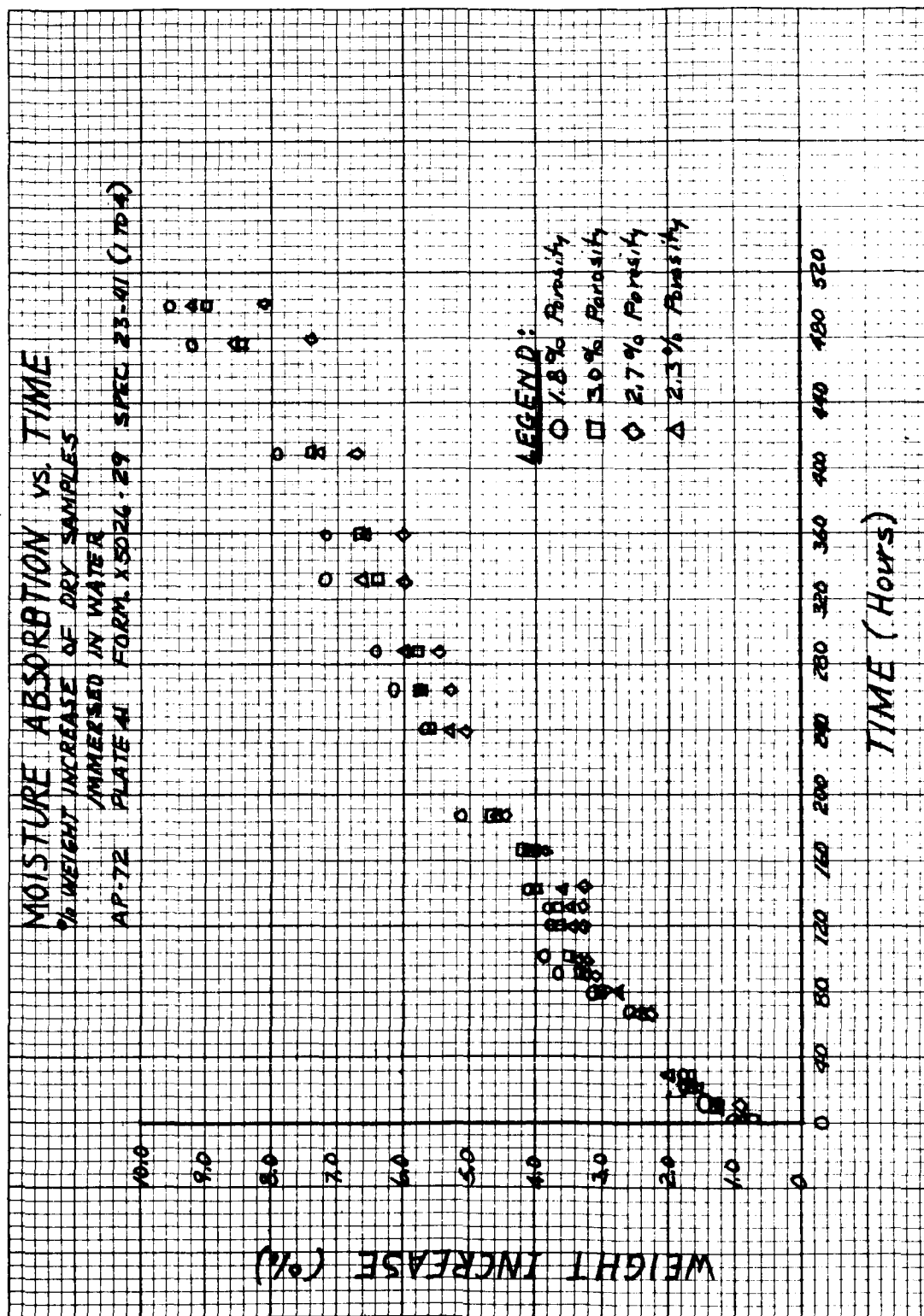


Figure 48 MOISTURE ABSORPTION VERSUS TIME

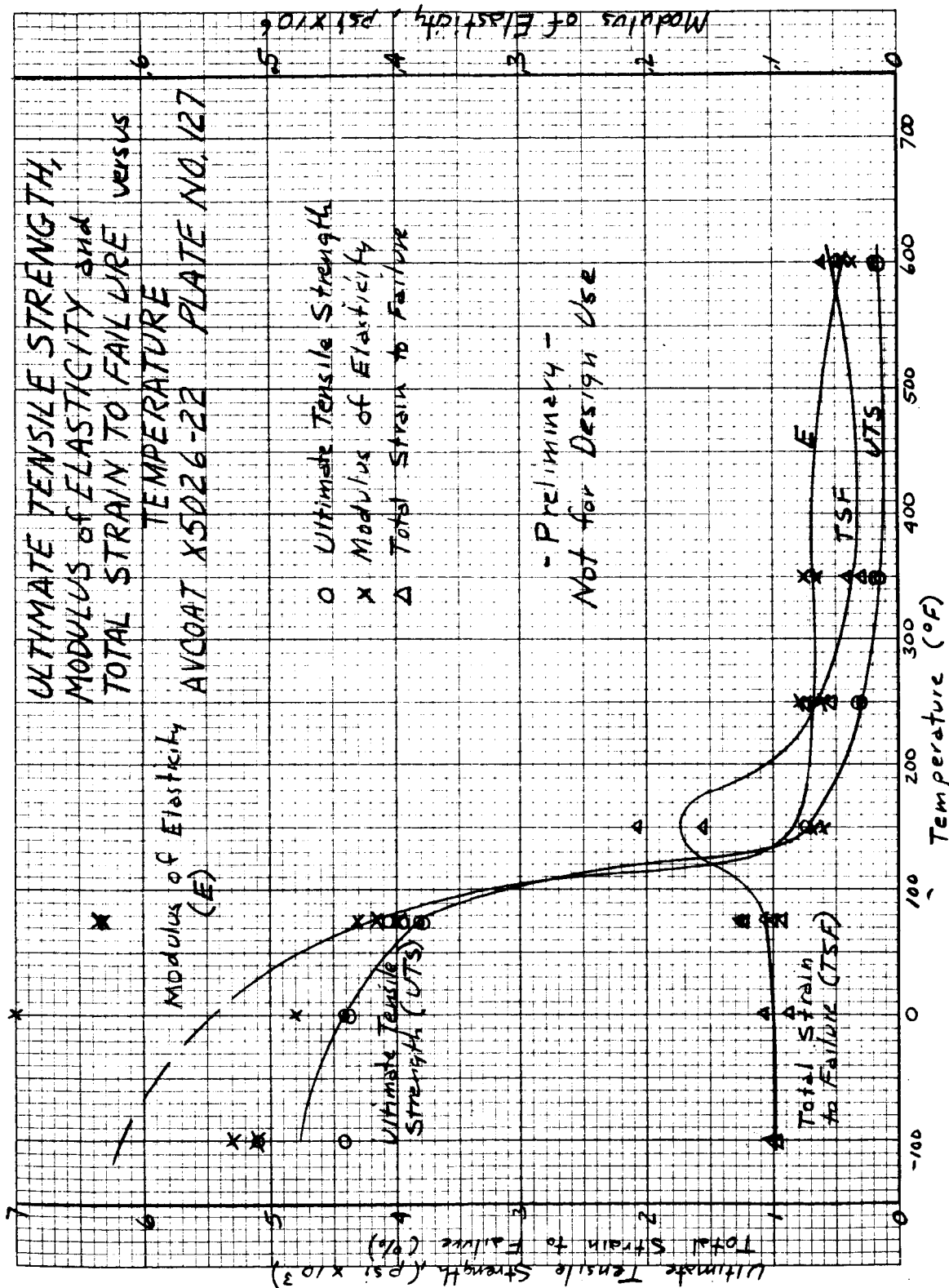


Figure 49 ULTIMATE TENSILE STRENGTH, MODULUS OF ELASTICITY,
AND TOTAL STRAIN TO FAILURE VERSUS TEMPERATURE

3. Materials Evaluation

To date the following groups of Avcoat X5026 have been tested and partially reported. They are:

AP - 15	Plate - 2	Formulation - 22
AP - 21	Plate - 9	Formulation - 29
AP - 27	Plate - 10	Formulation - 29
AP - 33	Plate - 13	Formulation - 22
AP - 39	Plate - 16	Formulation - 22
AP - 1	Plate - 47	Formulation - 22
AP - 8	Plate - 50	Formulation - 22
AP - 45	Plate - 66	Formulation - 30

The first seven groups of samples gave nearly the same thermochemical heats of ablation (q^*). The last group (AP - 45) composed of samples cut from the parallel and transverse directions of the plate were tested at nearly the same conditions. The values of the q^* are about the same. Although no statistical evaluation has been performed, it appears that the two do not differ from each other. The quantity of emitted radiation is less for these samples (ablation rate is the same) than for the previous samples, so the q^* increased, and this group does show a difference in q^* level from the samples tested earlier. The chemical composition of the samples is slightly different. The increase of fiberglass and deletion of refrasil may have caused the radiation to decrease; however, a flame retarder was also added and this may have some effect.

The hot wall correction was made by taking the measured values of spectral emittance at 0.65 micron for several groups of samples and correcting the surface brightness temperatures to true temperatures for the ablating samples. The brightness temperature was measured with a manual (disappearing-filament type) pyrometer. The total radiation was also measured, so the value of total emittance of the sample can be determined from the Stefan-Boltzmann equation. This value of total emittance was used to get the true temperature for each sample in all the later tests from the measured radiation value.

In a past report it was noted that there was a discrepancy between the manual and the recording pyrometers. It has been found that the manual pyrometer employs a filter that covers a wide wavelength band, while the recording instrument responds to a narrow band of radiation. These numbers from the recording pyrometer would appear to be the more accurate since the band is very narrow (around 0.65 micron). When the pyrometer is completely calibrated, the results will be incorporated in the analysis. The value of emittance may change slightly. If so, then it will be necessary to recorrect the hot-wall heat flux, therefore changing the q^* values.

~~CONFIDENTIAL~~

The ablation rates obtained from the silhouette movies varied by a small amount from the length-loss rates, but the additional correction was not made at this time. If the heat flux has to be recorrected, the film ablation rate will be used to obtain the q^* values.

The values of density (ρ), laminar transpiration factor (η_L), q^* at 200 RT_O, and q_r at 200 RT_O are:

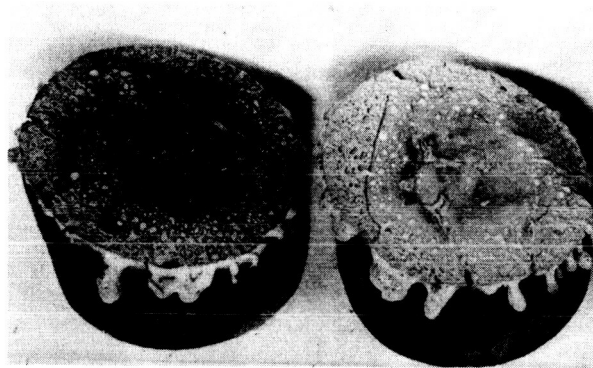
Code No.	η_L	q^* (Btu/lb)	(lb/ft ³)	q_r (Btu/ft ² sec)
AP1	0.87	5900	58	470
AP8	0.82	5900	58	470
AP45	1.20	7600	54	380

Figures 50 to 67 present the results of the present series of tests. All samples were 1-1/2 inches in overall diameter. The reference material in all these tests was X5026-22. Figures 50 and 51 present overall views of two test samples in which the phenolic microballoons of the standard X5026 formulations have been replaced by silica microballoons. The cracks in the char layer (and virgin material), as well as the deep char, are decidedly worse than in a comparable X5026 test sample (refer to previous progress report). Figures 52 and 53 present the test results on repeated tests on lower density ($\rho = 0.73$) X5026-22. These samples performed in a similar manner as those reported in the previous progress reports. Figures 54 and 55 present the test results on X5026 formulation having no phenolic microballoons. No improvement over the standard formulation is evident.

Figures 56 and 57 present the test results on three samples of X5026 where each was produced from approximately the same formulation, but different fabrication techniques which resulted in a different density of the material. From figure 57 the lowest density material had the larger ablation based on dimensional change. However, the cracks in the char were almost entirely eliminated. Further tests on this low density X5026 are planned. Figures 58 to 61 present results on silica-based materials containing either phenolic or epoxy impregnants. Although no cracking of the char is evident in any of these tests the char depth is greater than that in the standard X5026 material tests under the same conditions (Fig. 57).

Figures 62 and 63 present the test results on a foamed silica composite. Sample 4 (Figs. 62 and 63) showed excellent ablation characteristics (no cracking or other detrimental characteristics). The impregnated foamed silica (sample 3, Figs. 62 and 63) cracked during the test. No comparison from these tests can be made of the relative insulating qualities of foamed glass with that of X5026.

~~CONFIDENTIAL~~



A-1

A-3

Figure 50 OVERALL VIEW OF TESTED OVERS SAMPLES A-1 (PL148) AND A-3 (PL148) (sample composition similar to X5026-22, except phenolic microballoons have been replaced by silica microballoons)

Sample No.	Time (min)	Enthalpy (Btu/lb)	Heat Flux (Btu/ft ² -sec)
A-1 (PL148)	2	19,400	370
A-3 (PL148)	2	19,200	360
	2 (out)		
	5	8,000	44

~~CONFIDENTIAL~~



Figure 51 PHOTOMICROGRAPH OF HALF SECTION OF SAMPLE A-1 (LEFT)
AND SAMPLE A-3 (RIGHT) (refer to figure 50 for sample identification)

~~CONFIDENTIAL~~

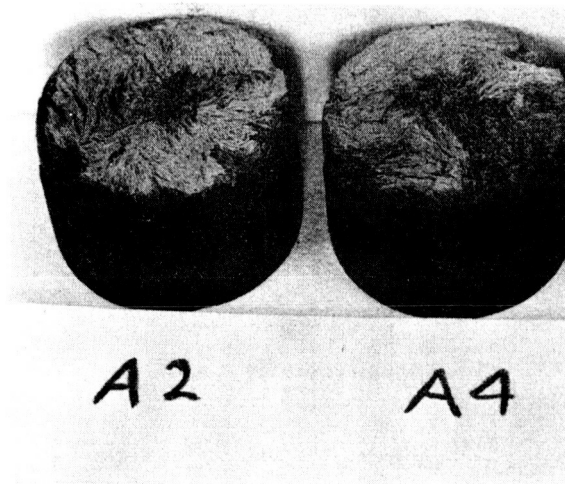


Figure 52 OVERALL VIEW OF OVERS TESTED SAMPLES A-2 AND A-4
(above samples (X5026-22B) had similar composition to X5026-22
but were less dense (S. G. = 0.73 vs S. G. = 9 for X5026-22)

Sample	Time (min)	Enthalpy (Btu/lb)	Heat Flux (Btu/ft ² -sec)
A-2	4	8400	39
A-4	4	8600	42

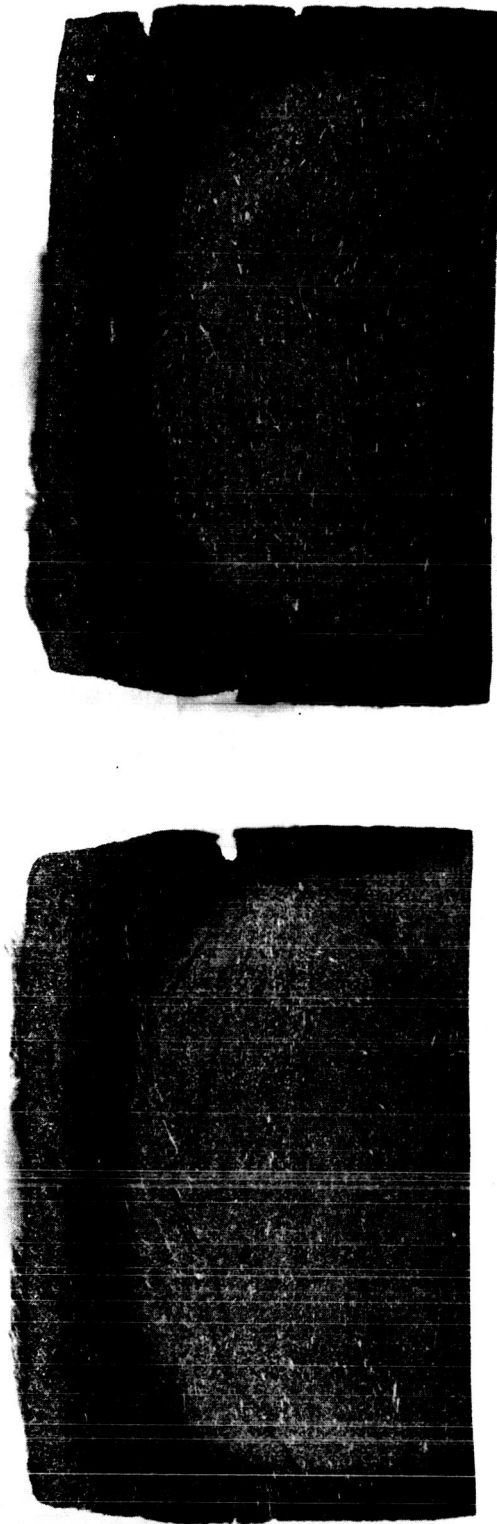


Figure 53 PHOTOMICROGRAPH OF HALF SECTION OF X5026-22B TEST
SAMPLES A-2 (LEFT) AND A-4 (RIGHT) (refer to figure 52 for
sample identification)

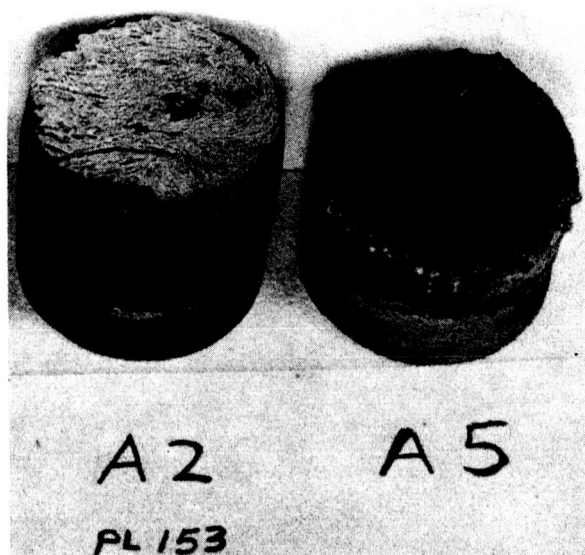


Figure 54 OVERALL VIEW OF OVERS TEST SAMPLES (PL 153) A-2 AND A-5 MATERIAL (similar to 5026-22 except phenolic microballoons omitted from formulation)

Sample	Time (min)	Enthalpy (Btu/lb)	Heat Flux (Btu/ft ² -sec)
A-2((PL 153)	4	8800	41
A-5 (PL 153)	2	19,000	390

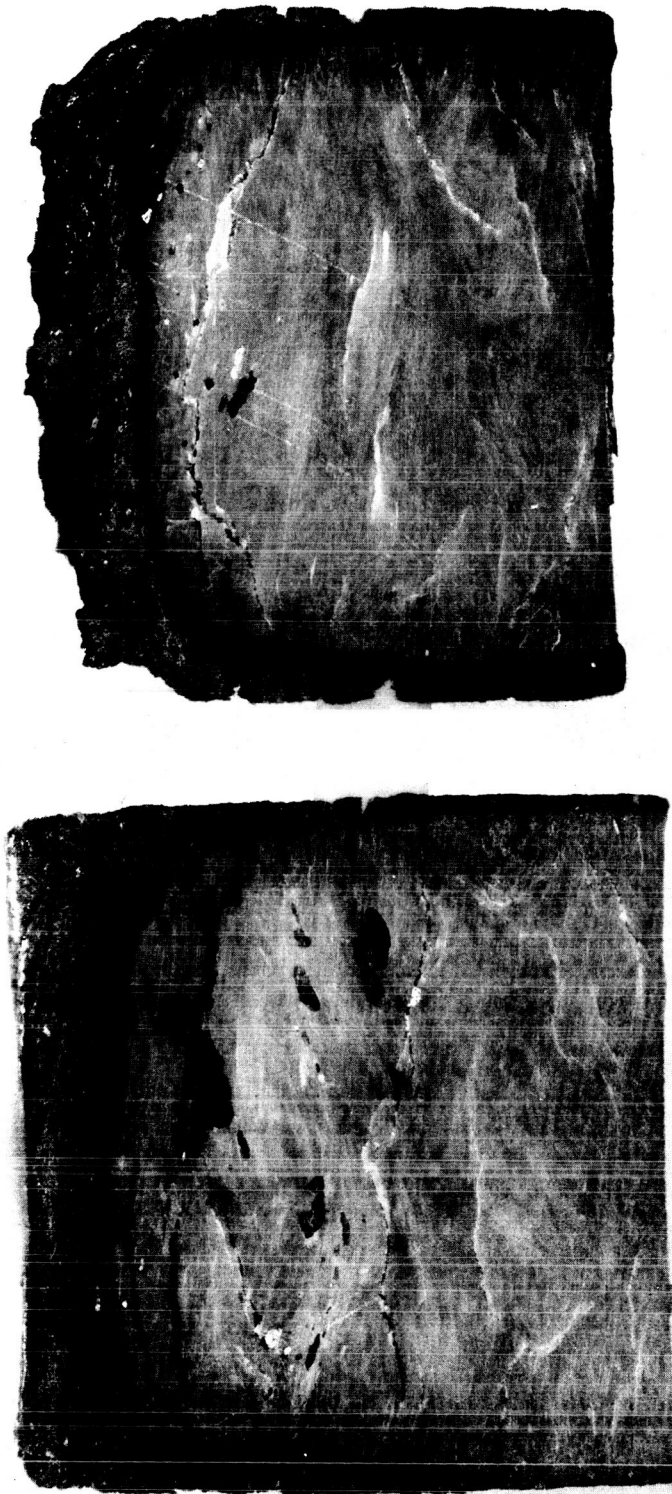
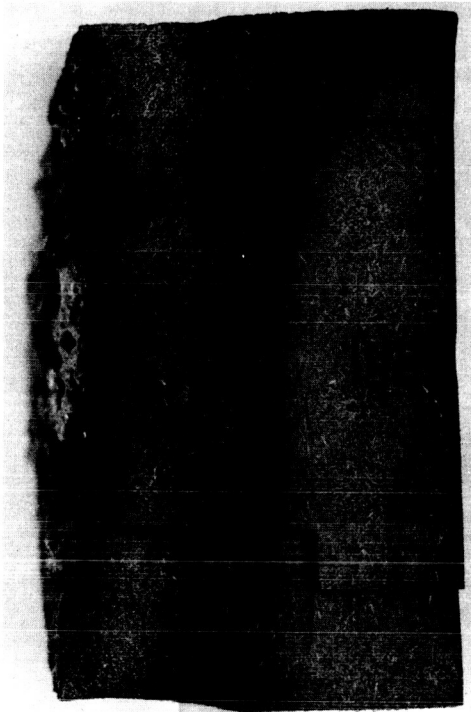


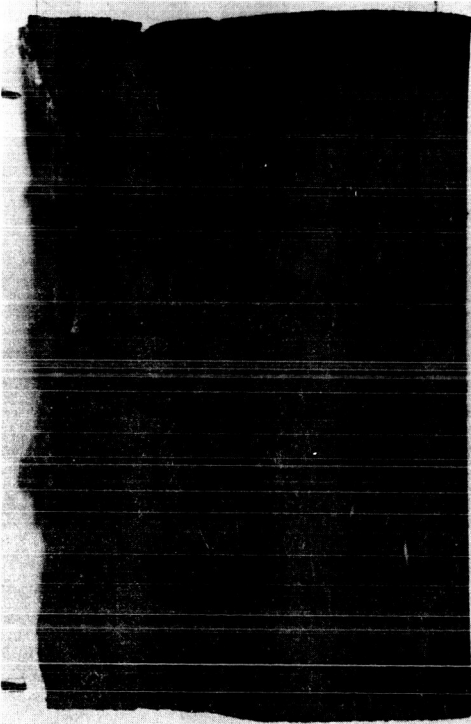
Figure 55 PHOTOMICROGRAPHS OF HALF SECTION OF TEST SAMPLES
(PL 153) A-2 (LEFT) AND A-5 (RIGHT) (refer to figure 54 for
sample identification)



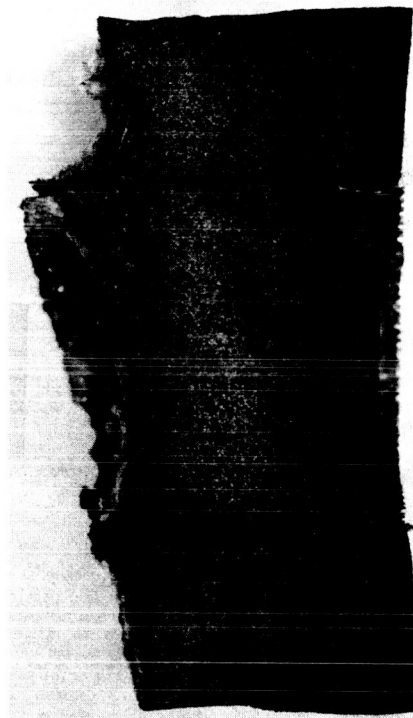
Figure 56 OVERALL VIEW OF OVERS TESTED SAMPLES A-3 (X5026-22B, S.G. 6 0.73), PL-2 (5026-22 AND DB3 (X5026, S.G. = 0.487) (the samples were tested at an enthalpy and heat flux of 6800 Btu/lb and 73 Btu/ft-sec, respectively for 8 minutes)



-B-



-A-



-C-

Figure 57 PHOTOMICROGRAPHS OF
HALF-SECTION OF TESTED
SAMPLES A-3 (A), PL-2 (B)
AND DB 3 (C) (refer to
figure 56 for sample
identification)

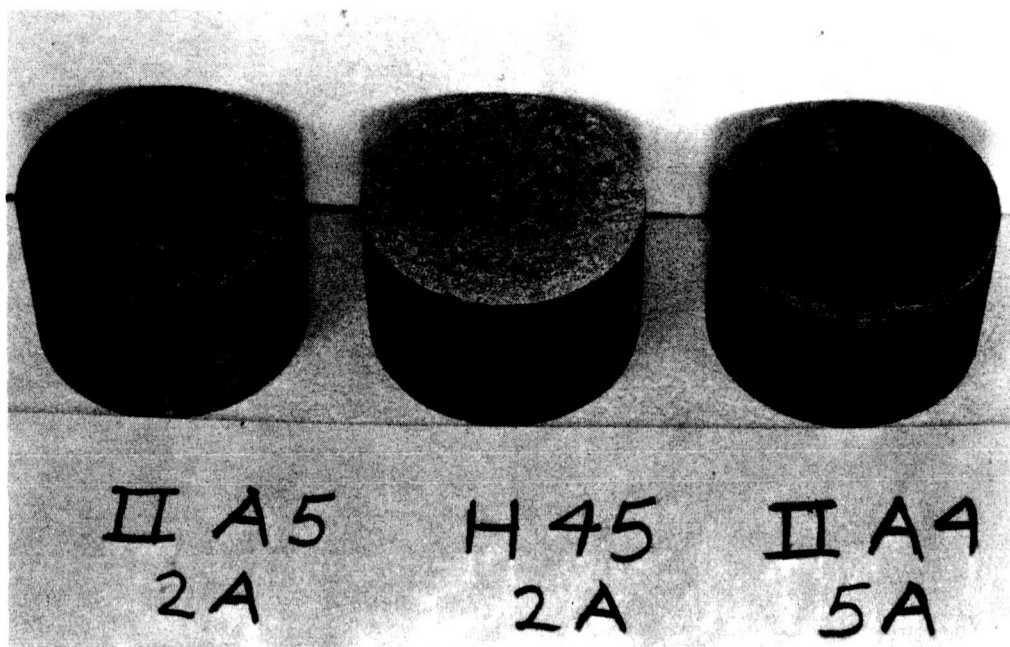
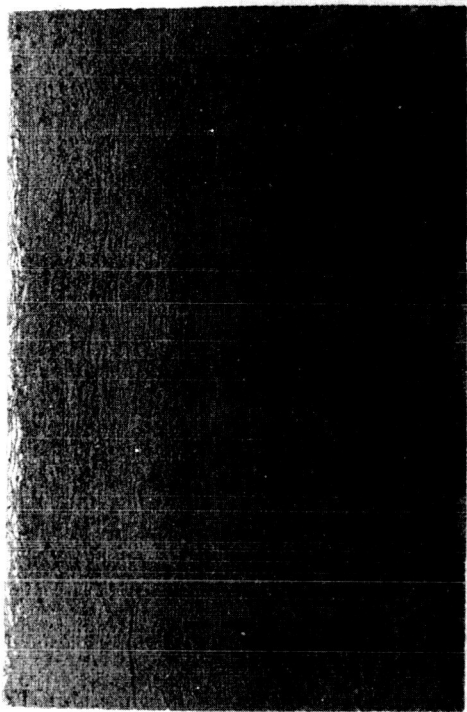


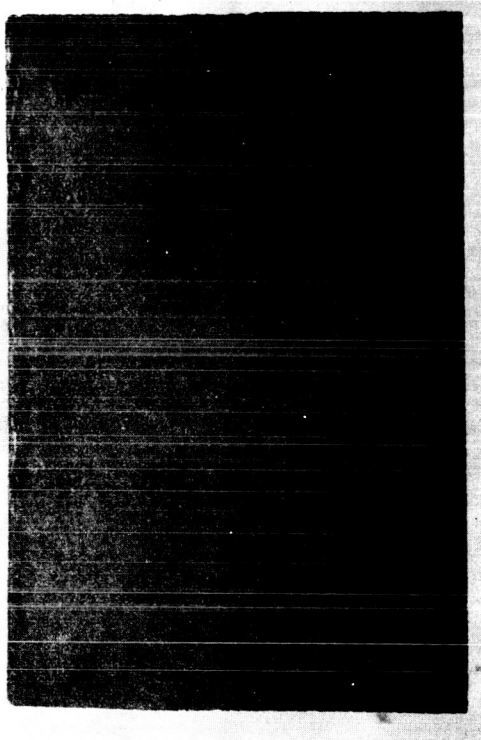
Figure 58 OVERALL VIEW OF OVERS TESTED SAMPLES II A5-2A, H45-2A, and II A4-5A

Sample	Composition	Time (min)	Enthalpy (Btu/lb)	Heat Flux (Btu/ft-sec)
II A5-2A	15% Ecco spheres + phenolic (S. G. = 0.85)	8	6800	73
H45-2A	15.5% Ecco spheres + glass, rock slips and phenolic, (S. G. = 0.82)	8	6800	73
II A4-5A	8% Ecco spheres + phenolic (S. G. = 0.99)	8	6800	73

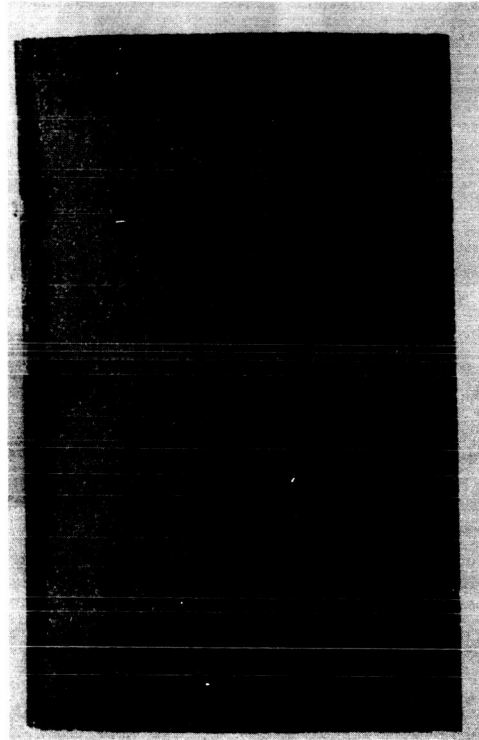


-B-

Figure 59 PHOTOMICROGRAPH OF
HALF SECTION OF TESTED
SAMPLES II A5-2A (A),
H45-2A (B), AND II
A4-5A (C) (refer to
figure 58 for sample
identification)



-A-



-C-

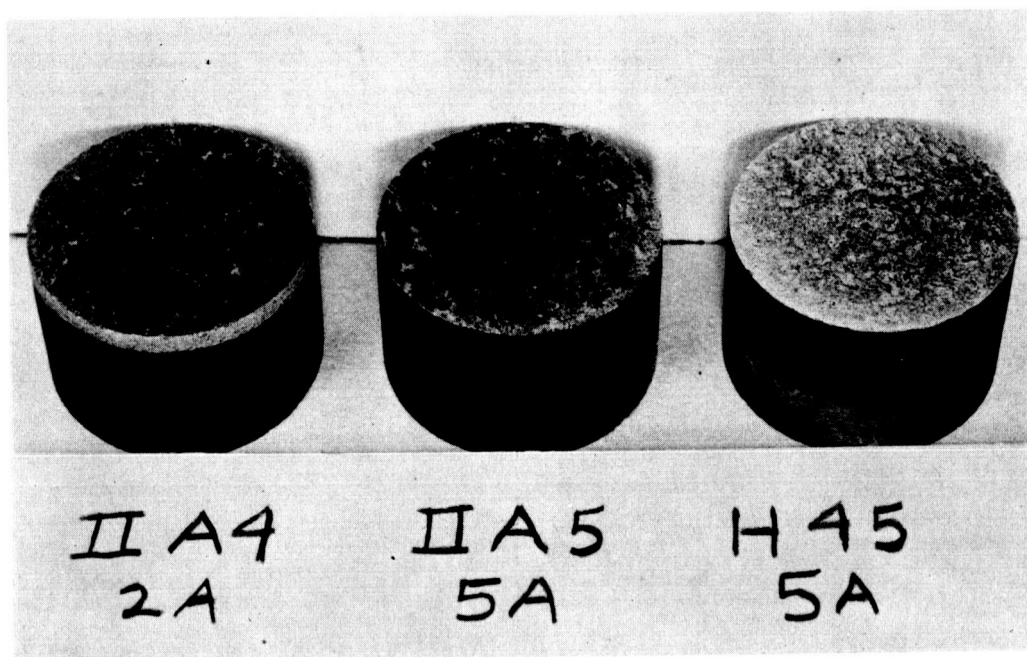
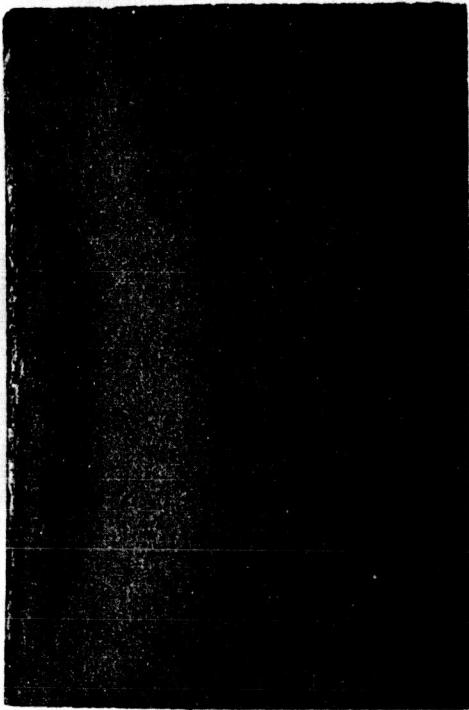


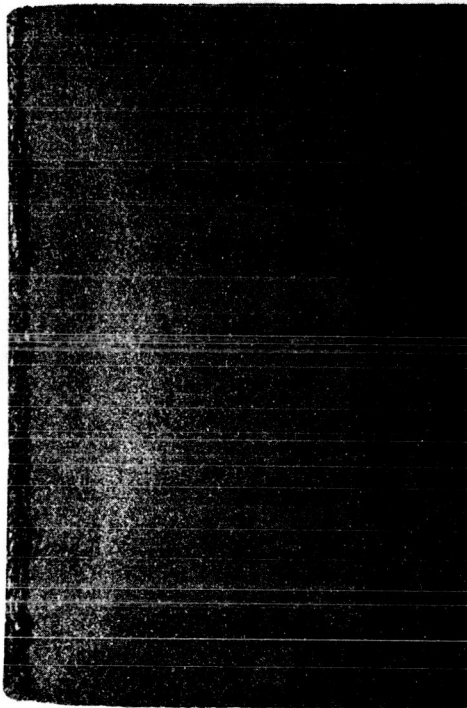
Figure 60 OVERALL VIEW OF OVERS TESTED SAMPLES II A4-2A,
II A5-5A, AND H45-5A

Sample	Composition	Time (min)	Enthalpy (Btu/lb)	Heat Flux (Btu/ft-sec)
II A4-2A	8% Ecco spheres plus epoxy (S. G. = 1.04)	8	6800	73
II A5-5A	15% Ecco spheres plus epoxy (S. G. = 0.92)	8	6800	73
H45-5A	15.5% Ecco spheres plus glass rock slip and epoxy (S. G. = 0.84)	8	6800	73

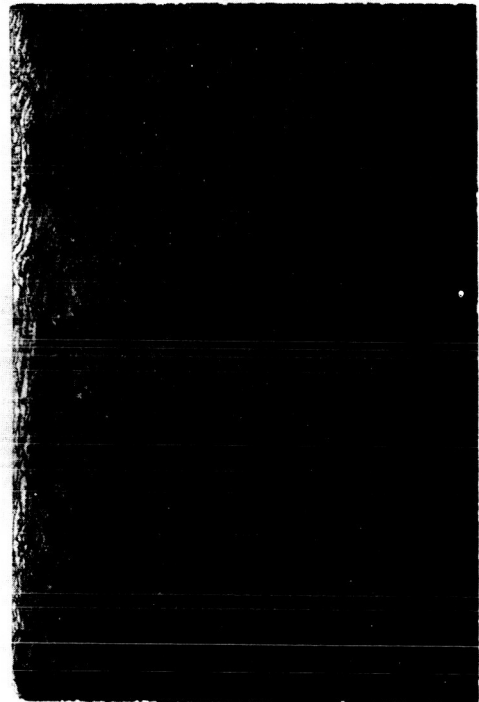


-B-

Figure 61 PHOTOMICROGRAPHS
OF HALF SECTION OF TESTED
SAMPLES II A4-2A (A), II A5-5A
(B) AND H45-5A (C) (refer to
figure 60 for sample
identification)



-A-



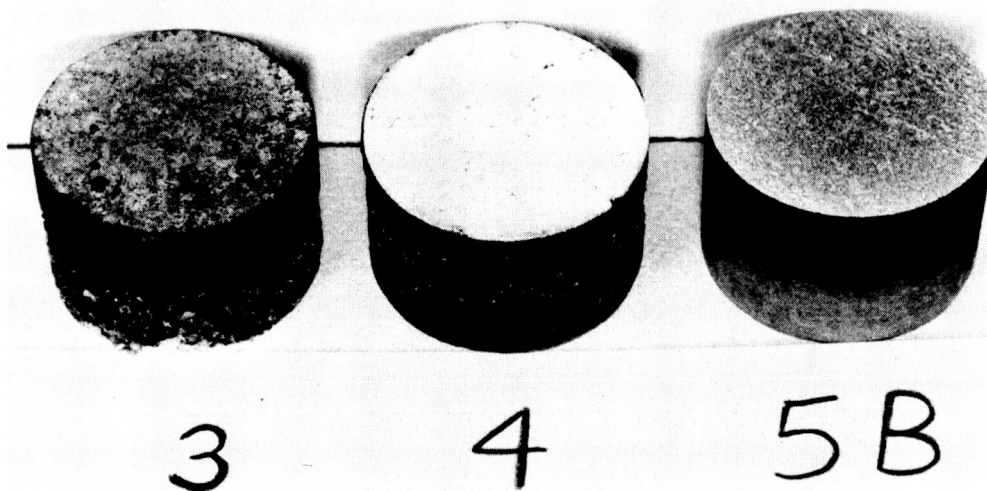


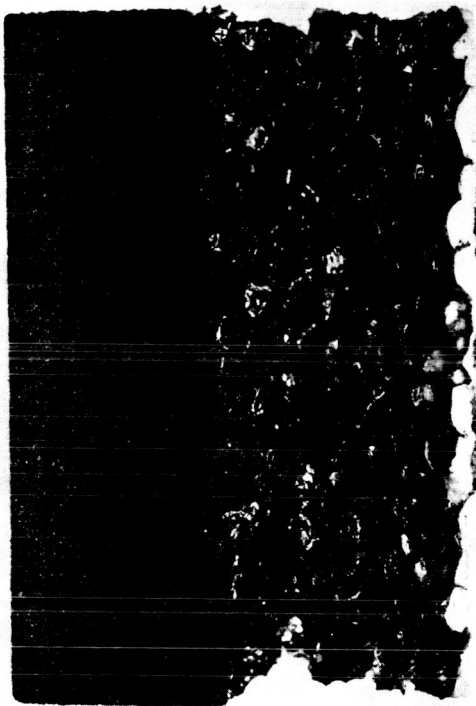
Figure 62 OVERALL VIEW OF OVERS TESTED SAMPLES 3, 4, AND 5B (H46)

Sample	Composition	Time (min)	Enthalpy (Btu/lb)	Heat Flux (Btu/ft-sec)
3	7/16-inch glass impregnated with spoxy on foamed glass (S. G. = 0.77)	1.5 (sample cracked)	6800	73
4	1/16-inch glass skeleton on foamed glass, (S. G. = 0.38)	8	6800	73
5B (H46)	8% Ecco spheres with glass rock slip and epoxy	8	6800	73

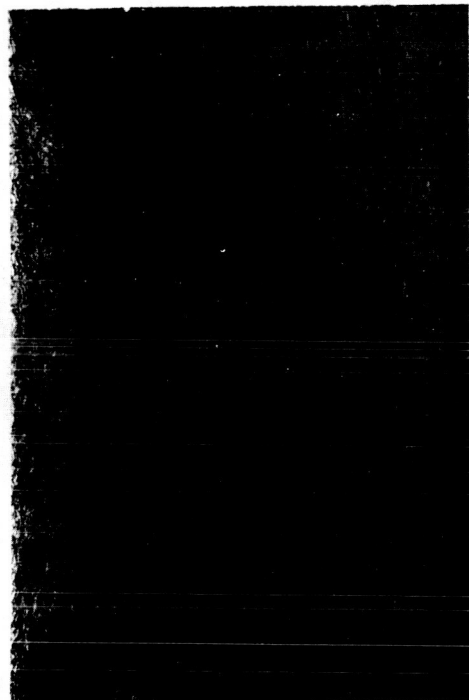


- B -

Figure 63 PHOTOMICROGRAPH OF
HALF SECTION OF TESTED
SAMPLES 3(A), 4(B) AND
5B(C) (refer to figure 62
for sample identification)



- A -



~~CONFIDENTIAL~~



Figure 64 OVERALL VIEW OF INSTRUMENTED OVERS TEST SAMPLES - TWO SAMPLES (LEFT) OF 5026-29, TWO SAMPLES (CENTER) OF 5026-22 AND TWO SAMPLES (RIGHT) OF 5026-23 (refer to table VIII for test conditions)

~~CONFIDENTIAL~~

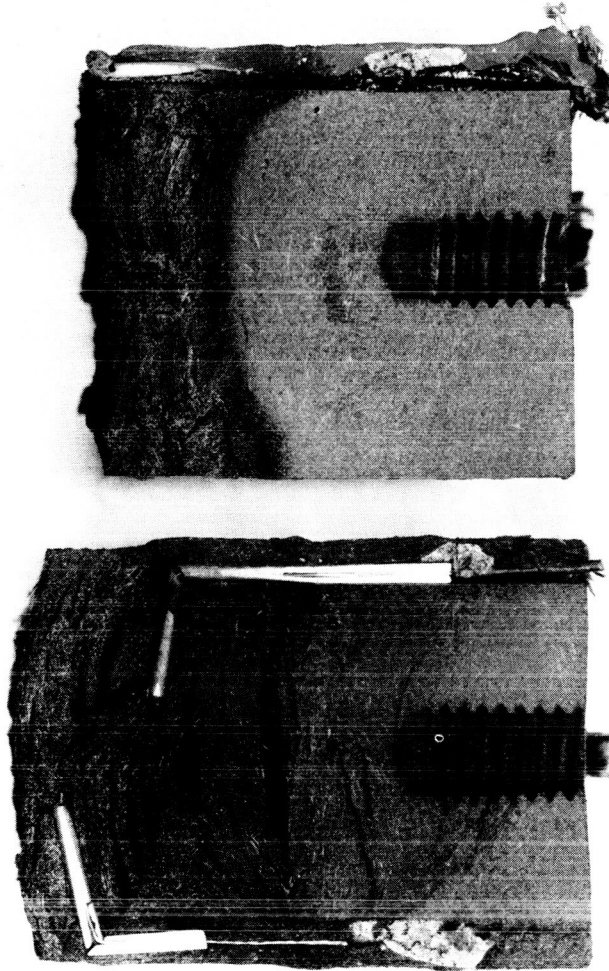


Figure 65 PHOTOMICROGRAPHS OF TESTED SAMPLES X5026-29 LOW
HEAT FLUX (LEFT) AND HIGH HEAT FLUX (RIGHT) (refer to
Table VIII for test conditions)

~~CONFIDENTIAL~~

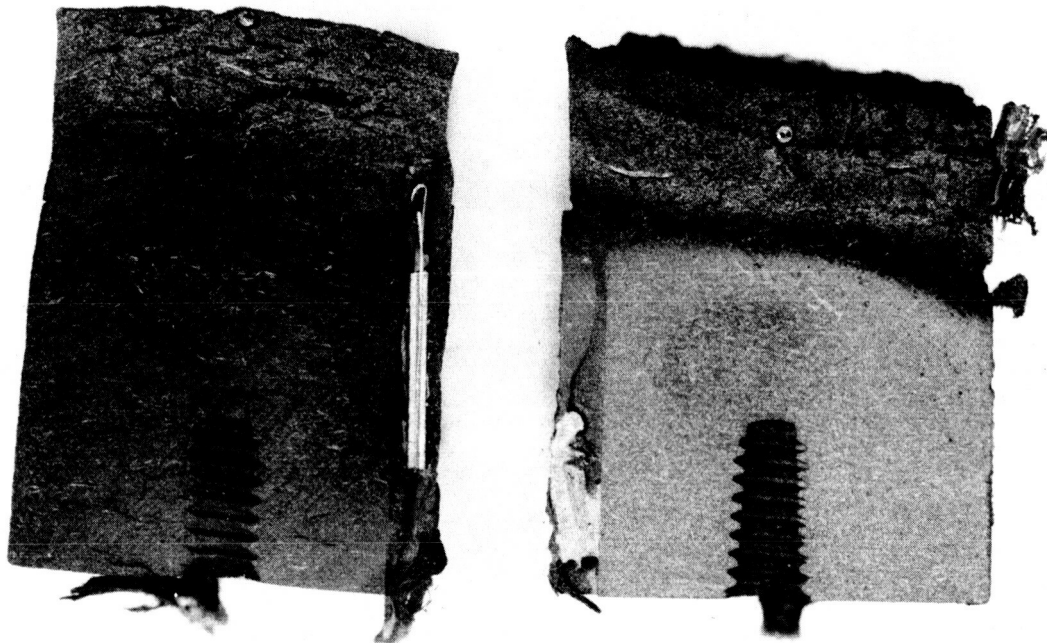


Figure 66 PHOTOMICROGRAPHS OF TESTED SAMPLES X5026-22 LOW
HEAT FLUX (LEFT) AND HIGH HEAT FLUX (RIGHT) (refer to
table VIII for test conditions)

~~CONFIDENTIAL~~

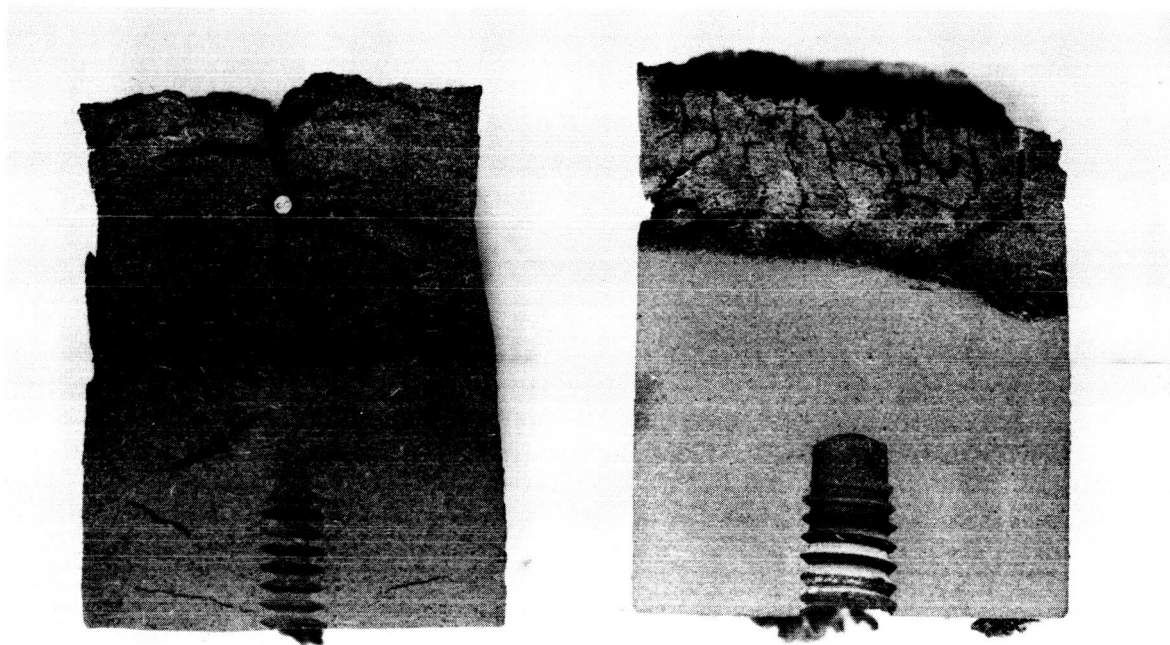


Figure 67 PHOTOMICROGRAPHS OF TESTED SAMPLES X5026-23 LOW
HEAT FLUX (LEFT) AND HIGH HEAT FLUX (RIGHT) (refer to
table VIII for test conditions)

In addition to the screening tests six samples of X5026 formulation were tested. Each of these samples was instrumented with four thermocouples. Table VIII presents the test conditions and the ablation characteristics of each of the tested samples. Figures 64 to 67 show the overall view of the tested samples as well as photomicrographs of the half section of each of the samples respectively. As is evident from the photomicrographs the cracking in the charred material is worse in samples tested at the low heat-flux level as compared to the samples tested at the high heat-flux level. The recorded brightness temperature, as well as the weight losses and dimensional changes for each of the tested samples, is given in Table VIII.

Slopes of the time-temperature data for specimen 21, plate 16 and specimen 21, plate 52 are shown in figures 68 and 69. A similarity between the shape of the curves for thermocouple 1 may be noted; the slope appears to level off in the vicinity of 800° F. This phenomenon is compatible with results computed for Avcoat X5026-22, specimens S and T. Similarities between the shapes of the curves for thermocouples 2, 3, and 4 may also be observed in both figures. In figure 68 the slopes determined for data from thermocouples 3 and 4 in plate 16, sample 21 (Avcoat X5026-22) rise considerably after a temperature of approximately 800° F is reached, and converge with the slopes determined for thermocouple 2 near a temperature of 1200° F. Several valleys are evident in the curves for thermocouples 2, 3, and 4, plate 52, sample 21, notably around 400° and 1050° F. These anomalies, which are more pronounced at the spatial positions occupied by thermocouples 2, 3, and 4, point toward the presence of chemical reactions. A number of cracks were noted in the specimens after sectioning which would also affect the slopes. The good correlation between the slopes below 1200° F, however, suggests that random cracks did not appear until after this temperature (or at least they did not greatly affect the thermocouple readings).

Figures 70 and 71 present the temperature distribution history for the data examined. The families of curves for the two specimens plate 16, sample 21 and plate 52, sample 21 are similar. Note that the second derivative of temperature with respect to distance from the heat surface tends to become negative at later times in the region bounded by thermocouples 2 and 4 (about 1800° F).

Effective thermal diffusivities, α , are listed in Tables IX and X. These values have been obtained from program 1077 which utilizes a simple heat-conduction model. The α -values for Avcoat X5026-22 (Table IX) determined at comparable temperatures during the heating period are consistent with those calculated for Avcoat X5026-22, specimens S and T. The α -values for Avcoat X5026-23 (Table X) are comparable until 1200° F. In Table X a maximum α is noted at approximately 1600° F and then α drops to quite low values. This result could be caused by the appearance of cracks. The presented thermal diffusivities are effective values because they are dependent on the effects of chemical reactions, transpiration, and cracks and as such are not functions of temperature only.

~~CONFIDENTIAL~~

TABLE VIII
OVERS ARC TEST DATA ON INSTRUMENTED TEST SAMPLES

Material	Sample No.	Gas Enthalpy (Btu/lb)	Stagnation Point Cold-Wall Heat Flux (Btu/ft ² -sec)	Stagnation Point Pressure (mm Hg)	Time of Test Results	Sample Weight (gm)		Sample Length (in.)		Sample Diameter (in.)		Recorded Brightness Temp. of Surface (°F)
						Before	After	Before	After	Before	After	
X5026-22	21	8200	45	2.30	8	23.7	20.3	1.004	0.987	0.740	0.713	2540
Plate 16	20	18600	320	11.6	2	23.3	21.0	1.000	0.880	0.744	0.754	3870
X5026-23	21	8200	45	2.30	8	23.3	19.5	1.004	0.975	0.744	0.716	2320
Plate 52	22	18600	320	11.6	2	23.3	21.0	1.007	0.868	0.745	0.749	3840
X5026-29	21	18600	320	11.9	2	22.8	20.3	0.991	0.804	0.745	0.747	4040
Plate 9	20	8200	45	2.30	8	22.9	20.0	0.993	0.985	0.742	0.712	2490

~~CONFIDENTIAL~~

~~CONFIDENTIAL~~

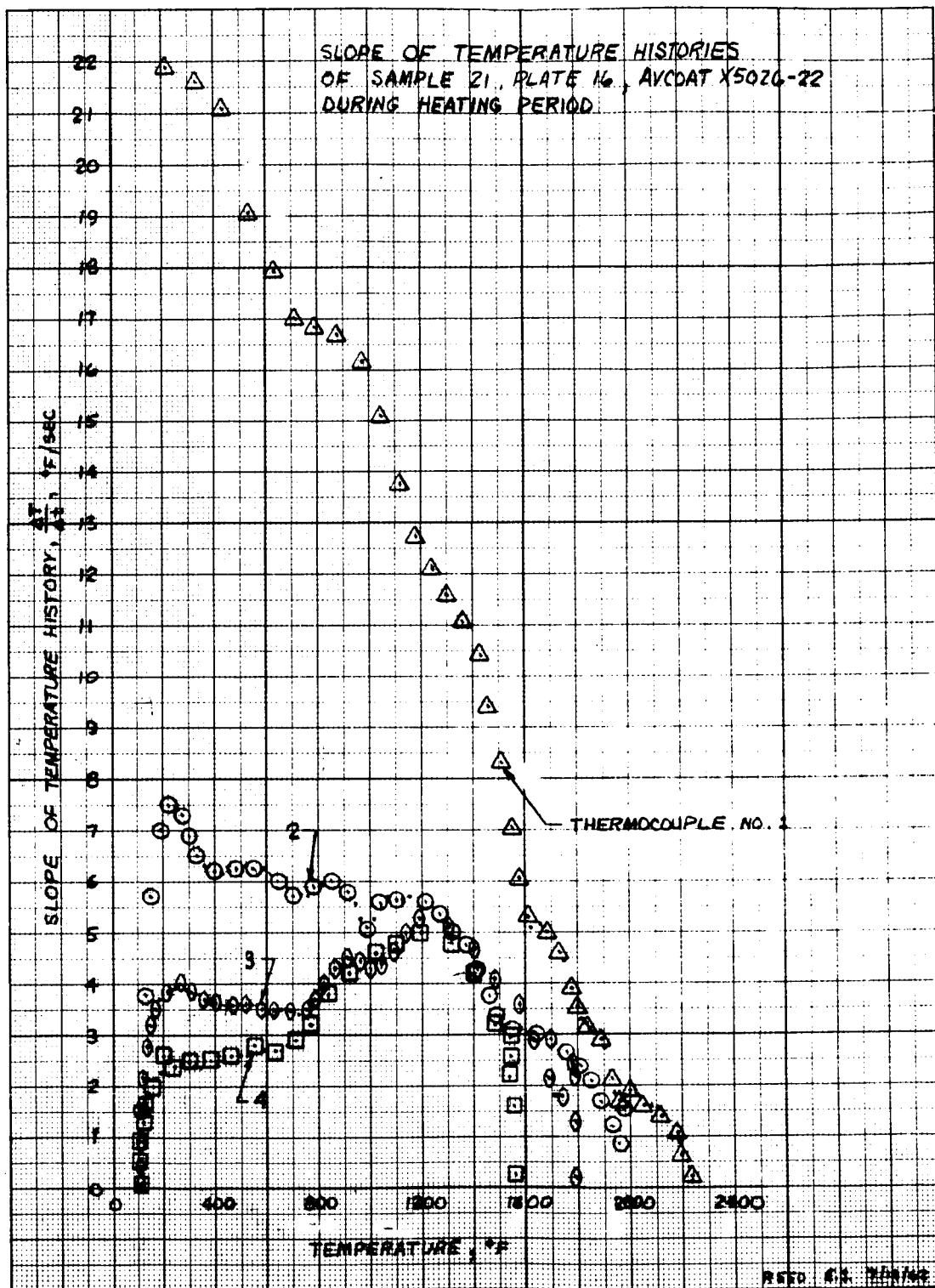


Figure 68 SLOPE OF TEMPERATURE HISTORIES OF SAMPLE 21, PLATE 16,
AVCOAT X5026-22 DURING HEATING PERIOD

~~CONFIDENTIAL~~

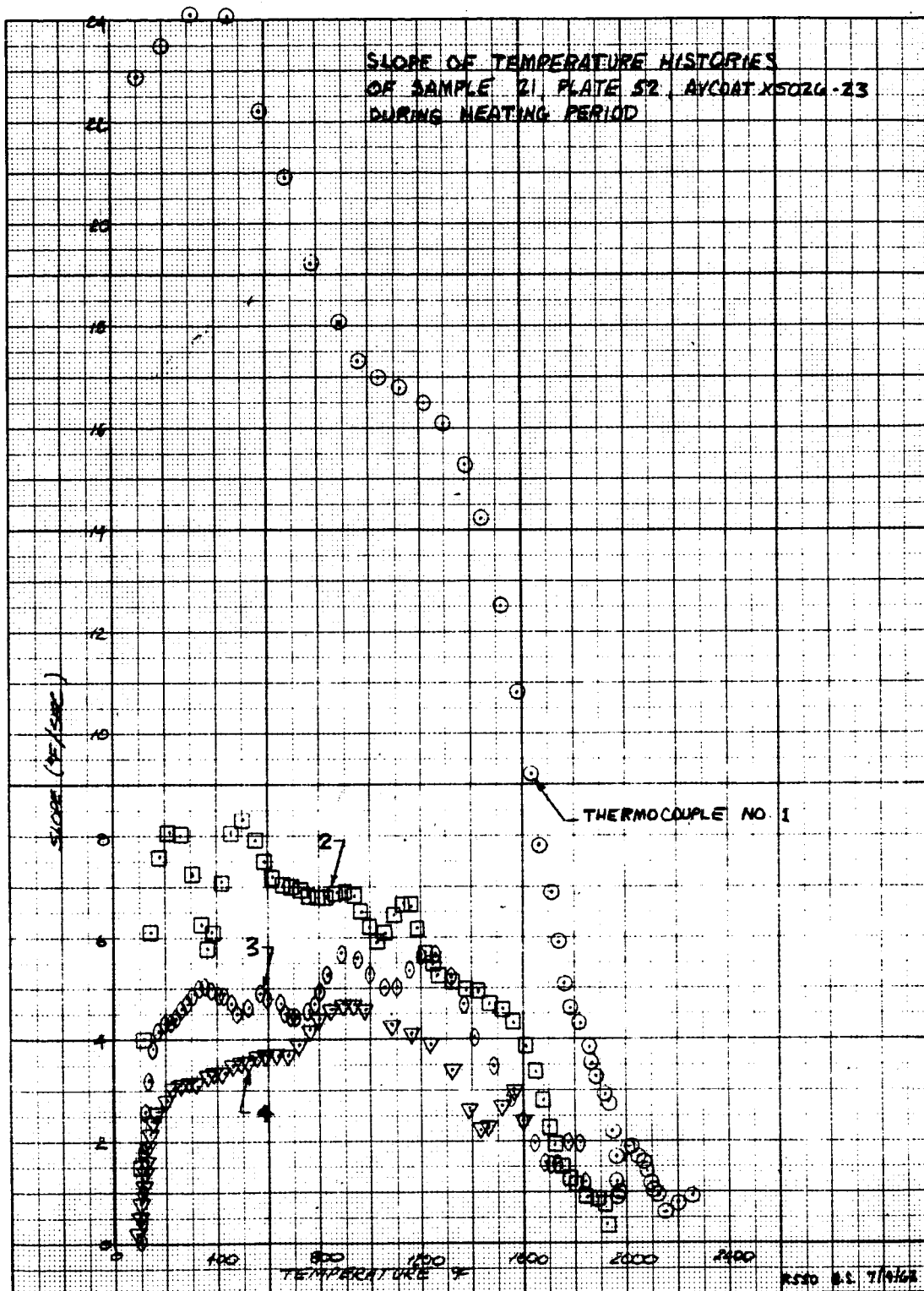


Figure 69 SLOPE OF TEMPERATURE HISTORIES OF SAMPLE 21, PLATE 52, AVCOAT X5026-23 DURING HEATING PERIOD

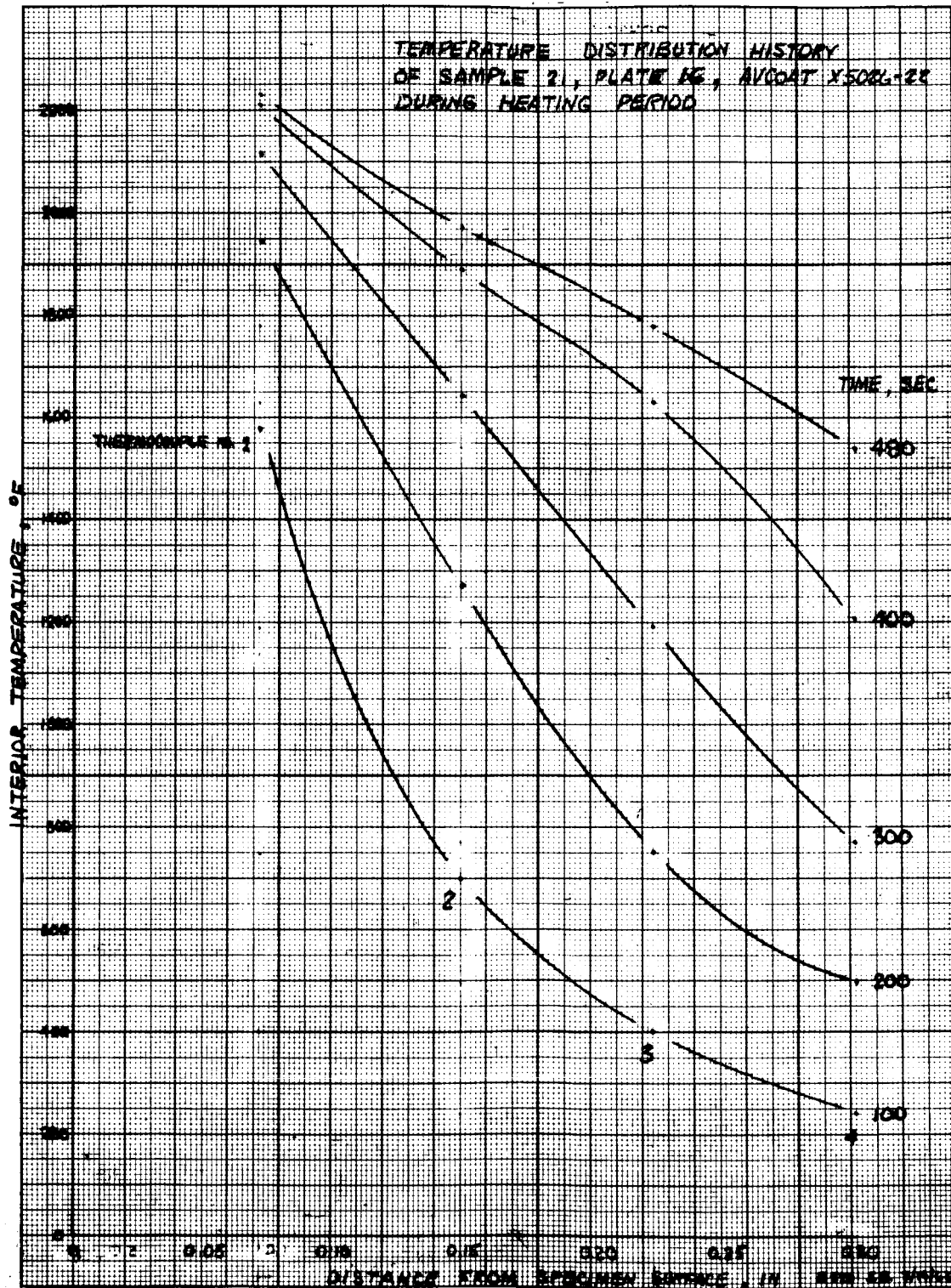


Figure 70 TEMPERATURE DISTRIBUTION HISTORY OF SAMPLE 21, PLATE 16,
AVCOAT X5026-22 DURING HEATING PERIOD

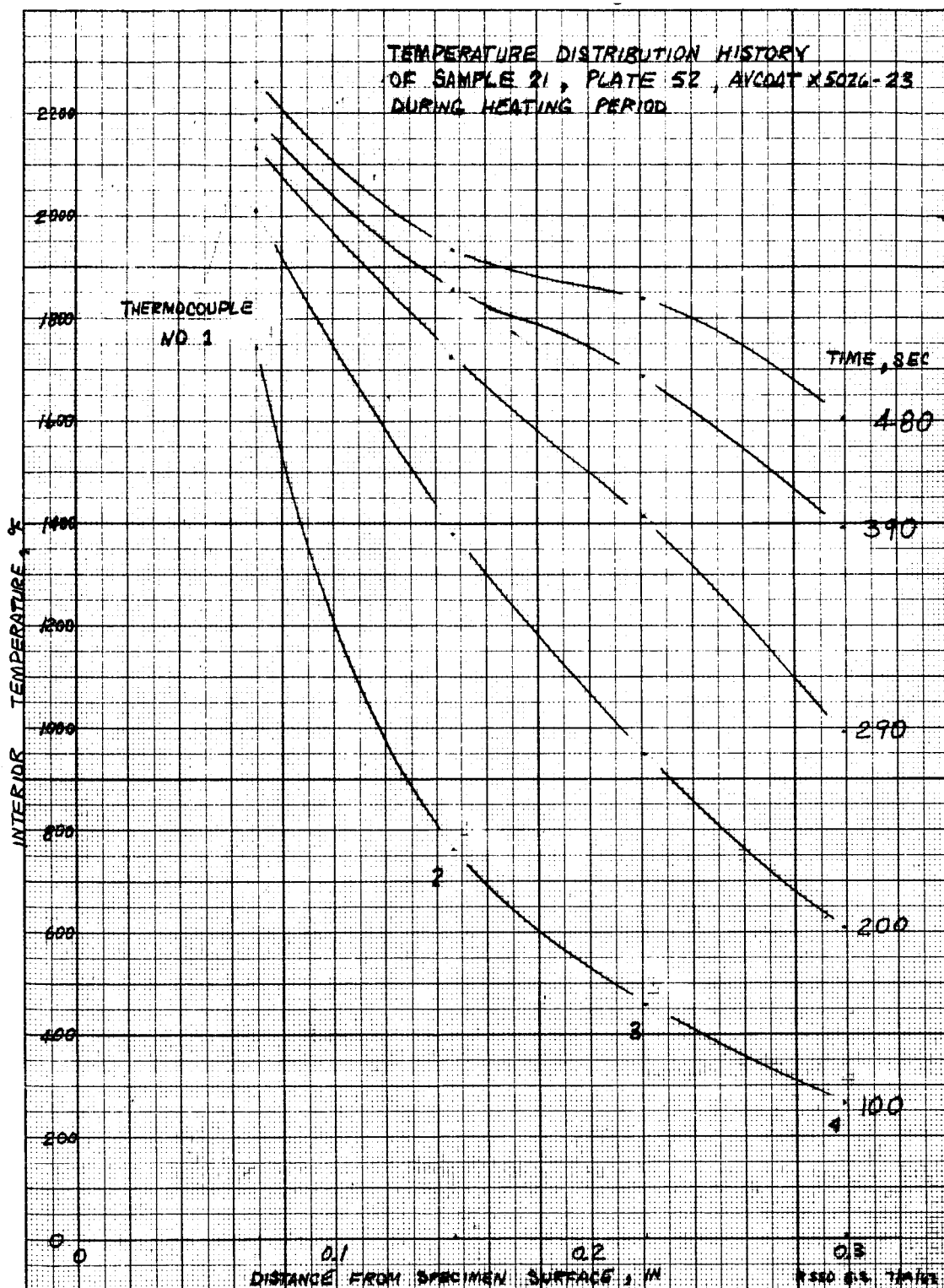


Figure 71 TEMPERATURE DISTRIBUTION HISTORY OF SAMPLE 21, PLATE 52, AVCOAT X5026-23 DURING HEATING PERIOD

~~CONFIDENTIAL~~

TABLE IX

EFFECTIVE THERMAL DIFFUSIVITIES CALCULATED USING
PROGRAM 1077 FOR SAMPLE 21, PLATE 16,
AVCOAT X5026-22

From Thermocouples No. 1, 2, and 3		
Avg. Temp. (°F)	Temp. Range (°F)	Thermal Diffusivity (ft ² /hr)
167	104 to 717	0.0042
363	137 to 1185	0.0025
550	245 to 1512	0.0016
730	362 to 1684	0.0015
905	471 to 1812	0.0018
1070	578 to 1905	0.0023
1239	682 to 1963	0.0046
1390	787 to 2018	0.0209

TABLE X

EFFECTIVE THERMAL DIFFUSIVITIES CALCULATED USING
PROGRAM FOR SAMPLE 21, PLATE 52,
AVCOAT X5026-23

From Thermocouples No. 1, 2, and 3		
Avg. Temp. (°F)	Temp. Range (°F)	Thermal Diffusivity (ft ² /hr)
160	99 to 783	0.0039
365	136 to 1298	0.0025
584	263 to 1671	0.0017
799	409 to 1835	0.0015
1000	550 to 1935	0.0018
1189	693 to 1976	0.0025
1353	831 to 2031	0.0036
1500	1005 to 2081	0.0055
1629	1152 to 2114	0.0089
1712	1324 to 2130	0.0036
1762	1453 to 2155	0.0019
1803	1554 to 2173	0.0012
1833	1626 to 2187	0.0009
1866	1683 to 2202	0.0009
1890	1725 to 2231	0.0007
1922	1775 to 2260	0.0009
1605	1080 to 1838*	0.0305

*Cooling period

~~CONFIDENTIAL~~

~~CONFIDENTIAL~~

Results calculated by program 958 for the OVERS test of 25 June on specimen X5020-29, sample 20, indicate a maximum surface temperature of 2550° F. A value of 2485° F was measured with the optical pyrometer. Emissivities computed for this test were several times larger than anticipated, in fact, exceeding unity. A study is underway to explain these large discrepancies.

It was noted that when a temperature, T_E , was supplied to program 958 which was in error, large oscillation resulted in the values of emissivity. As an example of this, case 4E was generated with a temperature at 50 seconds which was different by 100° F from the value used in case 4. In figure 72, the values of emissivities calculated for these two cases are shown. Notice that the oscillations (which reach values as large as $\epsilon = 50$) persist for 30 seconds after the error occurs. In order to diminish this oscillation, values of surface temperature T_0 and heat flux q_0 were smoothed by fitting a parabola, subject to a least-squares fit, through five successive points. The oscillations in emissivity were only slightly reduced. It is expected that an improvement can be made by reducing the degree of the curve to a linear one, increasing the number of points employed from five to ten, and operating directly on the emissivity rather than on T_0 and q_0 .

The results of thermal property measurements since the last reporting period are as follows:

a. Thermal Conductivity

Material	Density (lb/ft ³)	Thermal Conductivity (Btu/hr-ft °R at 710°R)	Temperature Range (°R)
Avcoat X5026-22 (AP-143)	57.03	0.095	550 to 850
Avcoat X5026-22 (AP-143)	55.94	0.093	550 to 850
Avcoat X5026-33 (AP-186)	64.62	0.141	550 to 850
Avcoat X5026-22B (AP-197)	42.26	0.075	550 to 850

b. Specific Heat (all values average of 4 tests)

Material	Density (lb/ft ³)	Specific Heat (Btu/lb °R)	Temperature Range (°R)
Avcoat X5026-22 (AP-6)	56.71	0.395	500 to 900
Avcoat X5026-22 (AP-13)	58.41	0.395	500 to 900
Avcoat X5026-22 (AP-58)	53.69	0.400	500 to 900
Avcoat X5026-22 (AP-108)	62.37	0.400	500 to 900
Avcoat X5026-33 (AP-183)	64.99	0.363	500 to 900

~~CONFIDENTIAL~~

~~CONFIDENTIAL~~

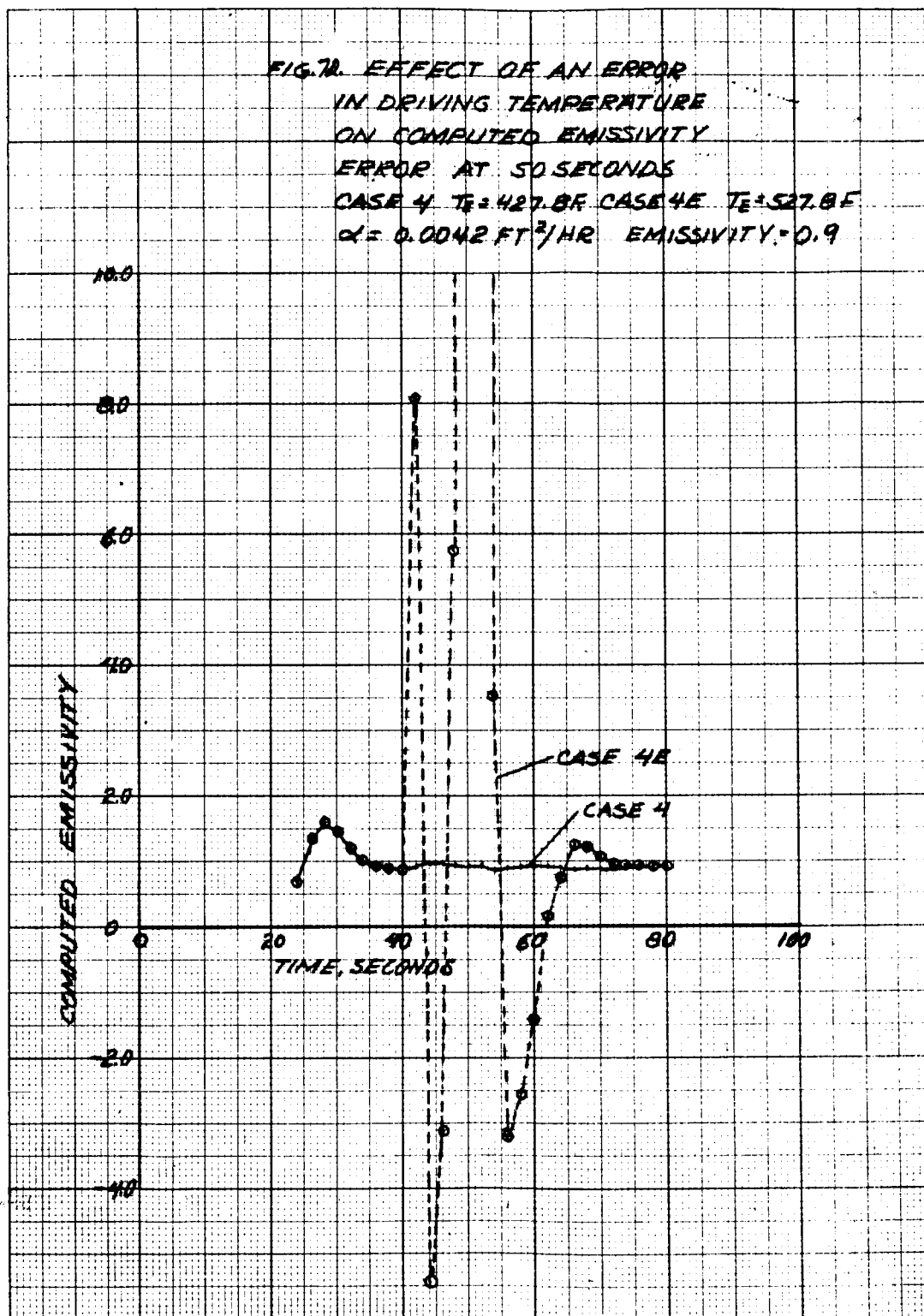


Figure 72 EFFECT OF AN ERROR IN DRIVING TEMPERATURE ON COMPUTED EMISSIVITY ERROR AT 50 SECONDS, CASE 4

~~CONFIDENTIAL~~

~~CONFIDENTIAL~~

The results of the aluminum and glass projectile firings completed to date are shown in figure 73. Also shown is the predicted penetration-energy relationship for glass into Avcoat X5026 at room temperature. These preliminary results indicate that glass and aluminum projectiles do not differ much in penetration into Avcoat X5026 at room temperature, for equivalent projectile energies. The actual depth of penetration is greater than the predicted values, which implies that the analysis of the system reliability is an optimistic evaluation, and the conditions should be worse than predicted.

The result of the "cold" target shots have been somewhat confusing. Early penetration data into a cold (-100° F) target at a penetration energy of 1400 joules show a penetration of about one-third that occurring at room temperature. Later shots have given somewhat deeper penetrations although still somewhat less than room temperature results (see points on figure 73). It is suspected that the very low penetration point may have been caused by a broken glass projectile. Impacts into a -100° F target also give significantly less spalling in all of the impacts than at room temperature. In the cold shots, the target was cooled to temperature by a cold soak in liquid nitrogen with the temperature being recorded 1/8- and 1/2-inch below the surface with iron-constantan thermocouples.

The effect of target temperature on the resulting impact damage should be investigated further to develop a better understanding of the phenomena and evaluate empirical constants which will allow a more accurate determination of system reliability. It is, therefore, recommended that tests be carried out at temperatures above and below room temperature. A suitable program would include about 40 tests, 10 each at temperatures of 350°, 200°, -100°, and -260° F over the velocity range obtainable with a light gas gun launching glass projectiles.

In previous results¹¹ from impacting an ablative target under hypervelocity conditions, it was shown that when the penetration depth was to the backup plate, a good deal of face spallation occurred which resulted in much larger crater diameters than have been observable in thicker targets at equivalent energies. Because of the thin (0.200-inch) heat shield used for most of the Apollo capsule, it is expected that an impact over this region would result in large losses of heat-shield materials. To understand this threat, six impact tests are planned into targets of 0.200-inch Avcoat X5026 bonded to a 0.012-inch thick steel plate. Three tests, each at maximum velocity (about 18,000 to 22,000 ft/sec), are planned with 0.100-gm glass spheres into targets cooled to -100° and -260° F. These hopefully will be accomplished during the next reporting period.

¹¹Rockowitz, M., Summary of Hypervelocity Impact of Ablation Re-entry Materials, Avco RAD Doc. 62-795 (July 1962).

~~CONFIDENTIAL~~

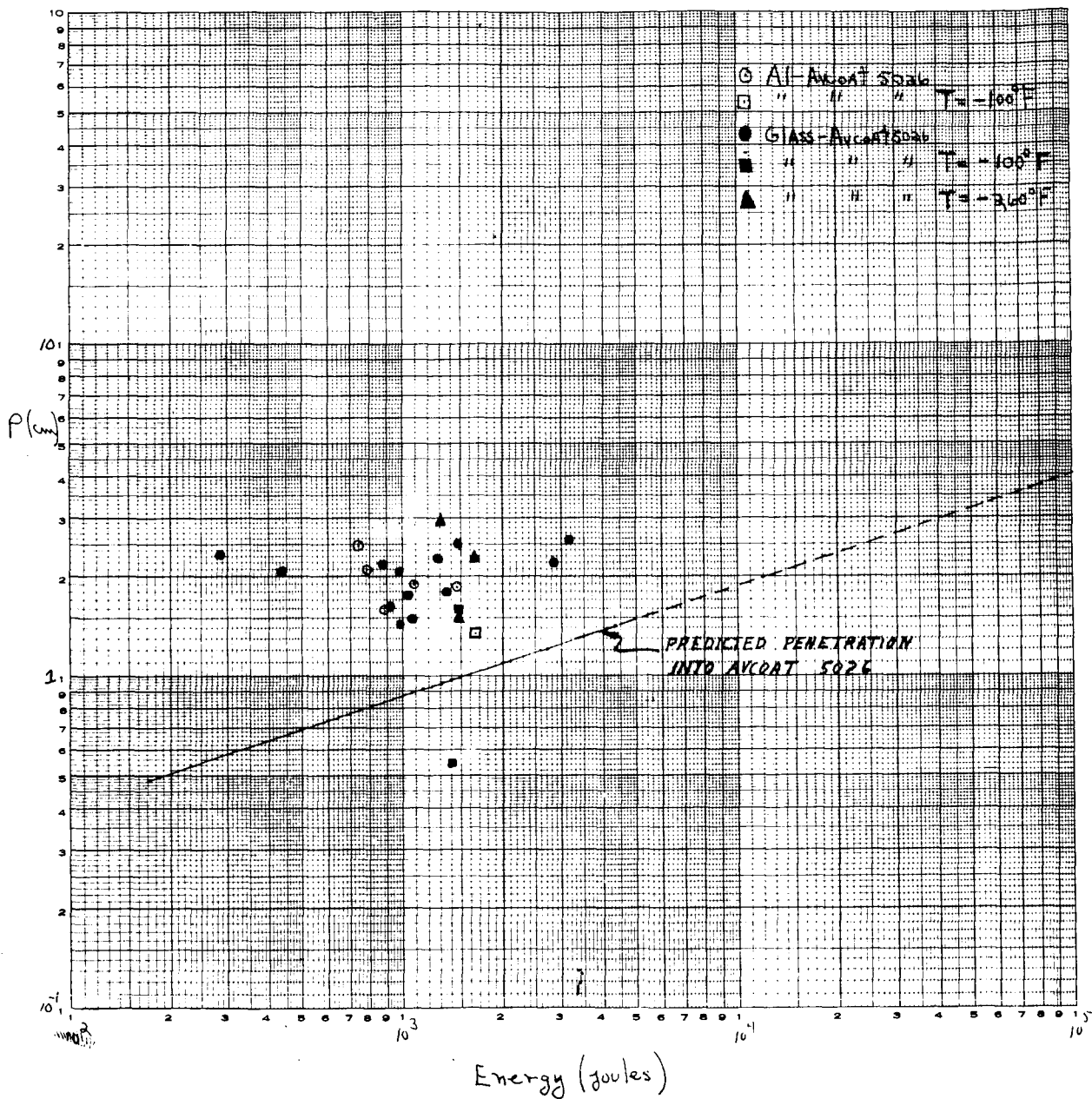


Figure 73 PREDICTED PENETRATION INTO AVCOAT X5026

~~CONFIDENTIAL~~

To determine whether the effects of re-entry heating on a puncture of the heat-shield skin would result in burn-through of the top plate of the stainless steel honeycomb specified for Apollo, calculations were made using a two-dimensional heat conduction program. The damage was assumed to be a cylindrical hole in the heat shield to the depth of the substructure. The hole was assumed to have a diameter twice that of the depth. This represents a maximum l/d ratio expected from impact, or in other words, a minimum heat flux to the substructure. The position on the capsule chosen for study was station 9, a point about midway along the windward side, and station 14, a point about midway along the center plane. The heat flux data used was taken from North American data assuming a maximum integrated heating trajectory (1). Since previous studies¹² have shown that the heat flux to the base of a cavity under turbulent flow conditions normal to the axis of the cavity is less than that to the surface, the heat-flux data were modified to take this effect into account. From the work of Hoercher, it was shown that the heat flux to the base of a cavity having an l/d of 0.5 under these flow conditions is 0.6 of the surface flux, if the Mach number of the flow is 2 or greater. Thus for lack of better information at this time, the flow is assumed to have a Mach number of 2 or greater. The results of the calculations are shown in figure 74. It is evident that burn-through of the stainless-steel face plate at station 9 occurs about 62 seconds after the start of re-entry. Stainless steel 17-7 having a melting temperature of 2600° F was used. This was assumed to be the condition at which burn-through would occur. The case for station 14 shows that burn-through will not occur over a 300-second period, which is long enough to insure that burn-through will not occur at all, since no appreciable heating will occur after that time. This last result indicates that punctures of the heat shield along the center plane having an $l/d < 0.5$ will have to be studied further to see if the increased hole diameter will lead to burn-through. Also the implication of this result is that puncture of the heat-shield material may not be a realistic choice of a mission failure criteria, and some other mode of failure may be necessary. This last point will be studied further in the next reporting periods.

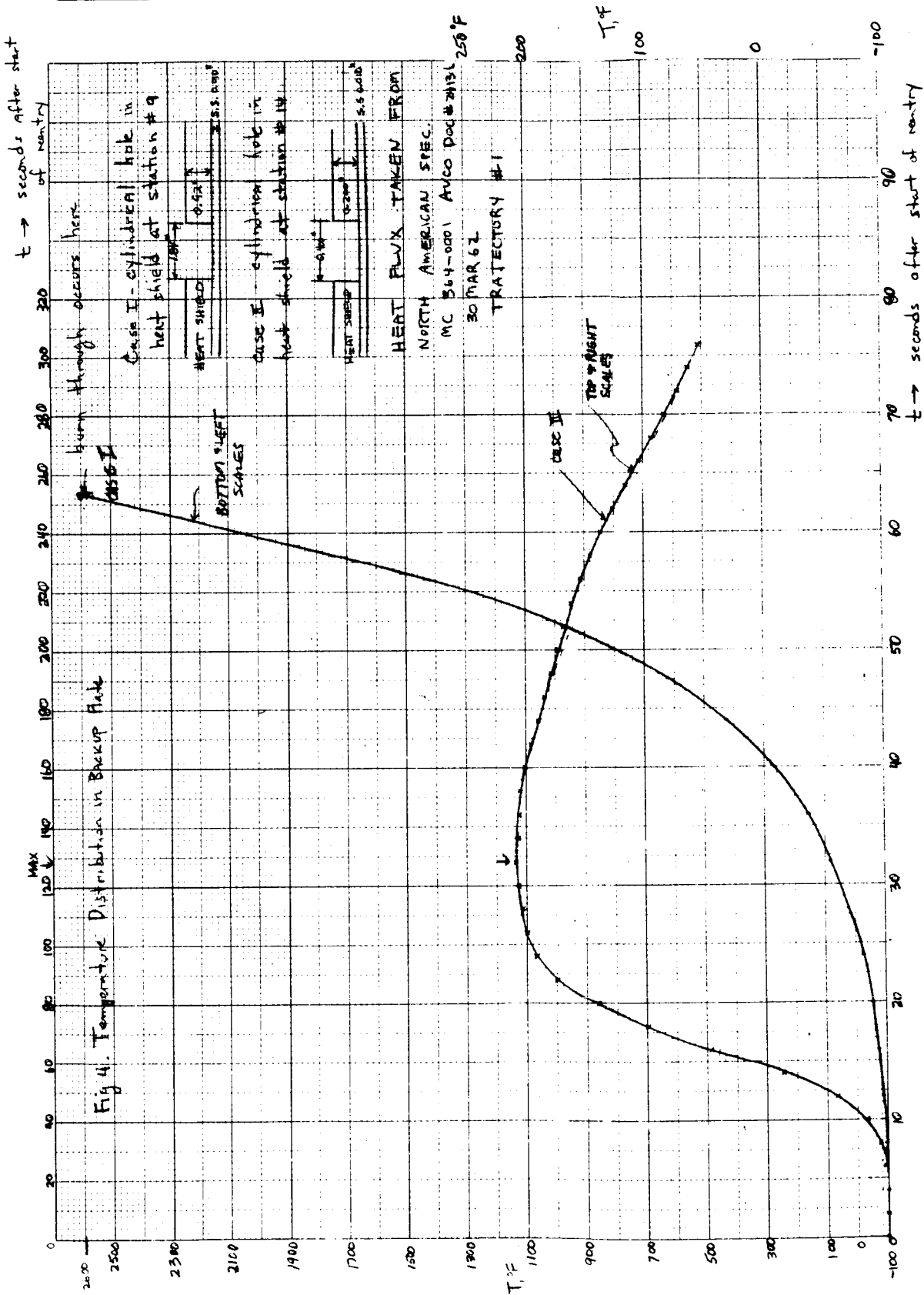
A computer program has been set up, and is currently being run, to see if the backup structure would also burn through at station 9. The backup structure assumed was another layer of stainless steel, plus one of insulation and one of aluminum. This should be a fairly realistic model of the actual spacecraft. This data should be available by the next reporting period.

The spectral emittance of the arc exposed Avcoat X5026-29 is given in figures 75 and 76. The operating conditions of the arc are stated on the figure.

¹²Hoercher, H., et al., Hypervelocity Kill Mechanisms Program, Aerothermal Phase," Avco RAD SR-61-164 (21 November 1961). Secret

~~CONFIDENTIAL~~

~~CONFIDENTIAL~~



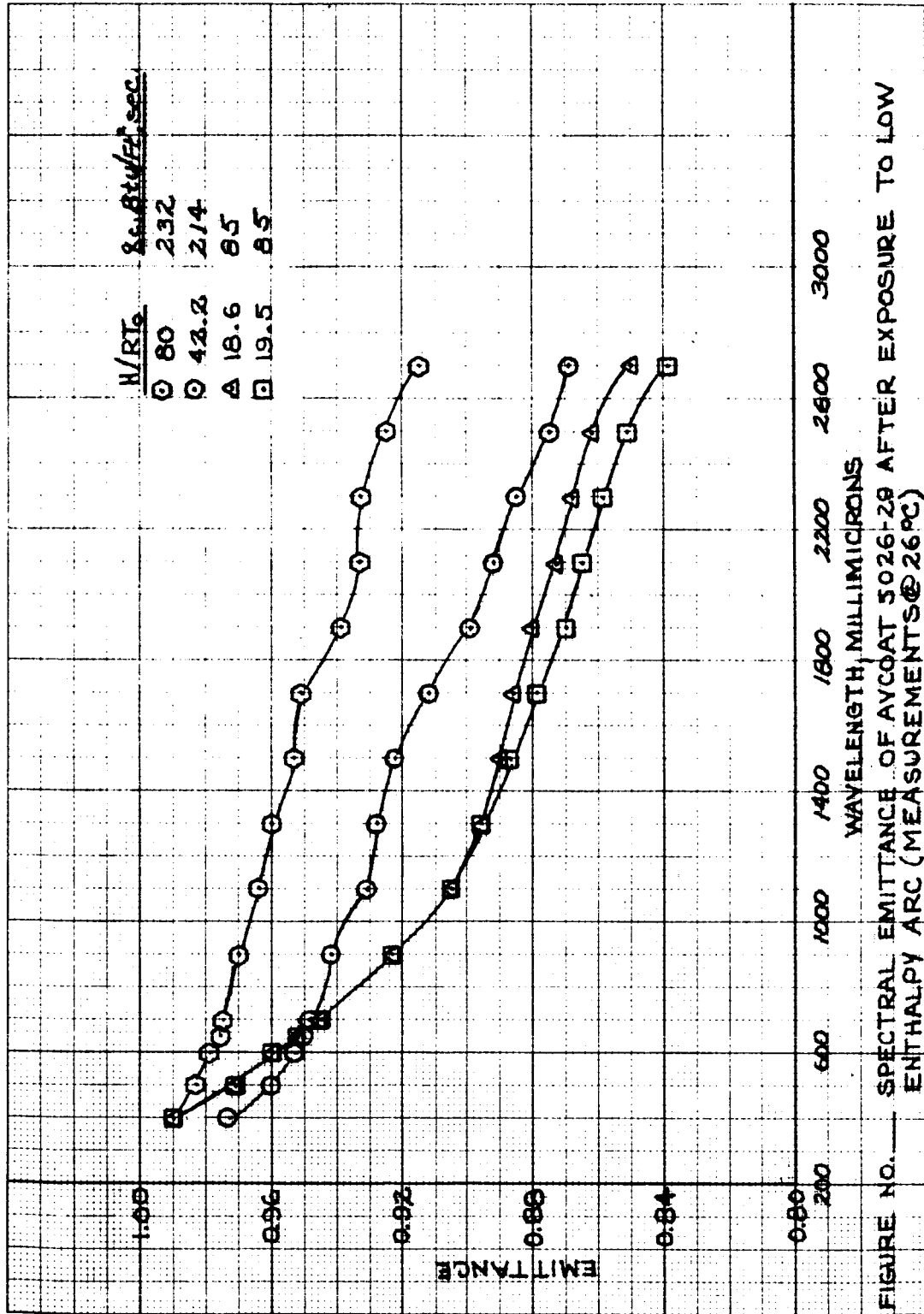


Figure 75 SPECTRAL EMITTANCE OF AVCOAT X5026-29 AFTER EXPOSURE TO LOW-ENTHALPY ARC (MEASUREMENTS AT 26°C)

~~CONFIDENTIAL~~

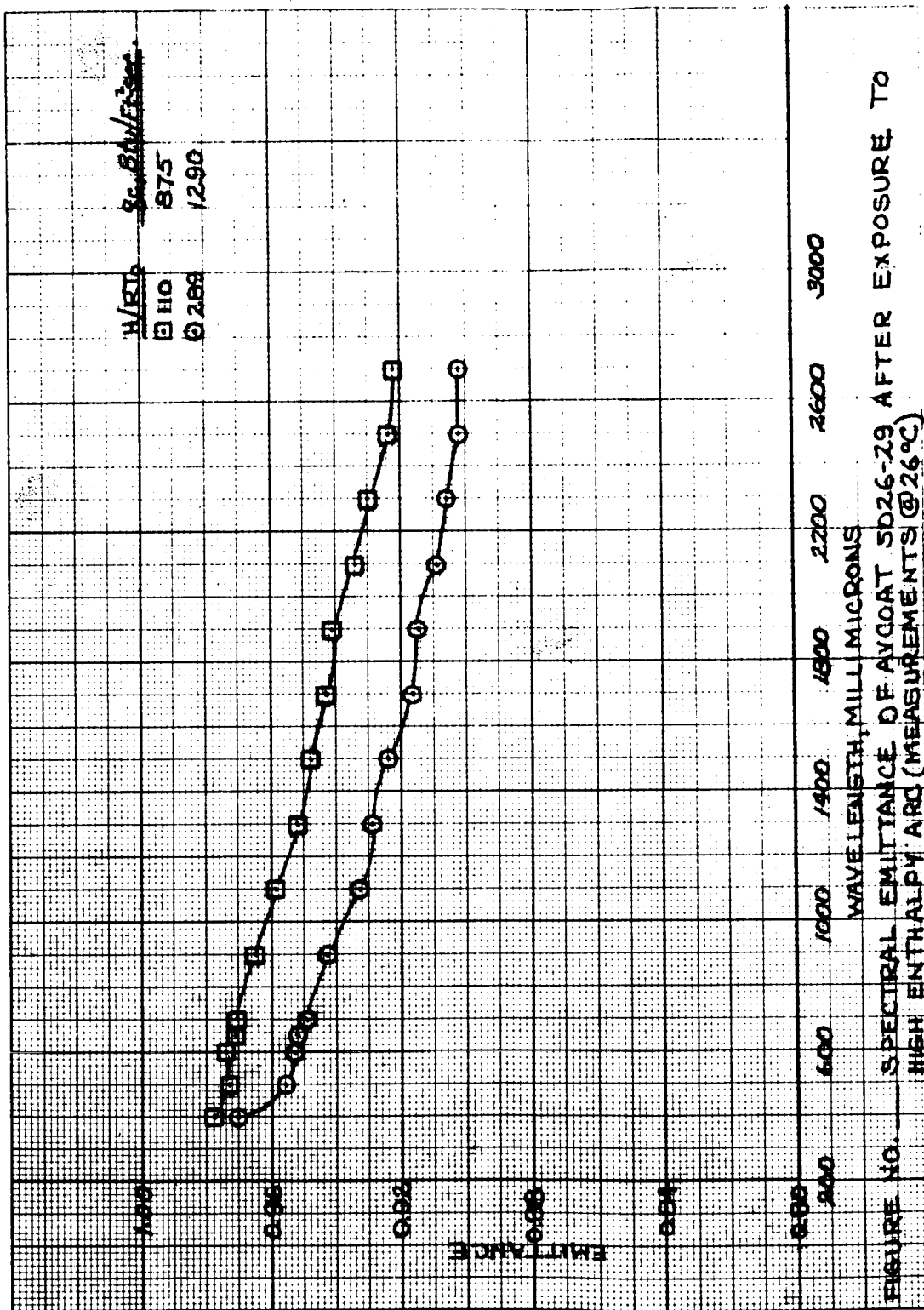


Figure 76 SPECTRAL EMITTANCE OF AVCOAT X5026-29 AFTER EXPOSURE TO HIGH-ENTHALPY ARC (MEASUREMENTS AT 26 °C)

~~CONFIDENTIAL~~

~~CONFIDENTIAL~~

The spectral emittance of the six samples tested for the purpose of brightness temperature correction are as follows:

Material — Avcoat X5026-29

	H/RT ₀	q _c Btu/ft ² sec	ε _λ at λ = 0.65 micron
In virgin state	-	-	0.86
In charred state (arc exposed)	18.6	85	0.95
	19.5	85	0.95
	42.2	214	0.95
	80.0	232	0.97
	110.0	875	0.97
	289.0	1290	0.95

The total emittance can be determined by the relationship

$$E_{tS} = \frac{\int_0^{\infty} E_{b\lambda} E_{S\lambda} d\lambda}{\int_0^{\infty} E_{b\lambda} d\lambda}$$

where

E_{tS} = total emittance of the specimen

$E_{b\lambda}$ = rate of energy emission, per unit wavelength interval, of a blackbody for the increment λ to $\lambda + d\lambda$

$E_{S\lambda}$ = emittance of the specimen between λ and $(\lambda + d\lambda)$

It was felt that for these preliminary measurements the following operation would give sufficient precision.

$$E_{tS} \approx \frac{\sum_{\lambda_1}^{\lambda_2} E_{b\lambda} E_{S\lambda} \Delta\lambda}{\sum_{\lambda_1}^{\lambda_2} E_{b\lambda} \Delta\lambda}$$

~~CONFIDENTIAL~~

~~CONFIDENTIAL~~

Since all values of $\Delta\lambda$ were chosen to be equal they cancelled numerically as well as dimensionally. The results of these evaluations over the wavelengths of 0.4 to 2.7 microns for 3500° K and 5800° K for the specimen tested at 42.2 RT₀ average are:

At 3800° F:

$$E_{tS} \cong 0.62, \text{ virgin state}$$

$$E_{tS} \cong 0.82$$

At 5800° K:

$$E_{tS} \cong 0.81, \text{ virgin state}$$

$$E_{tS} \cong 0.95.$$

4. Quality Assurance

X-rays of NAA honeycomb test panels show areas of heavy alloy flow, of twisted or crushed core, and of apparent repairs to the cells. Although no acceptance criteria exist, this is given for information.

~~CONFIDENTIAL~~

~~CONFIDENTIAL~~

DISTRIBUTION

<u>Addressee</u>	<u>No. of Copies</u>
NAA S&ID Attn: J.M. Kerr (+1 reproducible)	25
M. C. Adams	1
R. Alberts	1
M. T. Anderson	1
P. Andrews	1
E. Belason	1
R. Bentley	1
C. Berninger	1
W. Broding	1
C. Caputo	1
C. Cohen	1
J. Collings	1
W. deFee	1
R. E. Demming	1
F. Diederich	1
A. Diming	1
J. Edwards	1
J. Gillies	1
J. Graham	1
D. Haas	1
L. Hammond	1
B. Henshall	1
H. Hoercher	1
A. J. Hanawalt	1
C. Huffine	1
R. H. Huggins	1
E. Kaminsky	1
W. Ihnat	1
R. John	1
A. E. Johnson, Jr.	1
R. Knower	1
J. Kyger	1
G. Larson	1
R. Lurie	1
C. H. Leigh	1
E. G. Lowery, NAA Resident Representative	1
M. Malin	1
H. Manheimer	1
M. Mitrovich	1
T. Mix	1
D. Mosher	1
B. Nordquist	1

~~CONFIDENTIAL~~

~~CONFIDENTIAL~~

DISTRIBUTION (Concl'd)

<u>Addressee</u>	<u>No. of Copies</u>
E. Offenhartz	1
R. Peterson	1
P. Quaiel	1
G. Quayle	1
A. Rothstein	1
S. Ruby	1
I. Sacks	1
E. Schurmann	1
D. Stafford	1
V. Strang	1
H. Tereshkow	1
T. Vasilos	1
R. Wagner (Lycoming)	1
A. C. Walker	1
H. Weisblatt	1
W. Zeh	1
W. Zolla	1
Central Files	5
Document Control	2
Research Library	5
Apollo Central File (+1 reproducible)	

~~CONFIDENTIAL~~